The Unsaturated Hydraulic Characteristics of the BandelierTuff

Los Alamos
N A T I O N A L   L A B O R A T O R Y

An Affirmative Action/Equal Opportunity Employer

*The Unsaturated Hydraulic
Characteristics of the Bandelier Tuff*

David B. Rogers
Bruce M. Gallaher

Table of Contents

NOTE: The **Inside Back Cover** of **paper copies** of this report has a computer disk containing files on moisture retention and hydraulic data (Macintosh, tab-delimited text files).
In the **online version** of the report, these files have been added to the end of the report as **Special Appendix G.** The files are listed on the following page in the order they appear. These files have no page numbers.

Special Appendix G

NOTE: These files are contained on a disk inside the paper copies of this report (Macintosh, tab-delimited text files). In the online version they follow Appendix F. There are no page numbers.

AB Retent Data Txt

CDBM Retent Data Txt

Crsh Tuff Retent Data Txt

MCM5.1 Retent Data Txt

MCM5.9A Retent Data Txt

PC-4 Retent Data Txt

PC-4 SPOC Retent Data Txt

SIMO-1 Retent Data Txt

TA-54 LLC Retent Data Txt

TA-54-1001 Retent Data Txt

TA-54-1002 Retent Data Txt

TA-54-1003 Retent Data Txt

TA-54-1006 Retent Data Txt

TA-16 P-16 Retent Data Txt

Unsat Prop by Units Txt

Unsat Prop by Well Txt

List of Tables

List of Figures

The Unsaturated Hydraulic Characteristics
of the Bandelier Tuff

by

David B. Rogers and Bruce M. Gallaher

Abstract

This report summarizes the physical and unsaturated hydraulic properties of the Bandelier Tuff determined from laboratory measurements made on core samples collected at Los Alamos National Laboratory. We fit new van Genuchten-type moisture retention curves to this data, which was categorized according to member of the Bandelier Tuff and subunit of the Tshirege Member. Reasonable consistency was observed for hydraulic properties and retention curves within lithologic units, while distinct differences were observed for those properties between units. With the moisture retention data, we constructed vertical profiles of in situ matric suction and hydraulic head. These profiles give an indication of the likely direction of liquid water movement within the unsaturated zone and allow comparison of core-scale and field-scale estimates of water flow and solute transport parameters. Our core-derived transport velocities are much smaller than values estimated from tritium (^{3}H), Cl$^-$, and NO$_3^-$ contamination found recently in boreholes. The contaminant tracer-derived transport velocities from Los Alamos Canyon are 10- to 100-times greater than core-derived values found for the Otowi Member, and for Mortandad Canyon, 1300- to 5000-times greater than core-derived values for that borehole. The significant difference found for Mortandad Canyon suggests that fracture or other fast-path transport may be important there. The relatively small difference between observed and predicted velocities at Los Alamos Canyon may mean that vadose zone transport there occurs by unsaturated matrix flow.

Introduction

This report summarizes the physical and unsaturated hydraulic properties of the Bandelier Tuff, determined mainly from laboratory measurements made on core samples collected from boreholes at Los Alamos National Laboratory. A knowledge of these properties is essential for understanding the hydrologic behavior of the tuff, and is a fundamental requirement for interpreting water and contaminant movement beneath the Laboratory. The results presented here are an extension of work by Loeven and Springer (1993) and a compilation of four earlier reports by the authors (Rogers, 1994a, 1994b, 1995; Rogers and Gallaher, 1995).

We determined new moisture retention curve fits from retention data collected under contract by Daniel B. Stephens & Associates, Inc., Albuquerque, New Mexico, and for the crushed tuff data of Abeele (1979, 1984). We have determined van Genuchten-type fits (van Genuchten, 1980) for most of the available retention data using the program RETC (van Genuchten et al., 1991).

This report contains a summary of the available laboratory hydraulic data, the new retention curve fits, and vertical profiles of hydraulic properties (e.g., moisture content, porosity, hydraulic head, and matric suction). The data are divided according to member of the Bandelier Tuff, with the Tshirege Member further subdivided according to the correlation of Baltz et al. (1963). The canyon-bottom alluvium and weathered Tshirege Unit 1a are treated as separate lithologic units. The weathered Tshirege Unit 1a is essentially canyon-bottom alluvium.

Tshirege Unit 1a and the Otowi Member are represented by a large number of laboratory core analyses. The Tsankawi/Cerro Toledo sequence, vapor-phase notch (Tshirege Unit 1a/1b contact), the surge beds beneath Tshirege Unit 2b at Mesita del Buey, and the Guaje Pumice Bed are insufficiently characterized; these units are all believed to be significant corridors for water movement, whether by unsaturated flow related to higher saturation, flow of perched water, or water vapor flux. In addition, properties for the underlying and probably even more heterogeneous basalts and Puye formation are lacking, with the exception of a few test results from water supply wells (Purtymun, 1984; Purtymun and Stoker, 1988).

Most of the core data comes from boreholes at TA-54 and in Mortandad Canyon. The Bandelier Tuff is generally more welded towards the volcanic source at the west, so the lack of geographic coverage is a major limitation of this data set. The data also provide limited vertical continuity of coverage at most sites; often only a portion of the lithologic section is represented. For the most part, the hydraulic properties and retention curves within each lithologic unit are somewhat similar, with differences in properties between units. Some units, such as the Tshirege Unit 1a and the Tsankawi/Cerro Toledo, show a wider variability, perhaps in the first case due to large sample size and in the second to a diverse lithology. These patterns in hydraulic properties support the division of the Bandelier Tuff into eight separate hydrogeological units as described by Broxton et al. (1995a).

The core data provide the basis for constructing vertical profiles of in situ matric suction and hydraulic head, as well as profiles of porosity, moisture content, and water saturation. These profiles give an indication of the likely direction of liquid water movement within the unsaturated zone beneath parts of Los Alamos National Laboratory.

The data described here can be used as a basis for comparison of core-scale and field-scale estimates of water flow and solute transport parameters. The saturated permeability measured at large scale may be much greater than that measured for small samples, due to lithologic heterogeneities, as well as to the presence of faults or fractures. The core data and profiles allow estimates of effective vertical unsaturated hydraulic conductivities, and thus estimates of the travel times and velocities of infiltrating water. The core-derived travel times are much greater than values determined from the presence of recent ^{3}H, Cl$^-$, and NO$_3^-$ contamination found in boreholes a few hundred feet beneath two canyons. The tracer-derived values from Los Alamos Canyon are 10 to 100 times faster than the core values, and those for Mortandad Canyon are 1300 to 5000 times faster.

These last observations regarding travel times raise questions about the utility of collecting core samples for laboratory analysis, and the use of such results in modeling. This approach might be valid for dry locations such as mesas. The areas where tracer data and core results do not correspond may be limited to the vadose zone beneath some saturated canyon bottoms. In these latter locations, fast paths such as fracture flow might be a more effective transport mechanism.

Geologic and Hydrologic Setting

Los Alamos National Laboratory is located in Northern New Mexico on the Pajarito Plateau, which extends eastward from the Jemez Mountains. The plateau is capped by rocks of the Bandelier Tuff, an ignimbrite erupted from the Jemez volcanic center (Griggs, 1964). The plateau is semiarid, with ponderosa forest at higher elevations giving way to piñon-juniper as elevation decreases. The plateau is separated into finger mesas by canyons, which contain riparian vegetation and streams that are for the most part ephemeral or interrupted. Rainfall in the Los Alamos area totals about 18 in./yr, and varies greatly with elevation (Griggs, 1964; Bowen, 1990).

The Jemez Mountains volcanic center formed along faults at the western edge of the Rio Grande depression (Griggs, 1964). The oldest rocks discussed here are poorly consolidated sands, clays, and gravels of the Santa Fe Group, which are rift-filling sediments deposited from about 20 to 7 Ma (million years before present) (Goff et al., 1989). The volcanic highland west of the Laboratory is underlain by the Tschicoma Formation, which consists of a series of overlapping dacitic domes erupted from 7 to 3 Ma. Contemporaneous erosion resulted in volcanic sediments being shed eastward from these highlands, forming broad alluvial fan deposits of the Puye Formation (Goff et al., 1989).

The formation of the Bandelier Tuff began at 1.61 Ma (Izett and Obradovich, 1994) with eruption of the Otowi Member. The Guaje Pumice Bed at the base of the Otowi Member is a pumice-fall deposit, which was followed by nonwelded surge bed and pyroclastic flow deposits (Goff et al., 1989; Purtymun, 1995). After deposition of the Otowi Member, the Cerro Toledo Rhyolites were erupted. Beneath the Pajarito Plateau, the Cerro Toledo interval includes both pyroclastic and volcanogenic alluvial deposits (Goff, 1994).

The eruption of the Tshirege Member at 1.22 Ma (Izett and Obradovich, 1994) resulted in formation of the Valles Caldera atop the Jemez Mountains (Goff et al., 1989). The Tsankawi Pumice Bed is an air-fall deposit that lies at the base of the Tshirege Member. This pumice deposit was again followed by surge bed and pyroclastic eruptions (Goff et al., 1989). The Tshirege Member underlying the Pajarito Plateau consists of several distinct flow units, which differ in degree of welding and fracturing. Within individual flow units, welding is greatest to the west, near the volcanic source. Numerous correlation schemes have been derived for the lithologic subunits of the Tshirege Member, as discussed below.

Groundwater beneath the Pajarito Plateau occurs as (1) perched alluvial groundwater in canyon bottoms, (2) intermediate perched groundwater in the Guaje Pumice Bed and in volcanic sediments of the Puye Formation and intercalated basalts underlying the Bandelier Tuff, and (3) the main aquifer beneath the Pajarito Plateau, within the Santa Fe Group and the Puye Formation, at a depth of 1200 ft along the western edge of the plateau, and 600 ft along the eastern edge (Purtymun, 1995).

Sources of Data

Hydrologic property data are available for core samples from 21 boreholes; samples from a pit at TA-21 (Nyhan, 1979); and for crushed tuff mined from an outcrop near the entrance to TA-53. The crushed tuff properties were determined in the laboratory (Abeele, 1979; Stephens et al., 1994a) and from a caisson experiment (Abeele, 1984). Table 1 lists the data source for each sample, along with some comments on the type of moisture retention data that were obtained. The borehole locations are shown in Figures 1 and 2.

Lithologic Assignments

The lithologic units encountered by the boreholes are given in Table 2, along with the generalized hydrologic setting for each borehole. The lithologic data were obtained from logs of R. H. Gilkeson (personal communication, 1994), Stoker et al. (1991), and Purtymun (1995).

4

The various lithologic correlation schemes used for the Tshirege Member of the Bandelier Tuff are shown in Figure 3. The correlation used for the Tshirege Member in this report is that of Baltz et al. (1963) and Purtymun and Kennedy (Figure 2 in 1971), because most of the lithologic assignments for the boreholes were done by W. D. Purtymun according to this scheme. Purtymun (p. 193 in 1995) further subdivided Unit 3 at TA-16 into four subunits. There is some uncertainty about the correlation of Unit 3 from this area to other parts of the Laboratory (part of Purtymun's Unit 3 could be Unit 4; D. E. Broxton, personal communication, 1995). For boreholes 54-1001, -1002, -1003, and -1006, the Tshirege unit assignment according to the correlation of Vaniman and Wohletz (1990) and Vaniman (1991) is also given. For these boreholes, the Tshirege unit assignments for the scheme of Baltz et al. (1963) were inferred from Purtymun and Kennedy (Figure 2 in 1971).

Except for boreholes 54-1001, -1002, -1003, and -1006, no distinction is made between the Tsankawi Pumice Bed and the Cerro Toledo interval (the use of either term implies both units). In most cases the two units were not distinguished when logged. The Tsankawi Pumice Bed is rarely more than 2 ft thick in most places, so there must be a considerable thickness of Cerro Toledo deposits in these boreholes (D. E. Broxton, personal communication, 1995).

Hydraulic Data Presentation

Table 3 gives the types of laboratory data available for each of the samples. Appendix A summarizes statistics of the hydrologic data for each member of the Bandelier Tuff, and for each unit of the Tshirege Member. Appendix B lists the individual core data by lithologic unit, and Appendix C lists the data for each well. The retention curves for all of the core samples are plotted in Appendix D. Appendix E shows histograms and probability plots of bulk density, porosity, and saturated hydraulic conductivity for each member of the Bandelier Tuff, and Tshirege Units 1a and 3. Histograms and probability plots are not presented for other lithologic units due to the small number of hydraulic data. Appendix F gives unsaturated hydraulic properties computed for each core, arranged by well.

All of the moisture retention data for each core sample are included on the accompanying 3.5-in. computer disk. The disk is in Macintosh format, and contains tab-delimited text files. An additional data column identifies moisture retention values obtained with the thermocouple psychrometer, for cores which have them. Table 4 provides a cross-reference between the well or sample name and the disk file name. Two additional files on the disk include all of the hydraulic data, which forms the basis of the accompanying tables. One of the files is sorted by lithologic unit, the other by well or sample name.

The Moisture Retention Curve

The moisture retention curve relates the volumetric soil moisture content of unsaturated soils and rocks to the energy state of the soil water, and has three parts (Figure 4). The air entry region of the moisture retention curve is the portion at saturation, where a change in matric suction does not change the moisture content. The air entry suction is the value required to drain the first pore (Jury et al., 1991). In the capillary region the moisture content decreases with increasing suction, as increasingly smaller pores are drained. Fine-grained soils have a broad range of pore sizes. Coarser soils generally have larger pores and a narrower pore size distribution (sandy soil curve in Figure 4), and thus have a sharper transition through the capillary region than for finer soils (clay soil curve in Figure 4). Water in the adsorption region is held onto the soil matrix by surface forces. The higher particle surface area of finer-grained soils gives them a larger water content at high matric suctions (Jury et al., 1991).

The measurement of moisture characteristic curves, especially at low moisture contents, requires multiple laboratory techniques. Pressure plate measurements of matric suction are usually not valid outside a range of 300 to 1500 cm, but special porous ceramic plates may extend this to 15 bars (Jury et al., 1991). (Note that 1 bar = 1020 cm H_2O.) Thermocouple psychrometer measurements of soil water potential can be made up to 70 bars, although this measurement includes both matric suction and osmotic potential (Jury et al., 1991).

Van Genuchten Retention Curve Formula

The unsaturated hydraulic curve parameters that we derived for the samples are summarized in the accompanying tables (Appendices A, B, and C) and figures. The parameters follow from van Genuchten's formulation of the moisture characteristic curve (van Genuchten, 1980):

$$\tilde{\theta} = \frac{\theta - \theta_r}{\theta_s - \theta_r} = \frac{1}{\left[1 + |\alpha\psi|^N\right]^M} \quad , \tag{1}$$

where $\tilde{\theta}$ = effective saturation (volume percent),

θ = volumetric moisture content (volume percent),

θ_r = residual moisture content (volume percent),

θ_s = (also noted as θ_{sat}) saturated moisture content or effective porosity (volume percent),

ψ = matric suction (centimeters, positive if unsaturated),

α, N= van Genuchten fitting parameters (per centimeter and dimensionless, respectively), and

M = 1-1/N (dimensionless).

Van Genuchten et al. (p. 5 in 1991) state that "θ_r and θ_s in this study are viewed as being essentially empirical constants in soil water retention functions of the type given by [Equation (1)]." They note that, due to trapped or dissolved air, the saturated moisture content may be 5% to 10% less than the porosity. Alternatively, the saturated moisture content may be related to the effective porosity, which Bear (1972) defines as the ratio of the volume of interconnected pores to the total rock or soil volume.

There is some debate among soil physicists concerning the physical meaning of the residual saturation (θ_r), for which there are the following three interpretations:

1. θ_r is equivalent to a few monolayers of water bound to the soil grains by adsorption, or water that is held by surface forces rather than acted on by gravity, and corresponds to the moisture content below which the fluid phase becomes discontinuous and the fluid-phase permeability is zero (Luckner et al., 1989; van Genuchten et al., 1991);

2. θ_r is a fitting parameter as defined by van Genuchten (1980) [Equation (1)]. Van Genuchten et al. (1991, p. 5) state that "Formally, θ_r may be defined as the water content at which both $d\theta/d\psi$ and K go to zero when ψ becomes large. The residual water content is an extrapolated parameter and hence may not necessarily represent the smallest possible water content in a soil. This is especially true for arid regions where vapor phase transport may dry out soils to water contents well below θ_r."; or

3. θ_r is the lowest moisture content obtainable under natural conditions.

According to summary tables presented by van Genuchten et al. (Tables 3 and 4 in 1991), coarse soils (sand and loamy sand) have mean θ_r values around 2% to 6%. Clays and silty clays have average θ_r values of about 6% to 9%.

The van Genuchten parameters α and N control the shape of the moisture retention curve. The parameter α multiplies the matric suction in Equation (1), and has the effect of moving the retention curve up and down along the suction axis. A larger α gives the same moisture content at a smaller value of suction [Equation (1)], thus lowering the retention curve towards smaller suction values. Coarse soils have larger mean α values, around 0.11 to 0.14 cm^{-1} for sand and loamy sand. Clays and silty clays have average α values of 0.01 to 0.03 cm^{-1} (Tables 3 and 4 in van Genuchten et al., 1991).

The parameter N controls the slope of the retention curve: large N values lead to a more sand-like retention curve (Figure 4), for a very large change in moisture content with a small change in suction above the air entry suction (van Genuchten et al., 1991). Smaller values of N produce a curve with a gradual transition in moisture content as suction increases above the air entry value, giving a clay- or silt-like retention curve. Coarse soils have larger mean N values, around 1.5 to 2.7 for sand and loamy sand. Clays and silty clays have average N values of about 1.1 (Tables 3 and 4 in van Genuchten et al., 1991).

Unsaturated Hydraulic Conductivity

The values of unsaturated hydraulic conductivity are extremely low, and therefore laboratory measurement generally requires long time periods. This is especially true for conventional steady state methods, where up to a year may be required to achieve steady state flow for a single measurement (Conca and Wright, 1992). The lower laboratory limit for unsaturated hydraulic conductivity measurement is about 10^{-9} cm/sec (Conca and Wright, 1992).

The unsaturated hydraulic conductivity graphs discussed below extend to 10^{-22} cm/sec, in order to show the grouping of the curves. Hydraulic conductivity values in this region have uncertain physical meaning, however. Consider the average linear velocity (v) of fluid flow through a porous medium, given by:

$$v = \frac{q}{\theta} \qquad , \qquad (2)$$

where   q   =   specific discharge or Darcy flux (centimeters per second) and
        θ =   volumetric moisture content (dimensionless, $0 \leq \theta \leq 1$).

For saturated conditions, θ in Equation (2) is the porosity.

For a porosity of 50%, under saturated conditions, and a unit hydraulic gradient (steady state gravity flow, where specific discharge equals hydraulic conductivity; Jury et al., 1991), a hydraulic conductivity of 10^{-10} cm/sec implies a fluid travel distance of 6.3×10^{-3} cm in a year. This distance would be 10 times larger for a moisture content of 5%, but it is still quite small. The empirical formulas for hydraulic conductivity and the retention curve were not intended for use at such low moisture content values, where "it's all speculation, because the physics is out the door" (M. Th. van Genuchten, personal communication, 1994). At low moisture contents, vapor flow may be the dominant mode of water transport (Luckner et al., 1989).

Empirical Determination of Hydraulic Conductivity

One empirical expression for the unsaturated hydraulic conductivity (K) is:

$$K = K_s \widetilde{\theta}^{\frac{1}{2}} \left[1 - \left(1 - \widetilde{\theta}^{\frac{1}{M}} \right)^M \right]^2 \quad , \tag{3}$$

where K_s =   (also noted as K_{sat}) saturated hydraulic conductivity (centimeters per
                   second) and

         M =   1-1/N (dimensionless).

This equation uses Mualem's (1976a) empirical formula for unsaturated hydraulic conductivity
as implemented by van Genuchten (1980).

The retention curve parameters tabulated here use the restriction M = 1-1/N, which gives
a convenient expression [Equation (3)] for the unsaturated hydraulic conductivity (van
Genuchten, 1980). For several cores from boreholes 54-1001, -1002, -1003, and -1006 (Tshirege
units 1b, 2a, and 2b), the van Genuchten fit at high saturation values was unsatisfactory. Another
curve fit using independent N and M values was somewhat better for moisture contents near
saturation (see individual retention curves in Appendix D). Van Genuchten et al. (1991) indicate
that this parameterization always gives the best fit to the retention data but does not provide a
convenient form for the unsaturated hydraulic conductivity function. While adding more
parameters improves the curve fit, it may not increase understanding of the underlying process,
or yield a better extrapolation beyond the observed data. The use of more parameters may
provide a better functional form for uses such as modeling, however.

Statistical Distribution of Hydraulic Conductivity

Tables A1 through A20 contain the range of values for both K_{sat} and log K_{sat} because saturated
hydraulic conductivity is lognormally distributed for large data sets (de Marsily, 1986; Jury et al.,
1991; Gelhar, 1993). Note that the mean and standard deviations for normal and lognormal
distributions are not simple log transforms of each other (p. 280 in Jury et al., 1991). Variables
such as hydraulic conductivity are positive definite (values less than zero are not physically
possible) and have a large coefficient of variation (standard deviation divided by mean). These
variables cannot be normally distributed, because some values of the distribution must then be
negative (Jury et al., 1991). A lognormal distribution has no negative values; thus porosity and
bulk density may also have lognormal distributions.

Several different statistical means are useful in estimating the effective (or average) saturated hydraulic conductivity that applies to flow through heterogeneous media. For two-dimensional flow through a media with lognormally distributed permeability, the effective permeability is equal to the geometric mean K_m, where $\ln K_m = E(\ln K)$ (p. 82 in de Marsily, 1986). $E(x)$ is the expected value of the random variable x. The harmonic mean permeability K_m, where $1/K_m = E(1/K)$, is also given in the tables for each lithologic unit. The harmonic mean conductivity represents the effective hydraulic conductivity for flow perpendicular to strata of differing permeability, and the arithmetic mean is the effective hydraulic conductivity for flow parallel to such strata (de Marsily, 1986). The harmonic mean is more strongly affected by small values than the arithmetic mean. For parallel flow through media with spatially varying hydraulic conductivity, the effective hydraulic conductivity lies between the harmonic and arithmetic mean hydraulic conductivity (de Marsily, 1986).

Data Quality Considerations

Limitations of Geographic and Lithologic Coverage

Individual units within the Bandelier Tuff show a great variation in welding from east to west, which certainly exerts a great influence on bulk density, hydraulic conductivity, and other hydraulic properties. It is important to remind the reader that the conclusions presented here, regarding hydraulic properties both within and between lithologic units, reflect the limitations of geographic data coverage (Figure 1). For example, only one complete set of data are available for Tshirege Unit 3 (and possibly Unit 4), and this is from the western part of the Laboratory, where the units are likely to be more welded. At any one location, there has not been a systematic collection of hydraulic properties throughout the Bandelier Tuff, except at TA-54 and in Mortandad Canyon. In the latter case, drilling began on the canyon floor, so the upper part of the section is not represented. Some lithologic units that may have particular significance for hydrologic transport are the surge beds at the base of Tshirege Unit 2b, the vapor-phase notch between Tshirege Units 1a and 1b, the Cerro Toledo sequence, and the Tsankawi and Guaje Pumice Beds. Core samples are difficult to obtain from these units because the rock layers may be either thin or poorly consolidated.

Moisture Retention Measurements at Low Saturation

In most cases, Daniel B. Stephens & Associates, Inc., provided van Genuchten fits for their reported retention data. However, a reevaluation of these parameters is called for: they make the following observations regarding their pressure plate measurements of matric suction vs. water content in samples having relatively large pores (p. 2 in Stephens et al., 1992a):

"These samples often do not come to equilibrium at high tensions. Therefore, the data show an unrealistically large change in water content between the 15-bar pressure plate measurement and the 18-bar psychrometer measurement. The α and N values were determined on the entire data set for every sample to determine consistency of analysis. For greatest physical accuracy, the best choice would be use of pressure plate data to 1 bar plus use of the psychrometer data."

Figure 5(a) shows an example of one of the moisture retention data sets just described. Some of the pressure plate data above 0.5 bar (510 cm) apparently have not come to equilibrium when compared to the psychrometer value at 30,000 cm.

Several of the moisture retention data sets lack psychrometer measurements (Table 1). One consequence of the lack of psychrometer values for some moisture retention data sets is that only 4 of 10 data sets for borehole P-16, TA-16 (Stephens et al., 1988) are considered reliable in the dry range [e.g., Figure 5(b)]. In light of the problems with equilibration of the pressure plate data (described above), the dry portion of the retention curve in Figure 5(b) is probably not accurately defined by the moisture retention data.

For the individual retention curves shown in Appendix D, the moisture retention data are indicated by circles. Those pressure plate retention points judged not to have equilibrated are shown by solid black circles. Equilibrated pressure plate and psychrometer points are shown by open circles. The saturated moisture content (effective porosity) is plotted at an artificial suction value of 0.1 cm, so that it will appear on a log scale. The van Genuchten curve fits determined by the authors (solid line) and by Daniel B. Stephens & Associates, Inc., (dashed line) are displayed. In some cases additional curve fits are plotted, for example with variable van Genuchten (1980) parameters M and N, rather than the usual restriction of M = 1-1/N. The in situ moisture content for the sample is indicated on each plot by a solid vertical line.

The Residual Moisture Content

For the cases where moisture retention data for the Bandelier Tuff included psychrometer values, the residual moisture content (θ_r) determined with RETC was generally between 0% and 5%. We take this to be a reasonable range for θ_r in the Bandelier Tuff, and have omitted from the summary results presented here most curves with θ_r greater than 10%. Most of these lacked psychrometer values and are poorly defined in the dry portion of the retention curve, as discussed above. The measurements for boreholes LLC-85-14, -15, and -22 (Stephens et al., 1991c) are an exception to this. These retention curves lack psychrometer measurements, but the pressure plate measurements in the dry region appear to have equilibrated.

The determination that θ_r for the Bandelier Tuff lies between 0% and 5% is consistent with moisture retention data for sand presented by Mualem (1976b), and for coarse grained soils in the summary tables of van Genuchten et al. (1991). We consider sand to be appropriate for comparison to the Bandelier Tuff because the pore sizes of sand and tuff may be equivalent, and the shape of most of the tuff retention curves resembles those of soils with a narrow pore size distribution, i.e. sand (Figure 4) rather than clay or silt (Jury et al., 1991).

Some soil physicists question whether such low saturation values (between 0% and 5%) can be obtained under natural conditions. M. D. Ankeny (Daniel B. Stephens & Associates, Inc., personal communication, 1994) noted that laboratory measurements on tuff samples at the lowest moisture contents (~0% to 5%) were obtained after the samples were dried on the laboratory counter (in Albuquerque) at room temperature and humidity. The low values we obtained for θ_r are also consistent with field moisture contents observed in the Bandelier Tuff at TA-54 (Kearl et al., 1986a and b; R. H. Gilkeson, personal communication, 1994; B. M. Gallaher, personal communication, 1994). The question remains as to whether vapor-phase rather than liquid-phase transport has dried these rocks to a water content below θ_r as defined above by van Genuchten et al. (1991).

Comments on the Bendix Data

We consider the moisture retention data reported by Bendix Field Engineering Corporation (Kearl et al., 1986a and b) to be incomplete (an example is given in Figure 6). These data cover only a small portion of the saturation range, typically 50% to 100%. The data were obtained using a centrifuge, and the samples disaggregated at the highest speeds, preventing retention measurements at lower saturation values (p. 39 in Kearl et al., 1986a). Kearl et al. (1986a and b) concluded that their lowest moisture-content-data point represented the residual saturation, θ_r. In light of the limitations of their measurement techniques and the evidence provided by subsequent work (presented here and by Loeven and Springer, 1993), this conclusion appears to be unwarranted. The conclusions reached by IT Corp. (p. 4 in 1987), regarding the nature of liquid flow beneath Material Disposal Areas (MDA) G and L, TA-54, are based on the Bendix data and may also be unwarranted.

Some of the Bendix porosities (Kearl et al., 1986a and b) are extraordinarily high (up to 75%). The porosities are of uncertain value, due in part to the methods of sample collection. The Bendix core samples were subsampled from split spoon cores, and samples were prone to disaggregation during subsampling (p. 35 in Kearl et al., 1986a; A. K. Stoker, personal communication, 1994). The samples were repacked for laboratory analysis. It is difficult to

accept that reliable porosity measurements as high as 75% were made on repacked, disaggregated samples. As discussed below, the Bendix porosities are significantly higher than those obtained by Daniel B. Stephens & Associates, Inc. The latter values are supported by reasonable agreement with separate calculations of porosity based on bulk density measurements and an assumed particle density. No bulk density values are provided in the Bendix reports.

We consider the data of Daniel B. Stephens & Associates, Inc., to be the most reliable, due to the uniformity of their analysis procedures and the self consistency and completeness of their data set.

Discussion of Hydraulic Data

Tables A1 through A20 present summaries of the statistics for bulk density (ρ_b), saturated moisture content (or effective porosity, θ_{sat}), field saturation (S), saturated hydraulic conductivity (K_{sat}), log K_{sat}, and the van Genuchten parameters residual moisture content (θ_r), α, and N for each member or subunit of the Bandelier Tuff and the canyon-bottom alluvium. (The two crushed data sets are not included here.) The tables are divided in two ways. The data are presented for each member of the Bandelier Tuff, with the Tshirege Member divided into subunits. For each member or subunit having data from more than one source, tables present summaries both of all data and only of data obtained by Daniel B. Stephens & Associates, Inc. As can be seen from Tables A4 and A16, the additional data consist of 24 hydraulic conductivity values for Tshirege Unit 3 (Nyhan, 1979) and 20 values for θ_{sat} and K_{sat} for the Tshirege Units 1a, 1b, 2a, and 2b (Kearl et al., 1986a).

Figures 7 through 13 summarize the ranges of ρ_b, θ_{sat}, log K_{sat}, and the van Genuchten parameters α, N, and θ_r for each member or subunit of the Bandelier Tuff and the canyon-bottom alluvium. The results are discussed below.

Appendix E shows histograms and probability plots for bulk density, porosity, and log K_{sat} for the Bandelier Tuff as a whole, for each member of the Bandelier Tuff, and for Tshirege Units 1a and 3. If the data are normally distributed, they will plot as a straight line on a probability plot. For lognormally distributed data, the log of the data will plot as a straight line. Discontinuities in the plot may suggest the presence of more than one population within the data set, or that the data fit another type of distribution (Isaaks and Srivastava, 1989).

The comparison of hydraulic properties both within and between lithologic units is limited by the sparse geographic coverage of the boreholes.

Hydraulic Property Functions

Figures 14 through 22 are composites of all moisture characteristic and unsaturated hydraulic conductivity curves for each member of the Bandelier Tuff, with the Tshirege Member divided into units.

Except for Tshirege Unit 3 (Figure 15), the retention curves for each unit of the Tshirege Member (Figures 15 to 20) show a fairly good grouping, as do the unsaturated hydraulic conductivity functions. Recall that there is some uncertainty about the correlation of Unit 3 from this area to other parts of the Laboratory (D. E. Broxton, personal communication, 1995), and that the TA-16 moisture retention data sets lack psychrometer values, casting doubt on their reliability. In addition, the tuff at TA-16 is likely to have greater welding, as it is closer to the source.

The variability of the curves between units (which may be ascertained by comparing Figures 15 through 20) is in keeping with the alternating welded and nonwelded nature of the Tshirege Member. The variation in physical properties discerned from outcrops, along with other observations, led Broxton et al. (1995a) to divide the Tshirege Member beneath TA-21 into five separate hydrogeological units. These hydrogeological units correspond to Tshirege Units 1a, 1b, 2a, 2b, and 3.

The curves for the Tsankawi/Cerro Toledo Member (Figure 21) show the greatest scatter, partly due to a large variation in porosity. This is probably due to the diverse lithology of this unit, which is composed of pumice, ash, and fluvial deposits (Goff, 1995; Broxton et al., 1995a). Broxton et al. (1995a) divided the Tsankawi and Cerro Toledo interval beneath TA-21 into two separate hydrogeological units. Finally, curves for the Otowi Member (Figure 22) show the tightest grouping of the three members of the Bandelier Tuff. This grouping is consistent with the uniform nonwelded character observed for the Otowi Member by Broxton et al. (1995a), prompting their designation of this as one hydrogeological unit.

Bulk Density

The bulk density data (Figure 7) come from reports by Daniel B. Stephens & Associates, Inc. Tshirege Unit 3 shows the highest bulk density values. The Unit 3 data come from beneath MDA P, TA-16. The large difference in bulk density between Unit 3 and other units may reflect the fact that TA-16 is in the western part of the Laboratory, where flows are more welded. Purtymun (1995) describes Units 3c and 3d of the Tshirege at MDA P as being moderately welded (these may be Unit 4, D. E. Broxton, personal communication, 1995). On the other hand, no other

Tshirege Units are represented by the data collected at MDA P, and at any one location, lithologic observations of welding strongly indicate that the bulk density for Unit 2 will be significantly greater than Unit 3 (D. E. Broxton, personal communication, 1995).

The median bulk density decreases with depth through the Tshirege. Note that there is a fairly steep gradient of median bulk density across units 3, 2b, 2a, and 1b.

The bulk density probability plots for the Tshirege Unit 1a, the Tshirege Member, and the Bandelier Tuff (Figures E2, E3, and E6) show a discontinuity at about the 90th percentile, while the histograms suggest that the data are approximately normally distributed. If the log of bulk density is plotted for these units (not shown), the curves are more linear, but still show a slight discontinuity. The bulk density histogram for the Tsankawi is suggestive of a bimodal distribution, and the probability plot for the Tsankawi (Figure E4) shows a gap at about the 30th percentile. The probability plot for the Otowi (Figure E5) is strongly linear except for the highest value.

Porosity

There is very little variation in mean porosity values throughout the Bandelier Tuff (Figure 8). The mean value for the Tshirege is 49%, and 47% for the Tsankawi and Otowi. Tshirege Units 3, 1a, and the Tsankawi show the highest variation in porosity. These statements are based on the data obtained by Daniel B. Stephens & Associates, Inc. Figure 8 shows the high Bendix porosity values for comparison (Kearl et al., 1986a). Note the large variation in maximum porosities between the Bendix and Stephens et al. data for Tshirege Units 1b, 2a, and 2b (Tables A5 through A10, Figure 8).

The porosity probability plots for the Tshirege Unit 1a, the Tshirege Member, and the Bandelier Tuff are somewhat concave upwards (Figures E2, E3, and E6), while the histograms indicate that porosity is approximately normally or lognormally distributed. If the log of porosity is plotted (not shown), the probability plots are nearly linear. The histogram for the Tsankawi (Figure E4) appears bimodal, and the porosity probability plot shows a gap at about the 70th percentile. This corresponds to the gap in the bulk density plot at the 30th percentile: the high porosity samples have low bulk densities. The porosity probability plot for the Otowi (Figure E5) shows a strong discontinuity at the 50th percentile, which is not seen in the bulk density plot.

Saturated Hydraulic Conductivity

The values of log K_{sat} are shown in Figures 9 and 10 for the Stephens et al. data and for the complete data set. Figure 10 repeats Figure 9, except that the minimum, maximum, and median for the entire data set are indicated. Note (Figure 9) that there is a steep decrease in log K_{sat} across units 2b, 2a, and 1b. Tshirege Unit 2b and the Tsankawi Member appear to have the highest hydraulic conductivity values; Tshirege Unit 1b the lowest.

The hydraulic conductivity values of Nyhan (1979) for Tshirege Unit 3 at TA-21 (Table A3) are significantly lower than those found by Daniel B. Stephens & Associates, Inc., (Stephens et al., 1988) at TA-16 (Table A4). This could be due to differences in laboratory methods, or could indicate a variation of Unit 3 between the two locations.

The log K_{sat} probability plots for the Tshirege Unit 3, the Tshirege Member, and the Bandelier Tuff (Figures E1, E3, and E6) appear roughly linear, while the histograms indicate that K_{sat} is approximately normally or lognormally distributed. These distributions all have discontinuities, however, particularly at the 90th percentile. The probability plots for the Tshirege Unit 1a and the Otowi (Figures E2 and E5) are linear at the center, but not at the high and low values. The histogram for the Tsankawi (Figure E4) appears to be nearly flat.

Van Genuchten Parameters

The van Genuchten parameters α, N, and θ_r for each member of the Bandelier Tuff and each unit of the Tshirege member are plotted in Figures 11 through 13. The values of α (Figure 11) are plotted on a log scale due to their variation over several orders of magnitude; α may be lognormally distributed. The alluvium, Tshirege Unit 1a, and the Tsankawi have the highest mean α values; these units generally have the lowest suction values at a given moisture content. Nonetheless, these mean α values fall in the range described by van Genuchten et al. (1991) for clays and silty clays.

Tshirege Units 2a and 2b have the highest median N values (Figure 12). Units 2a and 1b show a large difference in this parameter, as do Units 3 and 2b. Most of the N values fall in the range given by van Genuchten et al. (1991) for sand and loamy sand.

For the residual moisture content (θ_r), Figure 13 shows that Tshirege Units 3, 2b, and weathered Unit 1a have higher mean values. The mean and median residual saturation values for the entire Tshirege are 2.1% and 0% (Table 18). These values fall at the low end or below the range given by van Genuchten et al. (1991) for sand and loamy sand. Recall that we eliminated many of the

retention fits with θ_r above 10%; most of these retention data sets lacked psychrometer measurements at low moisture contents.

Crushed Tuff Data

The hydrologic properties of crushed tuff are of interest because it is used, for example, to fill and line waste disposal pits at MDA G, TA-54. Two analyses of crushed tuff moisture retention data are presented here. All of the crushed tuff came from the quarry at the entrance to TA-53, which is in Tshirege Unit 3 (J. W. Nyhan, personal communication, 1995). The hydraulic properties for each crushed tuff data set are included in Table B-1; the individual moisture retention functions are shown in Figure D-19. Figure 23 shows the combined moisture retention and unsaturated hydraulic conductivity functions.

According to Abeele (p. 4 in 1984), the crushed tuff "can best be described as consisting mostly of silicic glass and having a grain size distribution close to that of silty sand." For the caisson experiment, the fill material was passed through a 12.5 mm screen.

The first crushed tuff sample in this analysis is a special case (Figure D-19). It is a composite of laboratory pressure plate measurements (Abeele, 1979) and tensiometer and neutron moisture probe measurements from a large-scale instantaneous moisture profile caisson experiment (Abeele, 1984). The moisture content ranges for the two data sets are complementary; neither moisture retention data set alone produces a reliable solution from RETC. Note that Abeele (1979, 1984) gives two values of K_{sat} for the crushed tuff (Table B-1). Both conductivity functions are shown in Figure 23.

The second crushed tuff sample is a conventional analysis by Daniel B. Stephens & Associates, Inc. (Stephens et al., 1994a).

Van Genuchten et al. (pp. 27–29 in 1991) report two retention and hydraulic conductivity curve fits for Abeele's (1979, 1984) crushed tuff data. Their fits also used the retention data from both the caisson and pressure plate experiments, as well as the hydraulic conductivity data from the caisson experiments. In the first fit, they allow θ_{sat} to be a free parameter, with a result of $\theta_{sat} = 33.20\%$. For the second fit, they use a "measured value" of $\theta_{sat} = 33.08\%$. However, Abeele lists the value of θ_{sat} for the crushed tuff as 40% (p. 3 in Abeele, 1979; p. 3 in Abeele, 1984).

Hydrologic Properties Profiles

Figures 24 through 34 are hydrologic property profiles for boreholes having a large enough number of cores. The top plot shows the saturation, porosity, moisture content, and residual moisture content; the lower plot shows head and in situ suction values (note that the head values are less than zero, and that the negative of the suction is plotted). The in situ suction values are determined from the following rearrangement of Equation (1) using the in situ moisture content:

$$|\psi| = \frac{1}{\alpha}\left[\left(\frac{1}{\tilde{\theta}}\right)^{\frac{1}{M}} - 1\right]^{\frac{1}{N}} \qquad . \tag{4}$$

The head values are determined from the formula:

$$H = z - \psi \qquad , \tag{5}$$

where   H = hydraulic head (centimeters),
         z = elevation head, or depth (centimeters, positive upwards, datum is ground
                 surface), and
         ψ = matric suction (centimeters, positive if unsaturated).

The in situ effective saturation [Equation (1)], suction, head, and in situ hydraulic conductivity [Equation (3)] are tabulated in the two hydraulic properties data files on the accompanying disk, and in Appendix F. The individual head and suction values must be regarded as having an unknown degree of uncertainty related to experimental errors and other uncertainties in the retention curves, but consistency within an individual profile, and comparison with psychrometer data (see below) gives confidence in the general patterns described here.

Cañada del Buey

The alluvium in Cañada del Buey is generally dry, except for discharge water from water supply well PM-4 (Purtymun, 1995). For borehole CDBM-1 (Figure 24), saturation increases from the surface down to the Tsankawi/Cerro Toledo sequence, and falls off somewhat below this level. Head values also increase with depth from the surface to about this horizon, and then fall off with increasing depth. The head gradient profile for CDBM-1 suggests that the direction of liquid water flow is both upwards and downwards away from the higher-saturation zone at the Cerro Toledo. Note that the suction profile for borehole CDBM-1 is fairly uniform below about 50 ft;

the head profile is dominated by the elevation term. The profiles for CDBM-2 (Figure 25) contain too few points for analysis.

TA-53, Mesita de los Alamos

Several boreholes have been drilled to monitor moisture conditions beneath the surface impoundments at the Los Alamos Meson Physics Facility (TA-53) on Mesita de los Alamos (Purtymun, 1995). Data for borehole AB-6 (Figure 26) indicate a saturation of about 90% near the base of Tshirege Unit 2b. The head values decrease uniformly with depth, suggesting downward liquid water flow below 40 ft.

Potrillo Canyon

Potrillo Canyon contains mostly dry alluvium, and has discontinuous stream flow (Becker, 1991; Purtymun, 1995). Borehole PC-4 (referred to as POTO-4 by Purtymun, 1995) was drilled at the upstream end of an area where stream flow was observed to infiltrate into the alluvium, with little flow beyond (Becker, 1991). Borehole PC-4 has a zone of nearly 90% saturation at the base of the Weathered Unit 1a (Figure 27). Saturation falls off below this depth, with only a slight increase in the Tsankawi Pumice, and remains constant at about 40% in the Otowi. In spite of the high saturation zone at the base of the Weathered Unit 1a, the hydraulic head decreases nearly monotonically with depth, as the elevation term dominates over suction. This indicates downward moisture movement beneath Potrillo Canyon.

Mortandad Canyon

Mortandad Canyon has received treated liquid radioactive waste discharges from the TA-50 treatment plant since 1963. At about the location of boreholes MCM-5.1 and MCM-5.9A, surface flow is intermittent. Storm water discharge may extend beyond this location, but has not left the Laboratory property (i.e. reached borehole SIMO-1) since observations began in 1960 (Stoker et al., 1991). Perched water in the alluvium seldom extends much beyond a point halfway between MCM-5.9A and SIMO-1 (Baltz et al., 1963; Purtymun, 1975).

The profiles for Mortandad Canyon borehole SIMO-1 (Figure 28) indicate no moisture buildup at the Tsankawi/Cerro Toledo sequence, but show an increase within the Otowi Member at the base of the borehole. A similar increase within the Otowi was noted by Stoker et al. (1991) for boreholes MCM-5.9A (Figure 30) and borehole MCM-8.2. The dry portions of the three retention data sets for borehole SIMO-1 are unreliable, so no head or suction values are shown.

Two zones of high saturation occur in Mortandad Canyon borehole MCM-5.1 (Figure 29): at the base of the canyon-bottom alluvium, and at the top of the Tsankawi/Cerro Toledo sequence. For this borehole and for MCM-5.9A, Daniel B. Stephens & Associates, Inc., (Stephens et al., 1991a) provided Richards thermocouple psychrometer potential measurements at the in situ moisture content (Figure 29). While these values are unreliable at moisture contents near saturation (Stephens et al., 1991a), the head values calculated from them agree well with the head calculated from the retention curves, except for a few points. The head values that depart most from the psychrometer head curve (i.e. at 54 and 82.5 ft) come from cores with low in situ moisture contents and retention curves that are poorly defined in the dry portion (Figures D10 and D11). Below a depth of 10 ft, the hydraulic head decreases uniformly with depth, indicating downward flow of water beneath the canyon floor.

The data for borehole MCM-5.9A again show a buildup of saturation at the top of the Tsankawi/Cerro Toledo sequence (Figure 30). Moisture content and saturation increase with depth in the Otowi Member, as noted by Stoker et al. (1991). Although a slight reversal in head occurs within the Tsankawi, suggesting the possibility of upward flow from this unit, the general trend for the borehole again indicates downward flow of water beneath the canyon floor. The psychrometer head value at 105 ft may be unreliable because of the high saturation at this depth (89%), causing it to deviate from the retention curve-derived head value.

MDA P, TA-16

MDA P is a landfill located on the canyon wall above Cañon de Valle at TA-16. Borehole P-16 was drilled on the mesa south of the landfill, away from the canyon rim (Purtymun, 1995). No saturation was found in any of the 30 test holes drilled near the landfill, 9 of which were located above the stream channel at the base of the canyon rim. The stream in this section of the canyon has a small flow due to discharge from an industrial outfall located upstream of MDA P (Hickmott and McCann, 1995).

Borehole P-16 (Figure 31) includes the only Tshirege Unit 3 (possibly Unit 4) retention data measurements. Because of the lack of psychrometer values, the retention curves are not well defined in the dry range, so the head and suction values at depths with low moisture content are unreliable (i.e., between 12 and 26 ft). There is a high saturation zone at the top of Unit 3d. Ignoring the low moisture content zone between 12 and 26 ft, the data appear to show a downward decrease of head, hence downward flow of water.

20

MDA L, TA-54, Mesita del Buey

TA-54 at Mesita del Buey includes the low-level radioactive waste disposal facility (MDA G) and a chemical waste storage facility (MDA L). These disposal areas occupy a mesa between Cañada del Buey and Pajarito Canyon, which contain interrupted streams (Purtymun and Kennedy, 1971).

Wells 54-1001, -1002, and -1006 (Figures 32, 33, and 34) are all from MDA L, TA-54, on Mesita del Buey (D. J. Krier, R. H. Gilkeson, and V. L. Trujillo, personal communication, 1994). The boreholes were drilled at angles, so both down hole depth and true vertical depth are indicated in the figures. The moisture profiles for all boreholes show higher moisture content at the vapor-phase notch and the Tsankawi/Cerro Toledo. The moisture content just above the vapor-phase notch level shows an increase with depth. The increase of moisture content is not as strong just above the Tsankawi/Cerro Toledo, and within this unit the moisture content is quite variable. This could be the result of varying hydrologic characteristics due to the diverse lithology of this unit, which is composed of pumice, ash, and fluvial deposits (Rogers and Gallaher, 1995; Broxton et al., 1995a).

For borehole 54-1001 (Figure 32), the suction and head values determined from the van Genuchten curve fit for the sample at depth 68 ft appear to be too low (~12,000 and 13,500 cm respectively) in comparison to a value we estimated from the psychrometer data presented by Daniel B. Stephens & Associates, Inc., (Stephens et al., 1994b) (see Figure D16). Both values are indicated on the head plot.

The profiles for boreholes 54-1001, -1002, and -1006 show low moisture contents, high suctions, and low head values in the upper part of Unit 2a. This horizon is associated with extremely low field moisture contents of about 1%, which are seen throughout both MDA G and MDA L in moisture profiles obtained in 1986 by Bendix Field Engineering Corporation (Kearl et al., 1986a and b). The low moisture zone may be related to pyroclastic surge deposits at the base of Unit 2b (Gallaher et al., 1994). The surge beds are known from earlier studies to be related to preferential migration of vapor-phase ^{3}H from disposal shafts (Purtymun, 1973).

The hydraulic head increases below the depth of the surge beds (the top of Unit 2a), indicating upward flow of liquid water within the mesa. Gallaher et al. (1994) hypothesized that the surge beds have higher air permeability than surrounding units of the Bandelier Tuff, and the mesa is dried out at this horizon by increased external air circulation through the mesa sides. This dry zone created by water vapor removal would therefore constitute a natural barrier to downward migration of liquid wastes beneath disposal areas at TA-54.

Summary of Vadose Zone Water Movement Beneath the Pajarito Plateau

In summary, most of the canyon-bottom and mesa hydraulic head profiles suggest that downward flow of water occurs beneath the ground surface. The exceptions are apparent upward flow above the Tsankawi/Cerro Toledo sequence in the upper 50 ft beneath Cañada del Buey (CDBM-1), in Mortandad Canyon (MCM-5.9A), and the possibility of upward flow from above the Tsankawi/Cerro Toledo sequence, up to the base of Tshirege Unit 2b, within Mesita del Buey at TA-54 (54-1001, -1002, and -1006). These observations suggest that the Tsankawi/Cerro Toledo sequence may provide a pathway for lateral movement of water by unsaturated flow.

In Situ Permeability and Travel Times

The Bandelier Tuff hydraulic property data provide a basis for comparison of core-scale and field-scale estimates of water flow and solute transport parameters. For highly faulted or fractured media, the saturated permeability measured at large scale may be three orders of magnitude greater than that of small samples (Neuzil, 1986). Similarly, for crystalline rocks, field-scale (e.g. pump test) measurements of saturated permeability are three orders of magnitude greater than laboratory measurements, again due to fractures (Brace, 1980). Bethke (1989) observed that, due to lithologic heterogeneities, fractures, and faulting, regional-scale saturated permeabilities for sedimentary basins can greatly exceed small-scale measurements. For unsaturated flow, differences in core- and field-scale permeability measurements might reflect the importance (at larger scale) of saturated fracture flow.

The unsaturated hydraulic conductivity functions that we determined for the Bandelier Tuff can be used to estimate the in situ unsaturated hydraulic conductivity by making use of the in situ moisture content values. Combining the in situ unsaturated hydraulic conductivity values for a borehole provides a means of estimating the effective unsaturated hydraulic conductivity or the travel times that apply to water flow through the Bandelier Tuff. Estimates of these travel times and effective unsaturated hydraulic conductivity values are the subject of the next section. Following that, we compare the effective unsaturated hydraulic conductivity estimates to tracer evidence. The core-derived hydraulic conductivity estimates are much lower than values inferred from the movement of recent ^3H, Cl^-, and NO_3^- contamination found a few hundred feet beneath two canyons.

Empirical Unsaturated Hydraulic Conductivities

Appendix F tabulates in situ unsaturated hydraulic conductivities for each core, calculated from Equation (3) using the K_{sat}, van Genuchten parameters, and in situ moisture content. The

arithmetic, geometric, and harmonic mean of the in situ unsaturated hydraulic conductivities for each well, based on the values in Appendix F, are listed in Table 5, along with the depth range for the cores. In calculating the means, the core conductivity values are not depth-weighted, but are treated as a random sample from within the depth interval. Where a sufficient number of cores is present for a borehole, the mean conductivity values are given for the individual lithologic units.

Moisture content variations exert a strong deterministic effect on the distribution and range of in situ (unsaturated) permeability values, so ordinary statistical arguments regarding distribution of the mean saturated permeability must be modified (Gelhar, 1993). The possible significance of the various permeability means was discussed in an earlier section (see "Statistical Distribution of Hydraulic Conductivity," pp. 9–10). The harmonic mean conductivity represents the effective vertical hydraulic conductivity for flow perpendicular to layered strata of varying permeability (de Marsily, 1986). It is strongly affected by the smaller hydraulic conductivity values, which generally reflect the lowest water contents.

Table 6 lists the arithmetic, geometric, and harmonic means of the average linear fluid velocities for the cores listed in Appendix F. The average linear velocity calculated with Equation (2) assumes a unit hydraulic gradient, or steady state gravity flow, where specific discharge equals hydraulic conductivity (Jury et al., 1991). The "mean average linear velocity" is henceforth referred to as the "mean velocity." Again, the individual velocity values are not depth-weighted, but are treated as a random sample in calculating the mean velocity values. The harmonic mean velocities range from about 4 times the harmonic mean unsaturated hydraulic conductivities in the relatively moist tuff beneath canyon bottoms (e.g., Mortandad Canyon), up to 50 to 150 times greater for the dry tuff beneath TA-54.

Table 7 gives the travel times applicable to the depth intervals represented by cores in Table 6 calculated from the three different mean velocities. For the purpose of comparison, the travel times are given as years required to travel 1 cm. The calculation assumes a unit hydraulic head gradient, and uses the respective mean fluid velocities from Table 6:

$$\text{unit travel time} = 1\,/\,\overline{v} = \overline{(\theta/q)} = \overline{\theta/(-Kdh/dl)} \quad , \tag{6}$$

where $\overline{v}$ =   mean (average linear) fluid velocity (centimeters per second),
        θ =   volumetric moisture content (dimensionless, $0 \leq \theta \leq 1$), and
   dh/dl   =   hydraulic gradient (dimensionless, assumed to equal 1).

The mean in situ unsaturated hydraulic conductivities (Table 5) and velocities (Table 6) are extremely low, and imply that the unsaturated Bandelier Tuff may have a permeability in the same range as saturated clays (Table 2.2 in Freeze and Cherry, 1979).

Note that the hydraulic conductivities and velocities described here are not measured, but depend on an empirical formulation for unsaturated hydraulic conductivity (Mualem, 1976a). These values would not apply if fast flow paths exist. The use of these values presumes that fluid flow only occurs through the unsaturated rock matrix.

Tracer Evidence for In Situ Travel Times

Contaminants of recent origin have been found in boreholes beneath two canyon bottoms at Los Alamos National Laboratory. The fluid transport velocities estimated from the presence of these contaminant tracers are significantly greater than core-based velocity estimates. This observation calls into question whether fluid transport through the unsaturated Bandelier Tuff occurs by unsaturated matrix flow or, alternatively, through fractures. The higher tracer-derived velocities also raise questions about the validity of using core-derived hydraulic conductivities to model fluid flow beneath the Laboratory.

Two boreholes recently drilled beneath Mortandad and Los Alamos Canyons revealed concentrations of ^{3}H, Cl^-, and NO_3^- that exceed background values (Stoker et al., 1991; Broxton et al., 1995b). The presence of these contaminants is due to industrial operations conducted at Los Alamos National Laboratory since the mid-1940s, and provides an upper limit on the time required for water to infiltrate through the Bandelier Tuff. While infiltration of ^{3}H through the vadose zone beneath the canyon bottom could occur partly in the vapor phase, the ionic species Cl^- and NO_3^- move only with the liquid phase.

Mortandad Canyon Tracer Velocities

The TA-50 radioactive liquid waste treatment plant at Mortandad Canyon began disposing of effluent with elevated levels of contaminants, including ^{3}H, Cl^-, and NO_3^-, in 1963. Measurements taken in 1961, before the TA-50 plant became operational, showed that the alluvial groundwater concentration of Cl^- was 5–11 mg/L, and the concentration of NO_3^- was 0-3 mg/L (Baltz et al., 1963). By 1990, the alluvial groundwater concentration for Cl^- was <0.5–34 mg/L and the NO_3^- concentration was 60–310 mg/L (Stoker et al., 1991).

The concentrations of ^{3}H, Cl^-, and NO_3^- (Figure 35) observed at depths of up to 200 ft beneath Mortandad Canyon (Stoker et al., 1991) suggest much shorter travel times through the Bandelier

Tuff than those predicted from core data. Borehole MCM-5.9A (Figure 35) penetrated 38 ft of alluvium, 60 ft of Tshirege Unit 1a, 20 ft of the Tsankawi/Cerro Toledo sequence, and 76 ft of the Otowi Member (Stoker et al., 1991). Analysis of cores for Cl^-, NO_3^-, and ^3H shows concentrations of these contaminants well above the 1961 alluvial groundwater levels, and suggests that the contaminants have propagated down to respective depths of about 100, 150, and 190+ ft over a period of 27 years (Stoker et al., 1991).

Let us assume that the travel distance is from the bottom of the alluvium, at 38 ft. For NO_3^-, the observed (maximum) unit travel time based on tracer evidence (over 27 years, from 38 ft to a depth of 150 ft) would be 7.9×10^{-3} yr/cm. This compares with a predicted 41 yr/cm for the Tshirege Unit 1a (from Table 7, using the harmonic mean velocity), and a predicted 10 yr/cm for the entire borehole MCM-5.9A. The observed and predicted fluid velocities are compared in Table 8. The observed (minimum) velocity implied by the NO_3^- data is 4.0×10^{-6} cm/sec, while the predicted (harmonic mean) velocity for the Tshirege Unit 1a from Table 6 is 7.8×10^{-10} cm/sec. The predicted velocity for the entire borehole is 3.1×10^{-9} cm/sec. The low velocity value for the Tshirege Unit 1a (compared to the velocity for all units encountered in the borehole) results from the very low unsaturated hydraulic conductivities of a few cores with low moisture contents.

The (minimum) fluid velocity values calculated from the NO_3^- measurements are much larger than the predicted velocity values estimated from the laboratory core data. The tracer values are about 5000 times larger than the (harmonic mean) core-derived value for Tshirege Unit 1a, and 1300 times larger than the core-derived value for the entire borehole. This suggests that infiltration beneath Mortandad Canyon may occur by other means than vertical unsaturated flow through the rock matrix. Some possible alternatives include saturated flow through fractures or infiltration farther upstream followed by lateral flow within the Tsankawi/Cerro Toledo interval. Vapor-phase flow may be responsible for the deeper movement of ^3H, especially below the Tsankawi/Cerro Toledo interval.

Los Alamos Canyon Tracer Velocities

Preliminary results from the drilling of borehole LADP-3 in Los Alamos Canyon lead to similar tracer-based travel time values. The borehole penetrated 65 ft of alluvium and 243 ft of the Otowi Member (Broxton et al., 1995b). ^3H (5.5 nC/L) and high Cl^- concentrations (46.8 mg/L) were found in perched groundwater at 325 ft in the underlying Guaje Pumice Bed. The contaminant source history in Los Alamos Canyon is not as well defined as for Mortandad Canyon, but a lower limit on the fluid velocity can be inferred by using the 50-year period since

the beginning of Laboratory operations. (Another time estimate may be the 38-year history of the Omega West Reactor, which has apparently been leaking tritiated cooling water into the alluvium since it began operation in 1956.) Let us assume that the travel distance is from the bottom of the alluvium, at 65 ft. This yields a maximum unit travel time of 6.3×10^{-3} yr/cm (over 50 years, from 65 ft to a depth of 325 ft), close to the Mortandad Canyon value for borehole MCM-5.9A. The corresponding minimum observed velocity is 5.0×10^{-6} cm/sec (Table 8).

Core data are not available for borehole LADP-3, but we can compare this minimum observed velocity value to predicted values for the Otowi Member (Table 6) from three other canyon-bottom boreholes (at in situ moisture contents). The predicted (harmonic mean) velocities through the Otowi Member are 5.1×10^{-8} cm/sec at CDBM-1, 3.9×10^{-7} cm/sec at PC-4, and 2.4×10^{-7} cm/sec at MCM-5.9A. The observed (minimum) velocity from LADP-3 is 10 to 100 times greater than the predicted values. The discrepancy between observed and predicted values may be less for the Otowi Member than for the Tshirege Member at MCM-5.9A because of the generally higher moisture contents of the Otowi.

The one or two order-of-magnitude difference between observed and predicted fluid velocities at borehole LADP-3 may not be significant. The unsaturated hydraulic conductivity values presented here for the Otowi Member are only empirical estimates, and may also have significant error due to variations in moisture content and rock properties. The Otowi Member beneath Los Alamos Canyon appears to have about the same volumetric moisture content as the other locations cited: 12% to 24% in LADP-3 (estimated from gravimetric moisture contents of 10% to 20% (Broxton et al., 1995b), by assuming a bulk density of 1.2 g/cm^3). This compares to volumetric moisture contents of 9% to 16% at CDBM-1, 12% to 15% at PC-4, and 18% to 23% at MCM-5.9A.

A second borehole, LAOI(A)-1.1, penetrated the Guaje Pumice about 3500 ft upstream from LADP-3. This borehole was drilled within the Guaje Mountain fault zone and also found perched water in the Guaje Pumice, but the ^3H concentration was at background levels (P. A. Longmire, personal communication, 1995). LAOI(A)-1.1 was drilled about 1000 ft downstream from the Omega West Reactor, which appears to have been leaking tritiated cooling water for up to 40 years. The lack of ^3H in the Guaje Pumice at this upstream borehole, together with the relatively small difference between the tracer and the core-derived fluid velocities at LADP-3, suggest that transport through the Otowi Member beneath the alluvium in Los Alamos Canyon could be occurring by unsaturated flow alone. In this case, it might not be necessary to call upon fractures or faults for accelerated fluid transport.

Conclusions

The results of this study suggest that in general, the moisture retention curves are similar within individual lithologic units. Hydraulic properties, such as bulk density and K_{sat}, appear to differ significantly between units. These conclusions could be an artifact of limited geographic coverage, however. The Tshirege correlation of Baltz et al. (1963) appears to serve as a good basis for dividing the Tshirege Member of the Bandelier Tuff into hydrogeological units as was done by Broxton et al. (1995a). The Tsankawi Pumice Bed, Cerro Toledo Interval, and the Otowi Member make up three additional hydrogeological units.

The core data provide the basis for constructing vertical profiles of in situ matric suction and hydraulic head, which give an indication of the likely direction of subsurface liquid water movement. The canyon-bottom and mesa hydraulic head profiles suggest that generally downward flow of water occurs beneath the surface of the Pajarito Plateau. However, exceptions are the apparent upward flow above the Tsankawi/Cerro Toledo sequence beneath Cañada del Buey and in Mortandad Canyon. Upward flow is also possible above the Tsankawi/Cerro Toledo sequence up to the base of Tshirege Unit 2b within Mesita del Buey at TA-54. These observations suggest that the Tsankawi/Cerro Toledo sequence may be a significant pathway for lateral movement of water by unsaturated flow. Upward flow within the mesas and beneath canyon bottoms would have significant implications for isolating waste storage facilities from ground and surface water.

The core data allow estimates of effective vertical unsaturated hydraulic conductivities and theoretical estimates of the travel times and velocities of infiltrating water. The results can be used as a basis for comparison of core-scale and field-scale estimates of water flow and solute transport rates. The core-derived travel times predict much slower transport than the travel times estimated from the presence of recent ^{3}H, Cl$^-$, and NO$_3^-$ beneath Los Alamos and Mortandad Canyons. In the case of Los Alamos Canyon, however, the observed travel times are only 10 to 100 times greater than those predicted from core measurements. Due to potential uncertainties in estimated unsaturated hydraulic conductivities, and variations of lithologic properties, this velocity difference does not rule out the possibility that vadose zone transport beneath Los Alamos Canyon occurs exclusively by unsaturated flow.

These canyon bottoms have perched alluvial groundwater systems, and may be a source of recharge to the main aquifer. In some canyons, the presence of relatively large amounts of water may facilitate downward water movement along fast paths such as saturated flow along faults and fractures. In other canyons and beneath the generally dryer mesas, the saturated conditions

that facilitate transport through fractures may not occur, and the use of core-derived travel times for modeling might be appropriate.

Remaining Questions and Further Study

The following questions remain concerning the mechanisms controlling flow through the unsaturated zone beneath the Pajarito Plateau and data needs for predicting the movement of moisture and contaminants:

1. Is the approach of estimating hydraulic properties from laboratory analysis of small cores and use of these values in groundwater flow models valid? The results from Mortandad Canyon suggest that, below canyon bottoms with perched alluvial groundwater systems, use of core values is not appropriate. The results from Los Alamos Canyon may not rule out the use of core-derived values.

2. Is the use of core-derived properties valid in some locations, such as the dry mesas and canyon bottoms, but not beneath some saturated canyon bottoms where fast paths, such as fracture flow, might be a more effective transport mechanism?

3. Is the use of laboratory core results and modeling methods valid, but do we lack enough data to completely represent flow within the lithologically heterogeneous system?

4. Do we need more laboratory measurements of core properties? What is the next step?

One basic problem with this data set is the limited geographic distribution of the boreholes, which frustrates both attempts to develop spatial trends for hydraulic properties for each unit, and to relate conclusions to the differing hydrologic settings of mesas or canyon bottoms. The well locations are biased towards the northeastern portion of the Laboratory, where units of the Bandelier Tuff are thinner and less welded. Tshirege Unit 3 is poorly represented (but is represented at both eastern and western ends of the Laboratory), and Unit 4 may not be represented at all. In addition, most of the cores have been collected either beneath saturated canyon bottoms or on Mesita del Buey. There is a need for more data to define the vertical and horizontal variation of hydraulic properties, in particular (1) east-west changes (such as welding) related to distance from the eruption source and (2) vertical changes at particular locations to clarify local contrasts between lithologic units.

A large body of core data exist for the Tshirege Unit 1a and the Otowi Member, but may not adequately reflect the areal variations that could occur within these units. The Tsankawi/Cerro Toledo sequence, the vapor-phase notch (Tshirege Unit 1a/1b contact), the surge beds beneath

28

Tshirege Unit 2b at Mesita del Buey, and the Guaje Pumice Bed are insufficiently characterized. These strata are all possible corridors for significant water movement by unsaturated flow, or for perched water or water vapor movement. In addition, properties for the underlying and probably even more heterogeneous basalts and Puye formation are lacking, with the exception of a few hydraulic test results from water supply wells (Purtymun, 1984; Purtymun and Stoker, 1988).

Given additional core analyses as described, it may be that the usefulness of these data for interpreting the hypothesized fast-path infiltration beneath canyon-bottom alluvial groundwater systems is limited. Other types of studies, along the lines of work done by Purtymun et al. (1989) or Stoker et al. (1991), could shed more light on the mechanisms of infiltration. If vapor transport beneath dry mesa locations, such as Mesita del Buey, has a significant effect on water movement, further investigations to understand this phenomenon are required.

Acknowledgments

References

W. V. Abeele, "Determination of Hydraulic Conductivity in Crushed Bandelier Tuff," Los Alamos Scientific Laboratory report LA-8147-MS (November 1979).

W. V. Abeele, "Hydraulic Testing of Crushed Bandelier Tuff," Los Alamos National Laboratory report LA-10037-MS (March 1984).

E. M. Baltz, J. H. Abrahams, and W. D. Purtymun, "Preliminary Report on Geology and Hydrology of Mortandad Canyon Near Los Alamos, New Mexico, with Reference to Disposal of Liquid Low-Level Radioactive Waste," U.S. Geological Survey Open-File Report (March 1963).

J. Bear, *Dynamics of Fluids in Porous Media* (American Elsevier, New York, 1972).

N. M. Becker, "Influence of Hydraulic and Geomorphologic Components of a Semi-Arid Watershed on Depleted Uranium Transport," Los Alamos National Laboratory report LA-UR-93-2165 (1991).

C. M. Bethke, "Modeling Subsurface Flow in Sedimentary Basins," *Geologische Rundschau* **78**, 129–154 (1989).

B. M. Bowen, "Los Alamos Climatology," Los Alamos National Laboratory report LA-11735-MS (May 1990).

W. F. Brace, "Permeability of Crystalline and Argillaceous Rocks," *International Journal of Rock Mechanics, Mineral Science, and Geomechanics* **17**, 241–251 (1980).

D. E. Broxton and S. Reneau, "A Proposed Nomenclature for Rocks on the Pajarito Plateau," Los Alamos National Laboratory Environmental Restoration Project technical session, Los Alamos National Laboratory (October 19, 1994).

D. E. Broxton, G. Heiken, S. J. Chipera, and F. M. Byers, Jr., "Stratigraphy, Petrography, and Mineralogy of Tuffs at Technical Area 21, Los Alamos National Laboratory, New Mexico," in "Geologic Studies at TA-21," D. E. Broxton and P. G. Eller (Eds.), Los Alamos National Laboratory report LA-12934-MS (1995a).

D. E. Broxton, P. A. Longmire, P. G. Eller, and D. Flores, "Preliminary Drilling Results for Bore Holes LADP-3 and LADP-4 at Technical Area 21, Los Alamos National Laboratory, New

Mexico," in "Geologic Studies at TA-21," D. E. Broxton and P. G. Eller (Eds.), Los Alamos National Laboratory report LA-12934-MS (1995b).

J. L. Conca and J. Wright, "Direct Determinations of Unsaturated Flow and Transport," in *Proceedings of the Twelfth Annual American Geophysical Union Hydrology Days Meeting* (Hydrology Days Publications, Fort Collins, Colorado, March 1992) pp. 103–116.

J. Constantz and W. N. Herkelrath, "A Submersible Pressure Outflow Cell for Measurement of Soil Water Retention and Diffusivity from 50° C to 95° C," *Soil Science Society of America Journal* **48**, 7–10 (1984).

B. M. Crowe, G. W. Linn, G. Heiken, and M. L. Bevier, "Stratigraphy of the Bandelier Tuff in the Pajarito Plateau: Applications to Waste Management," Los Alamos Scientific Laboratory report LA-7225-MS (April 1978).

Daniel B. Stephens & Associates, "Final Data Report on Laboratory Analysis of Soil Hydraulic Properties of Welded Tuffs at Los Alamos National Laboratory," prepared for Los Alamos National Laboratory, report no. DBSA/87-070/188-1 (January 1988).

Daniel B. Stephens & Associates, "Addendum to Laboratory Analysis of Hydraulic Testing for MCM 5.1 and MCC 5.9A Samples," prepared by Daniel B. Stephens & Associates, Inc., for Los Alamos National Laboratory, report no. DBSA/90-170/791-1 (July 1991a).

Daniel B. Stephens & Associates, "Laboratory Analysis of Soil Hydraulic Properties from TA-53 Impoundments Corehole #6, Corehole #7, and Corehole SIMO-1," prepared by Daniel B. Stephens & Associates, Inc., for Los Alamos National Laboratory, report no. DBSA/91-260/1191-1 (November 1991b).

Daniel B. Stephens & Associates, "Laboratory Analysis of Hydraulic Properties of Volcanic Tuff Samples," prepared by Daniel B. Stephens & Associates, Inc., for Los Alamos National Laboratory, report no. DBSA/91-110/1291-1 (December 1991c).

Daniel B. Stephens & Associates, "Laboratory Analysis of Soil Hydraulic Properties of PC4 Pressure Plate and SPOC Samples," prepared by Daniel B. Stephens & Associates, Inc., for Los Alamos National Laboratory, report no. DBSA/2830/892-1 (August 1992a).

Daniel B. Stephens & Associates, "Laboratory Analysis of Soil Hydraulic Properties of CDBM 2 and CDBM 3 Samples," prepared by Daniel B. Stephens & Associates, Inc., for Los Alamos National Laboratory, report no. DBSA/2830/1292-1 (December 1992b).

Daniel B. Stephens & Associates, "Laboratory Analysis of Soil Hydraulic Properties of Protective Barrier Landfill Cover Demonstration Samples," prepared by Daniel B. Stephens & Associates, Inc., for Los Alamos National Laboratory, report no. DBSA/4800/494-1 (April 1994a).

Daniel B. Stephens & Associates, "Laboratory Analysis of Soil Hydraulic Properties of Boreholes 54-1001, 1002, 1003, and 1006," prepared by Daniel B. Stephens & Associates, Inc., for Los Alamos National Laboratory, report no. DBSA/3854/794-1 (July 1994b).

G. de Marsily, *Quantitative Hydrogeology: Groundwater Hydrology for Engineers* (Academic Press, New York, 1986).

R. A. Freeze and J. A. Cherry, *Groundwater* (Prentice-Hall, Englewood Cliffs, New Jersey, 1979).

B. M. Gallaher, B. Gilkeson, D. B. Rogers, and D. Krier, "Hydraulic Gradients and Direction of Water Flow Beneath MDA G, TA-54," Los Alamos National Laboratory Environmental Restoration Project technical session, Los Alamos National Laboratory (October 19, 1994).

L. W. Gelhar, *Stochastic Subsurface Hydrology* (Prentice Hall, Englewood Cliffs, New Jersey, 1993).

F. Goff, "Geological Map of TA-21, Los Alamos National Laboratory, New Mexico," in "Geologic Studies at TA-21," D. E. Broxton and P. G. Eller (Eds.), Los Alamos National Laboratory report LA-12934-MS (1995).

F. Goff, J. N. Gardner, W. S. Baldridge, J. B. Hulen, D. L. Nielson, D. Vaniman, G. Heiken, M. A. Dungan, and D. Broxton, "Excursion 17b: Volcanic and Hydrothermal Evolution of Valles Caldera and Jemez Volcanic Field," New Mexico Bureau of Mines and Mineral Resources Memoir 46, pp. 381–434 (1989).

R. L. Griggs, "Geology and Ground-Water Resources of the Los Alamos Area, New Mexico," U.S. Geological Survey Water-Supply Paper 1753 (1964).

D. Hickmott and J. McCann, "Barium and HE in Cañon de Valle: Geochemistry and Preliminary Results," Los Alamos National Laboratory Environmental Restoration Project technical session, Los Alamos National Laboratory (April 19, 1995).

E. H. Isaaks and R. M. Srivastava, *Applied Geostatistics* (Oxford University Press, New York, 1989).

IT Corp., "Hydrogeologic Assessment of Technical Area 54, Areas G and L, Los Alamos National Laboratory," International Technology Corporation report NMHWA 001007 (March 1987).

G. A. Izett and J. D. Obradovich, "^{40}Ar/^{39}Ar Age Constraints for the Jaramillo Normal Subchron and the Matuyama-Brunhes Geomagnetic Boundary," *Journal of Geophysical Research* **99**, 2925–2934 (1994).

W. A. Jury, W. R. Gardner, and W. H. Gardner, *Soil Physics*, fifth edition (John Wiley and Sons, New York, 1991).

P. M. Kearl, J. J. Dexter, and M. Kautsky, "Vadose Zone Characterization of Technical Area 54, Waste Disposal Areas G and L, Los Alamos National Laboratory, New Mexico, Report 3, Preliminary Assessment of the Hydrologic System," Bendix Field Engineering Corp. report GJ-44 (March 1986a).

P. M. Kearl, J. J. Dexter, and M. Kautsky, "Vadose Zone Characterization of Technical Area 54, Waste Disposal Areas G and L, Los Alamos National Laboratory, New Mexico, Report 4: Preliminary Assessment of the Hydrologic System through Fiscal Year 1986," UNC Technical Services, Inc., report GJ-54 (December 1986b).

C. A. Loeven and E. P. Springer, "Validation of Continuum Concepts for Flow and Transport in Unsaturated Fractured Bandelier Tuff, Final Report," Los Alamos National Laboratory report LA-UR-93-2873 (August 1993).

L. Luckner, M. Th. van Genuchten, and D. R. Nielsen, "A Consistent Set of Parametric Models for the Two-Phase Flow of Immiscible Fluids in the Subsurface," *Water Resources Research* **25**, 2187–2193 (1989).

Y. Mualem, "A New Model for Predicting the Hydraulic Conductivity of Unsaturated Porous Media," *Water Resources Research* **12**, 513–522 (1976a).

Y. Mualem, "A Catalogue of the Hydraulic Properties of Unsaturated Soils," Technion Hydrodynamics and Hydraulic Laboratory research project report 442 (Israel Institute of Technology, Haifa, Israel, 1976b).

C. E. Neuzil, "Groundwater Flow in Low-Permeability Environments," *Water Resources Research* **22**, 1163–1195 (1986).

J. W. Nyhan, "Radioactive Waste Burial in Tuff at Los Alamos," in "Nuclear Waste Management Technology Development Activities, January-December 1978," L. J. Johnson and B. H. Desilets (Eds.), Los Alamos National Laboratory report LA-7921-PR (June 1979) pp. 53–55.

W. D. Purtymun, "Underground Movement of Tritium from Solid-Waste Storage Shafts," Los Alamos Scientific Laboratory report LA-5286-MS (May 1973).

W. D. Purtymun, "Geohydrology of the Pajarito Plateau, with Reference to Quality of Water, 1949-1972," Los Alamos Scientific Laboratory informal report (December 1975).

W. D. Purtymun, "Hydrologic Characteristics of the Main Aquifer in the Los Alamos Area: Development of Ground Water Supplies," Los Alamos National Laboratory report LA-9957-MS (January 1984).

W. D. Purtymun, "Geologic and Hydrologic Records of Observation Wells, Test Holes, Test Wells, Supply Wells, Springs, and Surface Water Stations in the Los Alamos Area," Los Alamos National Laboratory report LA-12883-MS (January 1995).

W. D. Purtymun and W. R. Kennedy, "Geology and Hydrology of Mesita del Buey," Los Alamos Scientific Laboratory report LA-4660 (May 1971).

W. D. Purtymun and A. K. Stoker, "Water Supply at Los Alamos: Current Status of Wells and Future Water Supply," Los Alamos National Laboratory report LA-11332-MS (August 1988).

W. D. Purtymun, E. A. Enyart, and S. G. McLin, "Hydrologic Characteristics of the Bandelier Tuff as Determined Through an Injection Well System," Los Alamos National Laboratory report LA-11511-MS (August 1989).

D. B. Rogers, "Landfill Cover Hydraulic Properties," Los Alamos National Laboratory memorandum ESH-8/WQ&H-94-247, to J. W. Nyhan (June 3, 1994a).

D. B. Rogers, "Well 54-1001: TA-54 Area L, Hydraulic Properties," Los Alamos National Laboratory memorandum ESH-8/WQ&H-94-344, to D. J. Krier (July 19, 1994b).

D. B. Rogers, "Unsaturated Hydraulic Characteristics of the Bandelier Tuff at TA-54," Los Alamos National Laboratory report LA-UR-95-1777 (May 1995).

D. B. Rogers and B. M. Gallaher, "Unsaturated Hydraulic Characteristics of the Bandelier Tuff," Los Alamos National Laboratory report LA-UR-95-1778 (May 1995).

M. A. Rogers, "Geologic Map of the Los Alamos National Laboratory Reservation, 1:400, 21 Sheets, New Mexico Environment Department (1995).

R. L. Smith and R. A. Bailey, "The Bandelier Tuff, a Study of Ash-Flow Eruption Cycles from Zoned Magma Chambers," *Bulletin Volcanologique* **29**, 83–104 (1966).

Stephens et al.---See Daniel B. Stephens & Associates

A. K. Stoker, W. D. Purtymun, S. G. McLin, and M. N. Maes, "Extent of Saturation in Mortandad Canyon," Los Alamos National Laboratory report LA-UR-91-1660 (May 1991).

M. Th. van Genuchten, "A Closed-Form Equation for Predicting the Hydraulic Conductivity of Unsaturated Soils," *Soil Science Society of America Journal* **44**, 892–898 (1980).

M. Th. van Genuchten, F. J. Leij, and S. R. Yates, "The RETC Code for Quantifying the Hydraulic Functions of Unsaturated Soils," U.S. Environmental Protection Agency report EPA/600/2-91/065 (1991).

D. Vaniman, "Revisions to Report EES1-SH90-17," Los Alamos National Laboratory memorandum EES1-SH91-12 (July 29, 1991).

D. Vaniman and K. Wohletz, "Results of Geological Mapping/Fracture Studies, TA-55 Area," Los Alamos National Laboratory memorandum EES1-SH90-17 (November 14, 1990).

J. E. Weir and W. D. Purtymun, "Geology and Hydrology of Technical Area 49, Frijoles Mesa, Los Alamos County, New Mexico," U.S. Geological Survey Administrative Release, Albuquerque, New Mexico (1962).

Tables

Table 1. Data sources and quality of Bandelier Tuff hydrologic property data.

Well/ Sample	Reference	Comments[1]
CDBM-1	Stephens et al., 1992b	(1)
CDBM-2	Stephens et al., 1992b	(1)
AB-6	Stephens et al., 1991b	(2); 1 of 5 retention curves unreliable
AB-7	Stephens et al., 1991b	(2); 2 of 2 retention curves unreliable
SIMO-1	Stephens et al., 1991b	(2); 3 of 3 retention curves unreliable
PC-4[2]	Stephens et al., 1992a	(1); 13 of 24 initial moisture values measured, 4 of 24 retention curves unreliable
MCM-5.1	Stephens et al., 1991a	(1); 1-5 of 12 retention curves unreliable
MCM-5.9A	Stephens et al., 1991a	(1); 1-4 of 8 retention curves unreliable
TA-16, P-16	Stephens et al., 1988	(2); 6 of 10 retention curves unreliable
LLC-85-14	Stephens et al., 1991c	(2); dry part of retention curves appears reliable
LLC-85-15	Stephens et al., 1991c	(2); dry part of retention curves appears reliable
LLC-86-22	Stephens et al., 1991c	(2); dry part of retention curves appears reliable
TA-21	Nyhan 1979	samples from pit near adsorption bed 1, MDA T
LLM-85-01	Kearl 1986a	retention data lack low θ values
LLM-85-02	Kearl 1986a	retention data lack low θ values
LLM-85-05	Kearl 1986a	retention data lack low θ values
LGM-85-06	Kearl 1986a	retention data lack low θ values
LGM-85-11	Kearl 1986a	retention data lack low θ values
54-1001	Stephens et al., 1994b	(1)
54-1002	Stephens et al., 1994b	(1)
54-1003	Stephens et al., 1994b	(1); 4 of 6 retention curves unreliable
54-1006	Stephens et al., 1994b	(1); 1 of 5 retention curves unreliable
Crushed Tuff 1	Stephens et al., 1994a	(1)
Crushed Tuff 2	Abeele 1979, 1984	(2); combination of pressure plate (Abeele, 1979) and caisson (Abeele, 1984) data

[1] Comments: (1) some pressure plate data > 1 bar not equilibrated, (2) no psychrometer values, so dry part of moisture retention curves may be poorly constrained.

[2] Referred to as POTO-4 by Purtymun (1995).

Table 2. Lithologic coverage and hydrologic setting of Bandelier Tuff hydrologic property samples.

Well	No. of Cores	Location, Hydrologic Setting	Lithologic Units Represented
CDBM-1	17	Cañada del Buey, dry	Tshirege 1a, Tsankawi, Otowi
CDBM-2	4	Cañada del Buey, dry	Tshirege 1a, Otowi
AB-6	5	TA-53, mesa	Tshirege 1a, 2a, 2b
AB-7	2	TA-53, mesa	Otowi
SIMO-1	9	Mortandad Canyon, wet	Tshirege 1a, Tsankawi, Otowi
PC-4	24	Potrillo Canyon, dry	Alluvium, Tshirege 1a, Tsankawi, Otowi
MCM-5.1	45	Mortandad Canyon, wet	Alluvium, Tshirege 1a, Tsankawi
MCM-5.9A	28	Mortandad Canyon, wet	Tshirege 1a, Tsankawi, Otowi
TA-16, P-16	10	TA-16 MDA P, mesa	Tshirege 3c, 3d
LLC-85-14	1	TA-54 MDA L, mesa	Tshirege 2b
LLC-85-15	1	TA-54 MDA L, mesa	Tshirege 2b
LLC-86-22	5	TA-54 MDA L, mesa	Tshirege 1b, 2a
TA-21	24	TA-21 MDA T, mesa	Tshirege 3
LLM-85-01	4	TA-54 MDA L, mesa	Tshirege 1a, 1b, 2a, 2b
LLM-85-02	4	TA-54 MDA L, mesa	Tshirege 1b, 2a, 2b
LLM-85-05	4	TA-54 MDA L, mesa	Tshirege 1a, 1b, 2b
LGM-85-06	4	TA-54 MDA G, mesa	Tshirege 1a, 1b, 2b
LGM-85-11	4	TA-54 MDA G, mesa	Tshirege 1a, 1b, 2b
54-1001	5	TA-54 MDA L, mesa	Tshirege 1b
54-1002	5	TA-54 MDA L, mesa	Tshirege 1a, 1b
54-1003	6	TA-54 MDA L, mesa	Tshirege 1a, 1b
54-1006	5	TA-54 MDA L, mesa	Tshirege 1a, 1b, 2b

Table 3. Los Alamos Bandelier Tuff hydrologic property samples: types of data.

Well	No. of cores	Bulk density	In situ moisture	K_{sat}	Moisture retention	Transient outflow	Air permeability	Other tests [3]
CDBM-1	17	X	X	X	X	X		
CDBM-2	4	X	X	X	X	X		
AB-6	5	X	X	X	X[1]			
AB-7	2	X	X	X	X[1]			
SIMO-1	3	X	X	X	X[1]			
SIMO-1	6	X	X					
PC-4	13	X	X	X	X	X		
PC-4	11			X	X[2]	X		
MCM-5.1	33	X	X					(1)
MCM-5.1	12	X	X	X	X[2]	X	X	
MCM-5.9A	19	X	X					(1)
MCM-5.9A	9	X	X	X	X[2]	X	X	
TA-16, P-16	10	X	X	X	X[1]			
LLC-85-14	1	X		X	X[1, 2]		X	(2)
LLC-85-15	1	X		X	X[1, 2]		X	(2)
LLC-86-22	5	X		X	X[1, 2]		X	(2)
TA-21	24			X				
LLM-85-01	4			X	X[1]		X	
LLM-85-02	4			X	X[1]		X	
LLM-85-05	4			X	X[1]		X	
LGM-85-06	4			X	X[1]		X	
LGM-85-11	4			X	X[1]		X	
54-1001	5	X	X	X	X		X	(2, 3, 4)
54-1002	5	X	X	X	X		X	(2, 3, 4)
54-1003	6	X	X	X	X		X	(2, 3, 4)
54-1006	5	X	X	X	X		X	(2, 3, 4)
Crushed Tuff 1	1	X	X	X	X	(Stephens et al.)		(5)
Crushed Tuff 2	-		X	X	X	(Abeele)		

[1] No psychrometer measurements in the dry portion of the retention curve.

[2] Moisture retention by SPOC (submersible pressure outflow cell, Constantz and Herkelrath, 1984) measurements.

[3] Other tests: (1) psychrometer suction at in situ moisture content, (2) particle density, (3) specific surface, (4) humidity/moisture content, (5) particle-size distribution.

Table 4. Contents of accompanying computer disk containing moisture
retention and hydraulic data.

Well or Sample ID, or File Contents	File Name
CDBM-1	CDBM Retent Data Txt
CDBM-2	CDBM Retent Data Txt
AB-6	AB Retent Data Txt
AB-7	AB Retent Data Txt
SIMO-1	SIMO-1 Retent Data Txt
PC-4	PC-4 Retent Data Txt
PC-4 SPOC	PC-4 SPOC Retent Data Txt
MCM-5.1	MCM5.1 Retent Data Txt
MCM-5.9A	MCM5.9A Retent Data Txt
TA-16, P-16	TA-16 P-16 Retent Data Txt
LLC-85-14	TA-54 LLC Retent Data Txt
LLC-85-15	TA-54 LLC Retent Data Txt
LLC-86-22	TA-54 LLC Retent Data Txt
TA-21	1
LLM-85-01	2
LLM-85-02	2
LLM-85-05	2
LGM-85-06	2
LGM-85-11	2
54-1001	TA-54-1001 Retent Data Txt
54-1002	TA-54-1002 Retent Data Txt
54-1003	TA-54-1003 Retent Data Txt
54-1006	TA-54-1006 Retent Data Txt
Crushed Tuff 1	Crsh Tuff Retent Data Txt
Crushed Tuff 2	Crsh Tuff Retent Data Txt
All hydraulic property data by lithologic unit	Unsat Prop by Units Txt
All hydraulic property data by well	Unsat Prop by Well Txt

[1] No retention data.

[2] See Kearl et al., 1986a and b.

Table 5. Mean, in situ, unsaturated hydraulic conductivities by well.

Well/Unit	Core depth range (ft)	Number of cores	In Situ Conductivity Means (cm/sec)		
			Harmonic	Geometric	Arithmetic
CDBM-1	24-189	17	3.13×10^{-10}	5.47×10^{-9}	1.74×10^{-8}
Tshirege 1a	24-64	5	9.54×10^{-11}	7.97×10^{-10}	3.30×10^{-9}
Tsankawi	89-94	2	1.34×10^{-8}	1.59×10^{-8}	1.89×10^{-8}
Otowi	104-189	10	5.41×10^{-9}	1.16×10^{-8}	2.41×10^{-8}
CDBM-2	28-68	4	3.99×10^{-10}	3.87×10^{-9}	1.86×10^{-8}
AB-6	40-150	4	5.65×10^{-7}	5.99×10^{-6}	2.95×10^{-4}
PC-4	4-168	12	5.42×10^{-8}	2.19×10^{-7}	1.57×10^{-6}
Alluvium	4-9	2	4.09×10^{-7}	5.19×10^{-7}	5.41×10^{-7}
Weathered 1a	14-59	3	2.57×10^{-8}	2.22×10^{-7}	1.32×10^{-6}
Tshirege 1a	64-84	2	6.87×10^{-8}	6.68×10^{-7}	6.50×10^{-6}
Tsankawi	89-104	2	1.28×10^{-7}	1.85×10^{-7}	2.65×10^{-7}
Otowi	118-168	3	5.35×10^{-8}	6.40×10^{-8}	8.05×10^{-8}
MCM-5.1	43-107	11	5.41×10^{-9}	5.78×10^{-8}	2.31×10^{-6}
Tshirege 1a	43-87	7	1.26×10^{-9}	1.67×10^{-8}	1.67×10^{-7}
Tsankawi	93-107	4	3.34×10^{-8}	5.05×10^{-7}	6.16×10^{-6}
MCM-5.9A	86-165	8	5.36×10^{-10}	8.01×10^{-8}	1.69×10^{-6}
Tshirege 1a	86-95	2	1.35×10^{-10}	7.81×10^{-10}	4.52×10^{-9}
Tsankawi	109	1	-	-	8.93×10^{-6}
Otowi	120-165	5	4.58×10^{-8}	1.99×10^{-7}	9.14×10^{-7}
TA-16, P-16	8-81	4	2.50×10^{-7}	8.49×10^{-7}	4.40×10^{-6}
LLC-86-22	54-131	5	8.92×10^{-13}	7.13×10^{-11}	4.74×10^{-9}
54-1001	68-142	5	2.76×10^{-11}	2.31×10^{-10}	7.90×10^{-10}
54-1002	92-244	5	1.86×10^{-11}	1.13×10^{-10}	1.56×10^{-9}
54-1003	102-157	2	4.51×10^{-13}	1.66×10^{-12}	6.10×10^{-12}
54-1006	42-161	4	1.36×10^{-13}	1.93×10^{-11}	8.06×10^{-10}

Table 6. Mean, unsaturated, average linear velocities by well.

Well/Unit	Core depth range (ft)	Number of cores	Average Linear Velocity Means (cm/sec)		
			Harmonic	Geometric	Arithmetic
CDBM-1	24-189	17	9.47×10^{-9}	5.52×10^{-8}	1.43×10^{-7}
Tshirege 1a	24-64	5	3.17×10^{-9}	1.17×10^{-8}	3.17×10^{-8}
Tsankawi	89-94	2	1.10×10^{-7}	1.17×10^{-7}	1.24×10^{-7}
Otowi	104-189	10	5.06×10^{-8}	1.03×10^{-7}	2.02×10^{-7}
CDBM-2	28-68	4	3.50×10^{-9}	3.57×10^{-8}	1.56×10^{-7}
AB-6	40-150	4	2.50×10^{-6}	2.24×10^{-5}	6.75×10^{-4}
PC-4	4-168	12	2.74×10^{-7}	1.10×10^{-6}	4.30×10^{-6}
Alluvium	4-9	2	2.01×10^{-6}	2.14×10^{-6}	2.28×10^{-6}
Weathered 1a	14-59	3	1.06×10^{-7}	7.50×10^{-7}	3.22×10^{-6}
Tshirege 1a	64-84	2	3.72×10^{-7}	2.45×10^{-6}	1.61×10^{-5}
Tsankawi	89-104	2	1.41×10^{-6}	1.56×10^{-6}	1.73×10^{-6}
Otowi	118-168	3	3.87×10^{-7}	4.73×10^{-7}	6.06×10^{-7}
MCM-5.1	43-107	11	8.10×10^{-9}	2.22×10^{-7}	5.65×10^{-6}
Tshirege 1a	43-87	7	5.37×10^{-9}	7.88×10^{-8}	4.08×10^{-7}
Tsankawi	93-107	4	7.45×10^{-8}	1.36×10^{-6}	1.48×10^{-5}
MCM-5.9A	86-165	8	3.08×10^{-9}	3.33×10^{-7}	5.36×10^{-6}
Tshirege 1a	86-95	2	7.77×10^{-10}	3.02×10^{-9}	1.17×10^{-8}
Tsankawi	109	1	-	-	2.01×10^{-5}
Otowi	120-165	5	2.38×10^{-7}	9.60×10^{-7}	4.55×10^{-6}
TA-16, P-16	8-81	4	1.19×10^{-6}	3.56×10^{-6}	1.35×10^{-5}
LLC-86-22	54-131	5	3.69×10^{-11}	1.61×10^{-9}	2.41×10^{-8}
54-1001	68-142	5	1.44×10^{-9}	4.41×10^{-9}	8.68×10^{-9}
54-1002	92-244	5	3.56×10^{-10}	2.32×10^{-9}	2.17×10^{-8}
54-1003	102-157	2	2.88×10^{-11}	6.12×10^{-11}	1.30×10^{-10}
54-1006	42-161	4	2.03×10^{-11}	7.36×10^{-10}	1.38×10^{-8}

Table 7. Calculated travel times by well.

Well/Unit	Core depth interval (ft)	Number of cores	Calculated Travel Times (yr/cm)		
			Harmonic	Geometric	Arithmetic
CDBM-1	165	17	3.3×10^0	5.7×10^{-1}	2.2×10^{-1}
Tshirege 1a	40	5	1.0×10^1	2.7×10^0	1.0×10^0
Tsankawi	5	2	2.9×10^{-1}	2.7×10^{-1}	2.6×10^{-1}
Otowi	85	10	6.3×10^{-1}	3.1×10^{-1}	1.6×10^{-1}
CDBM-2	40	4	9.1×10^0	8.9×10^{-1}	2.0×10^{-1}
AB-6	110	4	1.3×10^{-2}	1.4×10^{-3}	4.7×10^{-5}
PC-4	164	12	1.2×10^{-1}	2.9×10^{-2}	7.4×10^{-3}
Alluvium	5	2	1.6×10^{-2}	1.5×10^{-2}	1.4×10^{-2}
Weathered 1a	45	3	3.0×10^{-1}	4.2×10^{-2}	9.8×10^{-3}
Tshirege 1a	20	2	8.5×10^{-2}	1.3×10^{-2}	2.0×10^{-3}
Tsankawi	96	2	2.2×10^{-2}	2.0×10^{-2}	1.8×10^{-2}
Otowi	50	3	8.2×10^{-2}	6.7×10^{-2}	5.2×10^{-2}
MCM-5.1	64	11	3.9×10^0	1.4×10^{-1}	5.6×10^{-3}
Tshirege 1a	44	7	5.9×10^0	4.0×10^{-1}	7.8×10^{-2}
Tsankawi	14	4	4.3×10^{-1}	2.3×10^{-2}	2.1×10^{-3}
MCM-5.9A	79	8	1.0×10^1	9.5×10^{-2}	5.9×10^{-3}
Tshirege 1a	9	2	4.1×10^1	1.0×10^1	2.7×10^0
Tsankawi	4	1			1.6×10^{-3}
Otowi	45	5	1.3×10^{-1}	3.3×10^{-2}	7.0×10^{-3}
TA-16, P-16	73	4	2.7×10^{-2}	$8.9\times10{-3}$	2.3×10^{-3}
LLC-86-22	77	5	8.6×10^2	2.0×10^1	1.3×10^0
54-1001	74	5	2.2×10^1	7.2×10^0	3.7×10^0
54-1002	152	5	8.9×10^1	1.4×10^1	1.5×10^0
54-1003	55	2	1.1×10^3	5.2×10^2	2.4×10^2
54-1006	119	4	1.6×10^3	4.3×10^1	2.3×10^0

Table 8. Observed vs. predicted fluid velocities (cm/sec).

Well	Observed Velocity	Predicted Velocity	Source of Predicted Velocity*
MCM-5.9A	$> 4.0 \times 10^{-6}$	7.8×10^{-10}	MCM-5.9A (Tshirege 1a)
		3.1×10^{-9}	MCM-5.9A (entire well)
LADP-3	$> 5.0 \times 10^{-6}$	5.1×10^{-8}	CDBM-1 (Otowi)
		3.9×10^{-7}	PC-4 (Otowi)
		2.4×10^{-7}	MCM-5.9A (Otowi)

* Velocities are all harmonic means of unsaturated average linear velocities, determined for cores, from Table 6.

Figures
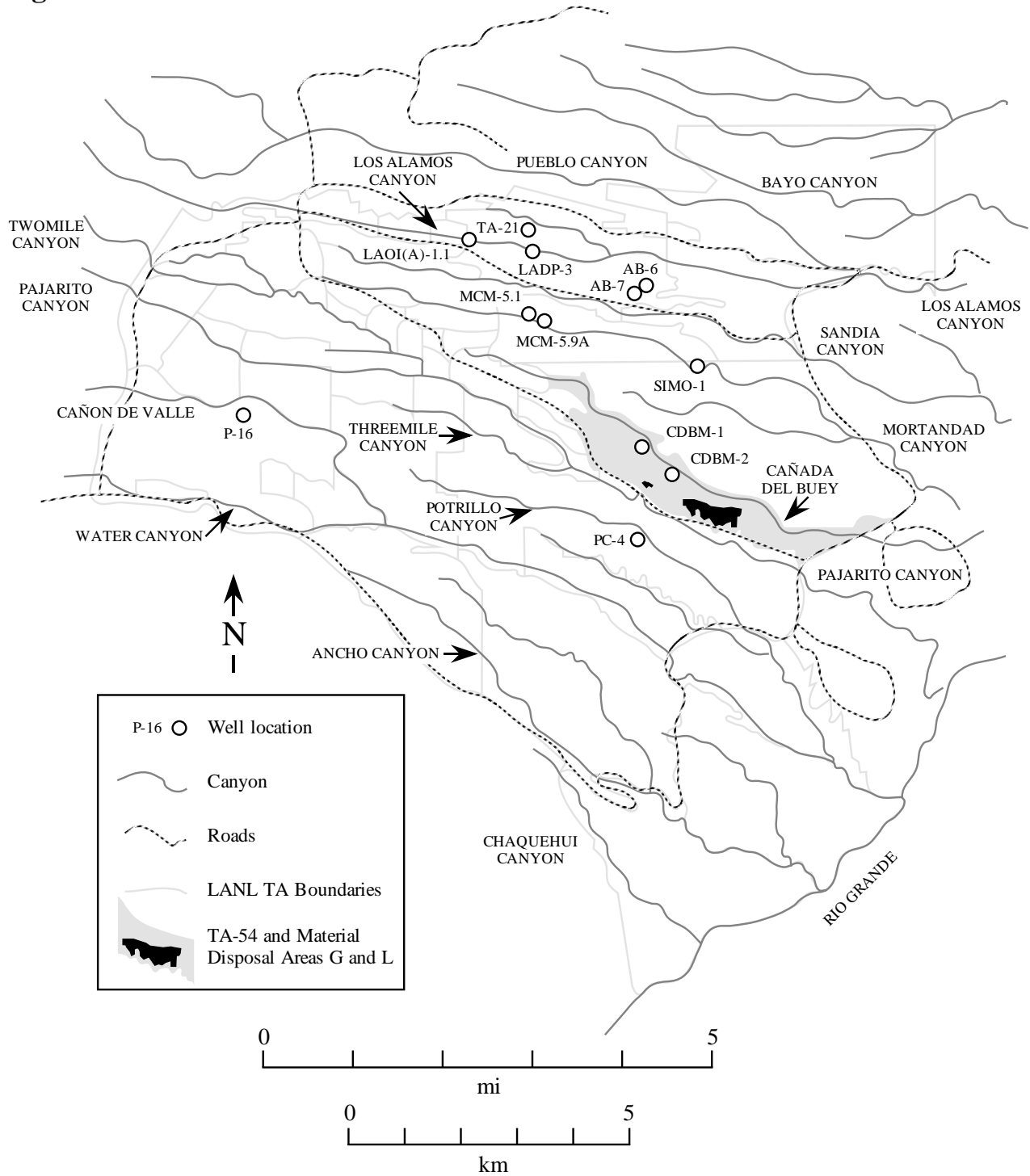
Figure 1. Map of Los Alamos National Laboratory, showing locations of hydrologic properties wells, canyons, roads, and Technical Area (TA) boundaries. The shaded area is TA-54, shown in Figure 2. Wells LADP-3 and LAOI(A)-1.1 are discussed in the section on travel time evidence from tracers.
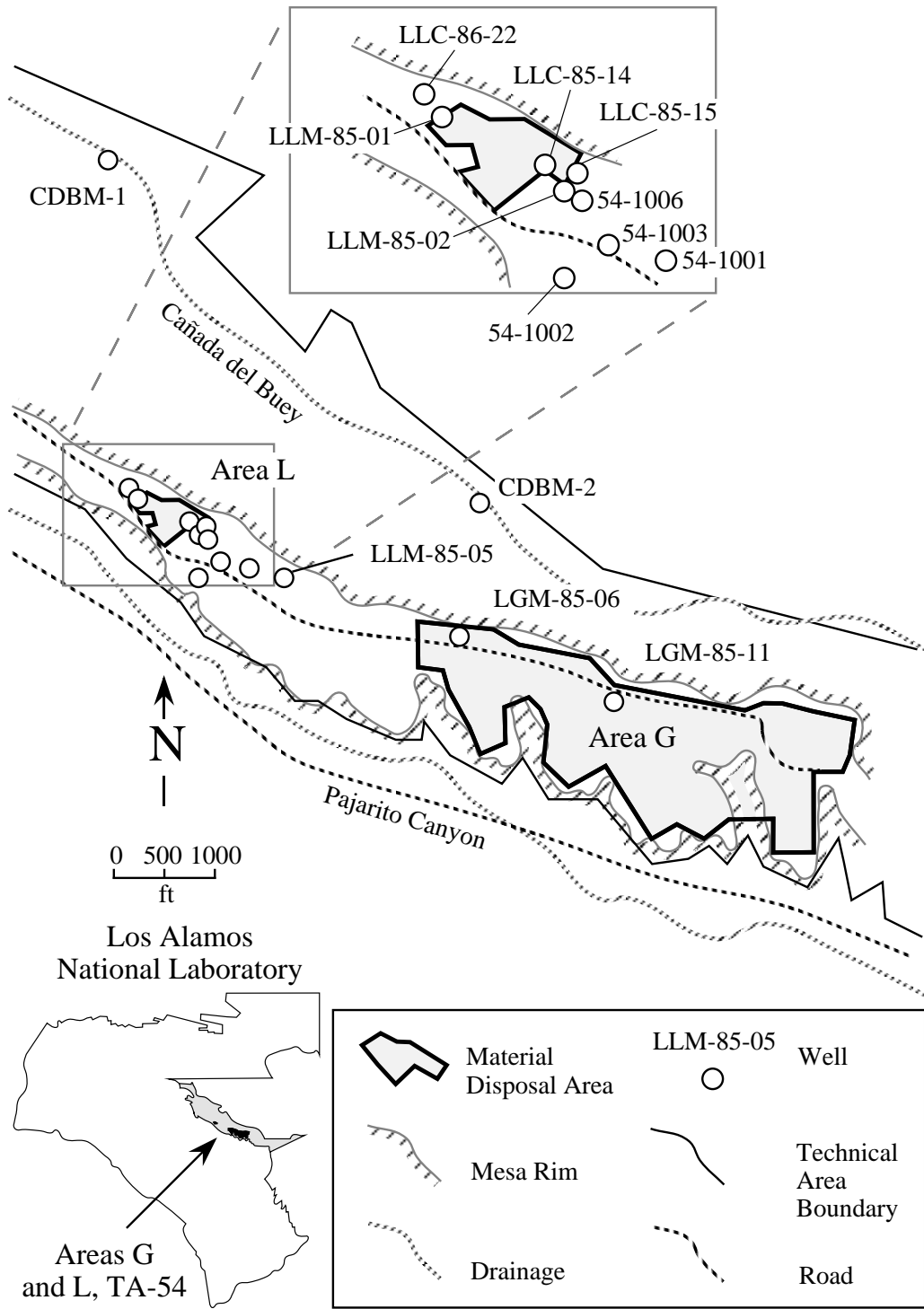
Figure 2. Detail of part of TA-54, showing locations of MDA L, MDA G, and locations of hydrologic properties wells [after Figure 2-3 in Kearl et al., (1986b); Purtymun (1995); and R. H. Gilkeson (personal communication, 1994)].

Correlation of Units within the Tshirege Member of the Bandelier Tuff

Smith and Bailey, 1966	Weir and Purtymun, 1962	Baltz et al., 1963	Purtymun and Kennedy, 1971	Crowe et al., 1978	Vaniman and Wohletz, 1990	M. A. Rogers, 1995	Broxton and Reneau, 1994
V	6	3		3	4	F	4
	5		2b			E	
IV	4	2b		2	3	D	3
	3		2a / 1b		nonwelded		
III		2a			2	C	2
II	2	1b	1a	1	nonwelded	B	1v
	1b	1a			1v		
I	1a				1g	A	1g
Jemez Volcanic Field	TA-49	Mortandad Canyon	TA-54	Ancho Canyon	Central LANL	LANL	LANL
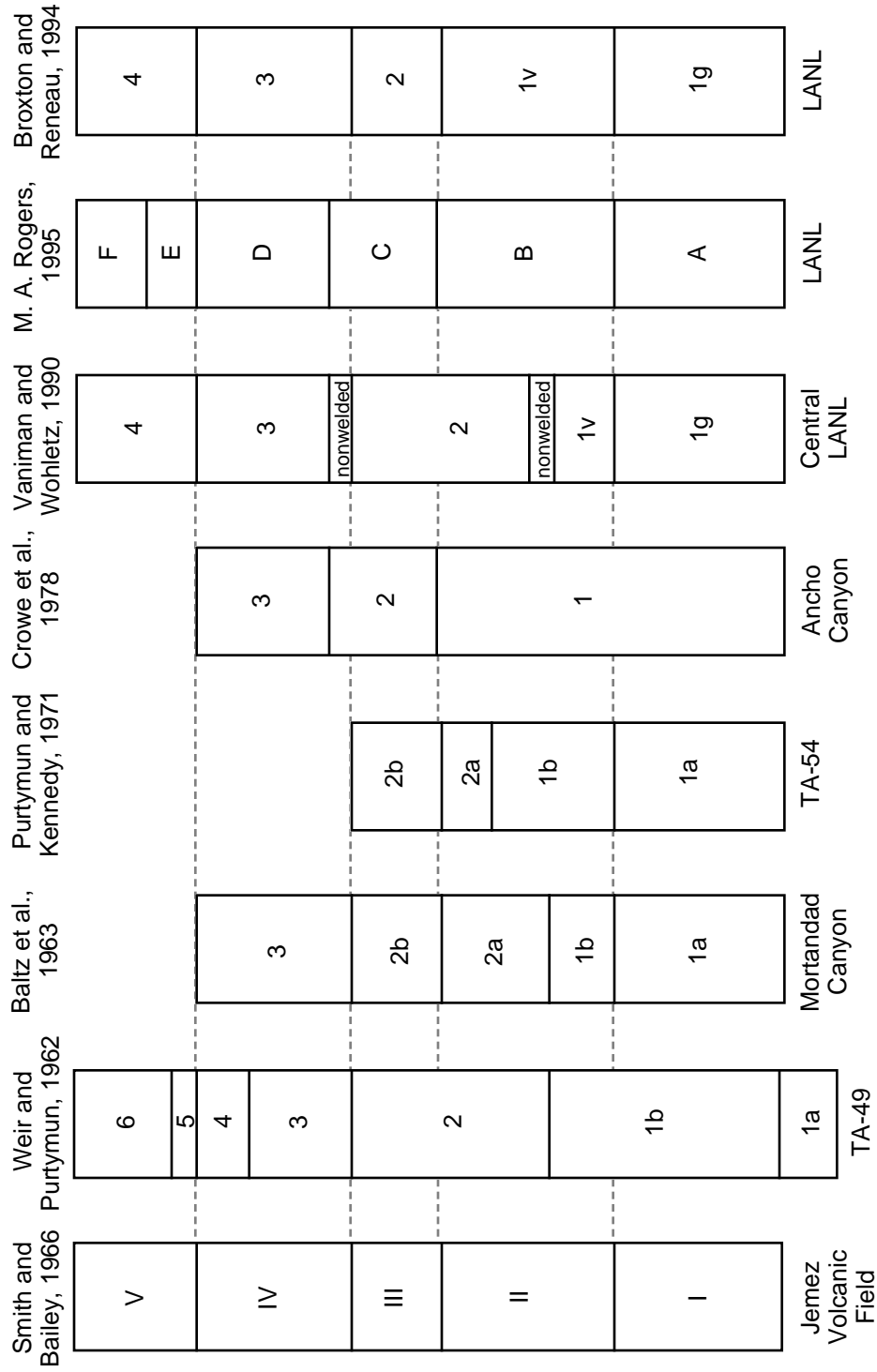
Figure 3. The various correlation schemes suggested for the Tshirege Member of the Bandelier Tuff (after Broxton and Reneau, 1994).
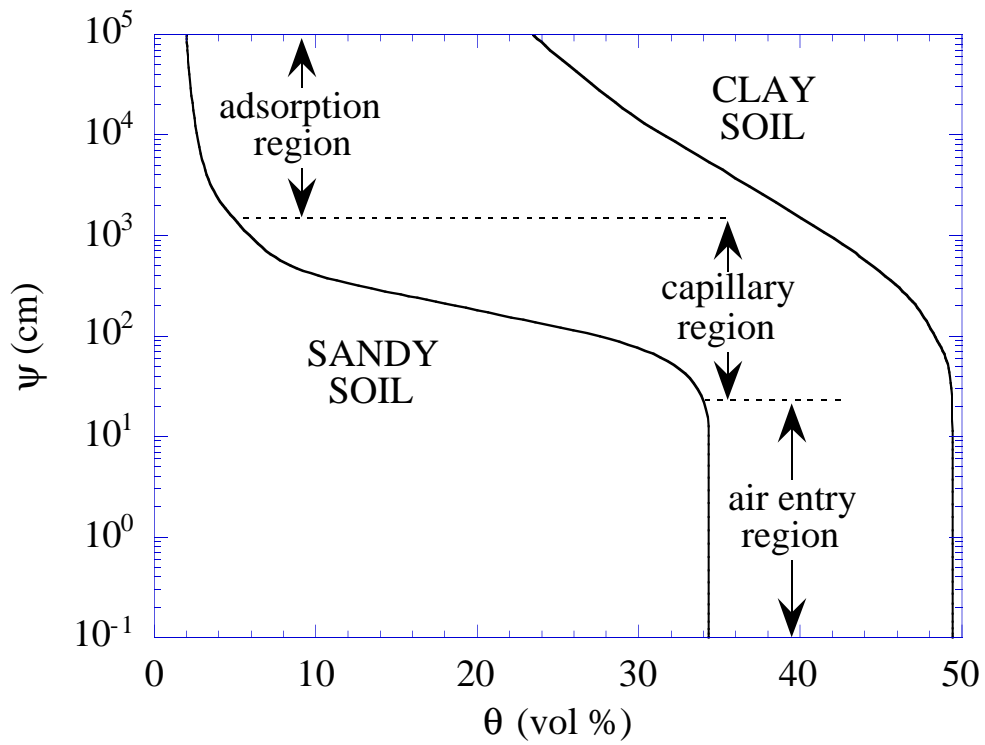
Figure 4. Idealized moisture retention curves (matric suction vs volumetric moisture content) for sandy soil and clayey soil, showing regions of the retention curve for sandy soil (after Figure 2.13 in Jury et al., 1991).

PC-4 104 ft Core Sample

P-16 17 ft Core Sample
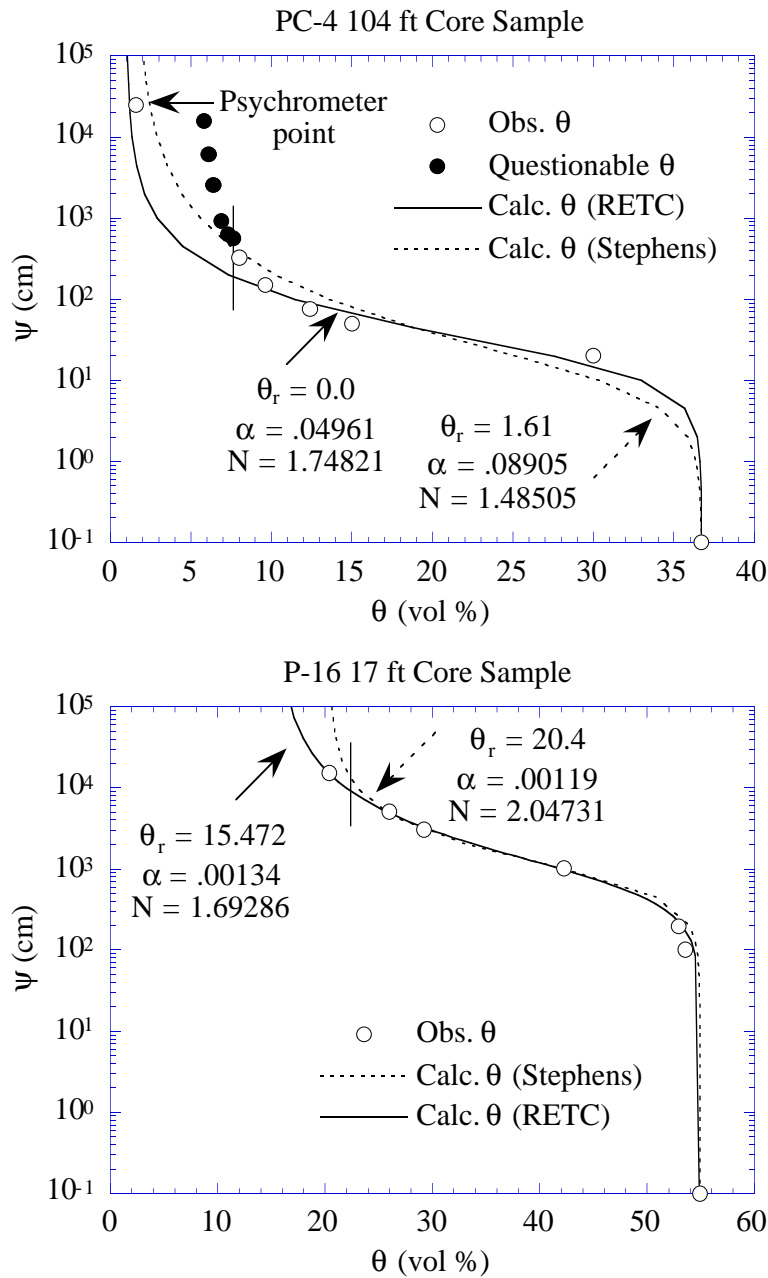
Figure 5. Example moisture retention curves showing (top) moisture retention data (black circles) which have not come to equilibrium above 0.5 bar (510 cm). The retention value at 3×10^4 cm is a psychrometer measurement. The in situ moisture content is indicated by the solid vertical line. (bottom) Moisture retention data for a case where no psychrometer values were obtained. Given the uncertainty with the pressure plate data near or above 1 bar (1020 cm), the dry portion of the retention curve is probably not well defined by the P-16 17 ft data set (bottom), leading to a high value of $\theta_r = 15.5\%$.
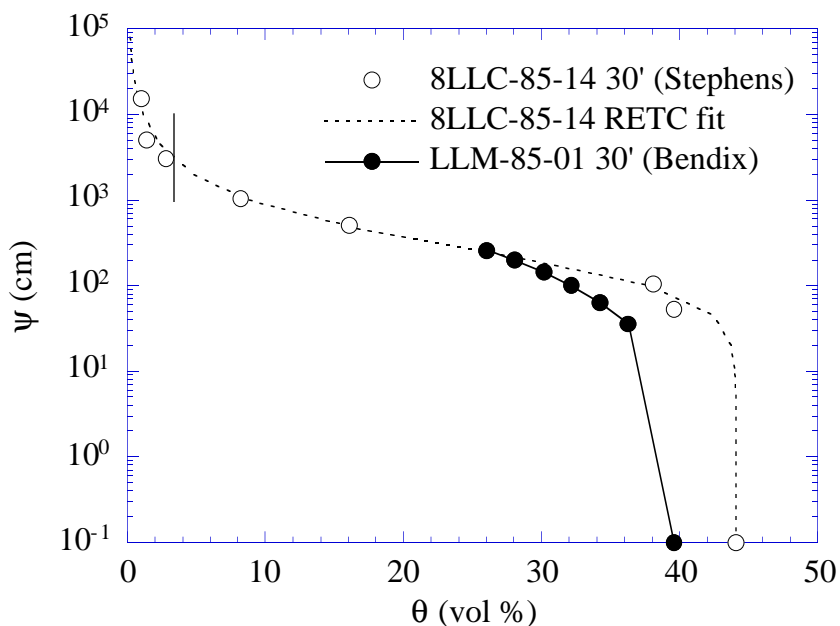
Figure 6. Comparison of moisture retention data for core from well LLM-85-01 at 30 ft (Kearl et al., 1986a) with data for nearby Area L well LLC-85-14 at 30 ft (sample no. 8LLC-85-14, Stephens et al., 1991c). The in situ moisture content is shown by the solid vertical line. The Bendix data cover only a small portion of the saturation range.
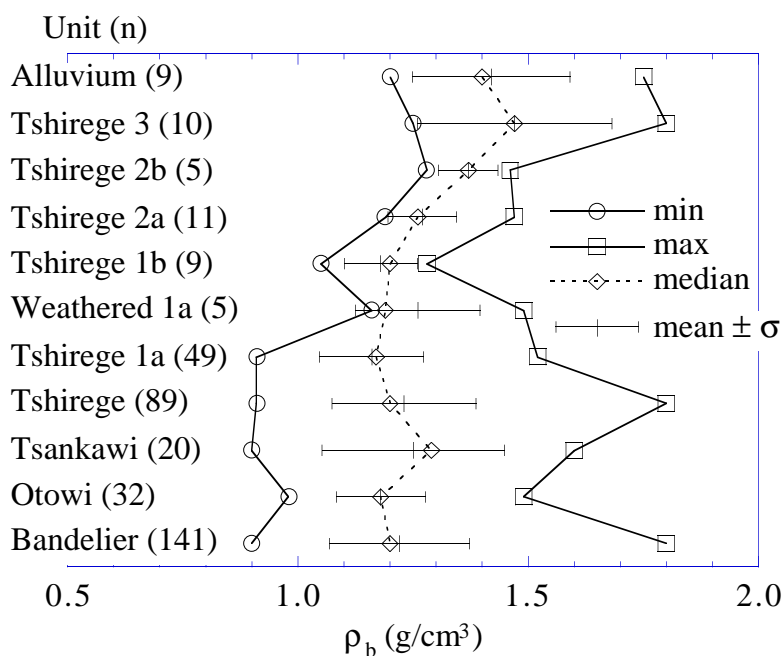
Figure 7. Statistical summary of bulk density data by member of the Bandelier Tuff and by unit for the Tshirege Member. The bulk density data come from reports by Daniel B. Stephens & Associates, Inc. The number of observations for each unit (n) is shown in parentheses.
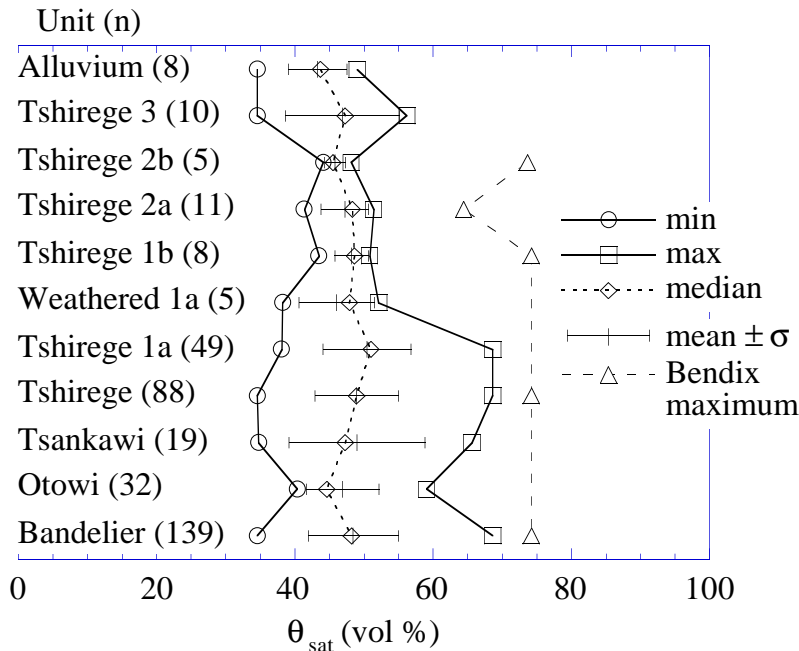
Figure 8. Statistical summary of saturated moisture content (porosity) data (of Daniel B. Stephens & Associates, Inc.) by member of the Bandelier Tuff and by unit for the Tshirege Member. The maximum porosity values from the Bendix data (Kearl et al., 1986a) are also shown. The number of (Stephens) observations for each unit (n) is shown in parentheses.
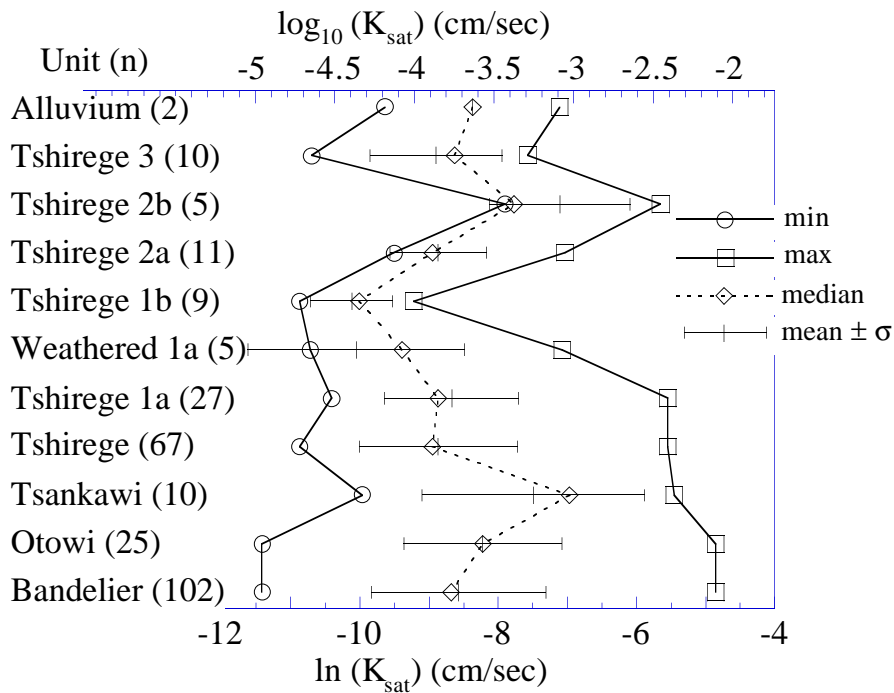
Figure 9. Statistical summary of log K_{sat} data (of Daniel B. Stephens & Associates, Inc.) by member of the Bandelier Tuff and by unit for the Tshirege Member. The number of observations for each unit (n) is shown in parentheses.
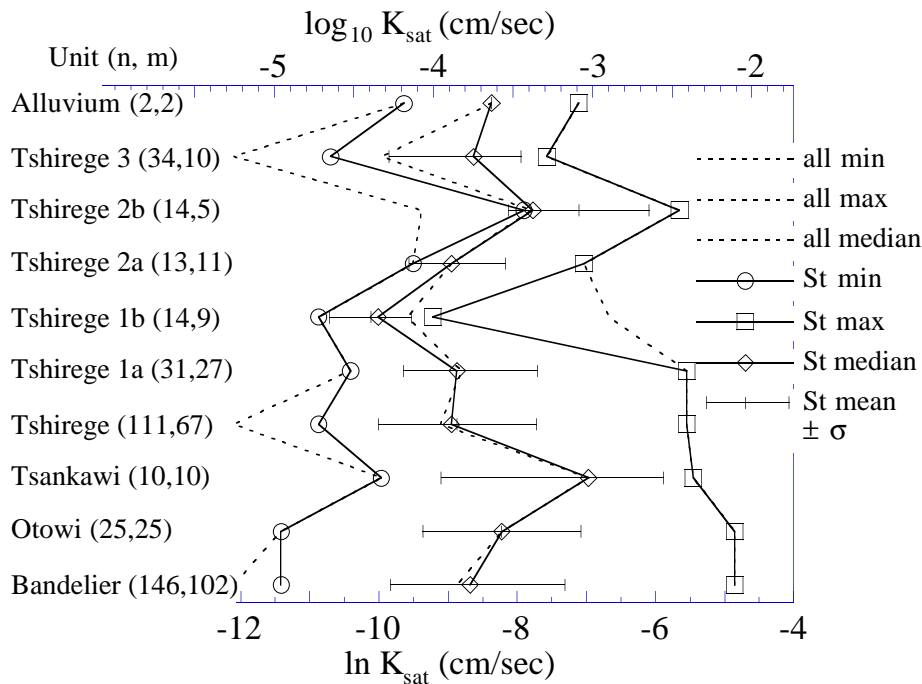
Figure 10. Statistical summary of log K_{sat} data of Daniel B. Stephens & Associates, Inc. (solid lines) and of the entire log K_{sat} data set (dashed lines) by member of the Bandelier Tuff and by unit for the Tshirege Member. The total number of observations for each unit (n), and the number due to Daniel B. Stephens & Associates, Inc. (m), are shown in parentheses.
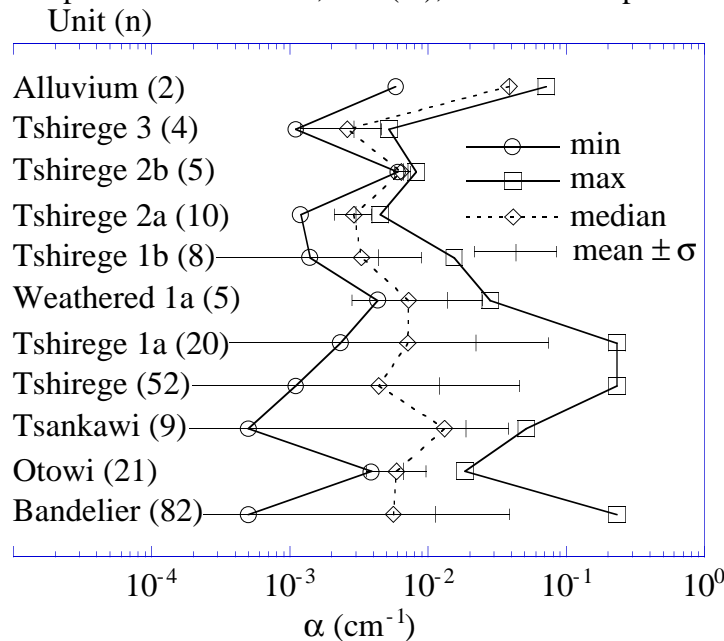
Figure 11. Statistical summary of the van Genuchten parameter α by member of the Bandelier Tuff and by unit for the Tshirege Member. All of the values are based on analyses of moisture retention data from Daniel B. Stephens & Associates, Inc. The number of observations for each unit (n) is shown in parentheses.
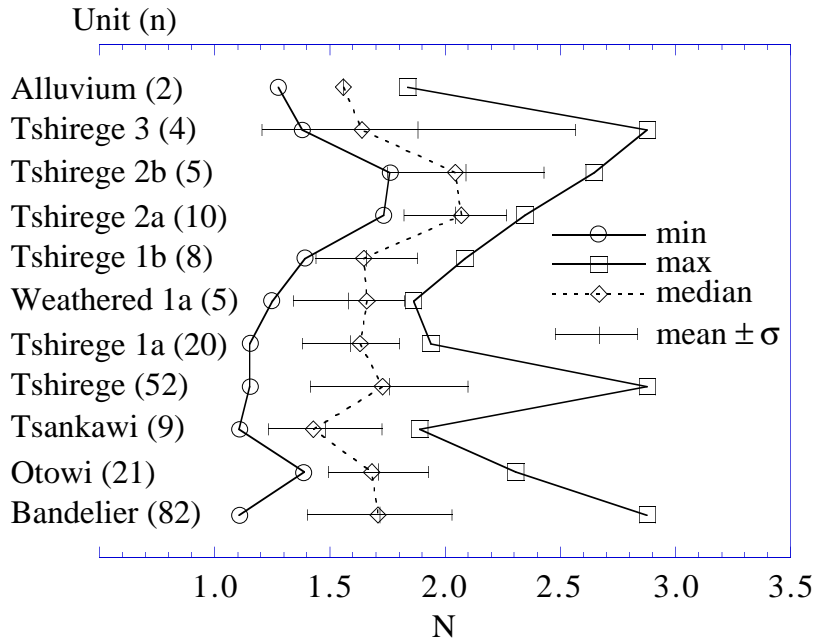
Figure 12. Statistical summary of the van Genuchten parameter N by member of the Bandelier Tuff and by unit for the Tshirege Member. All of the values are based on analyses of moisture retention data from Daniel B. Stephens & Associates, Inc. The number of observations for each unit (n) is shown in parentheses.
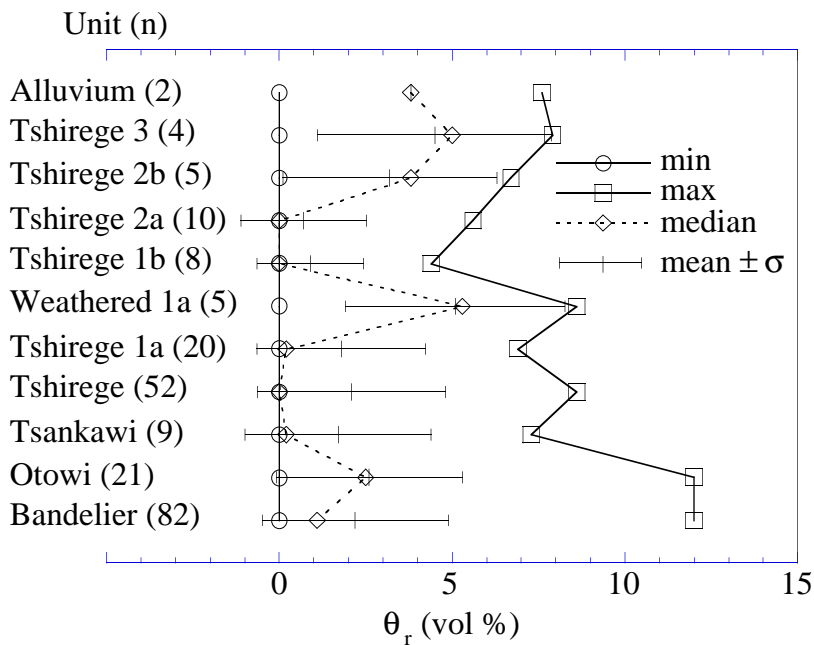
Figure 13. Statistical summary of the residual moisture content (van Genuchten parameter θ_r) by member of the Bandelier Tuff and by unit for the Tshirege Member. All of the values are based on analyses of moisture retention data from Daniel B. Stephens & Associates, Inc. The number of observations for each unit (n) is shown in parentheses.
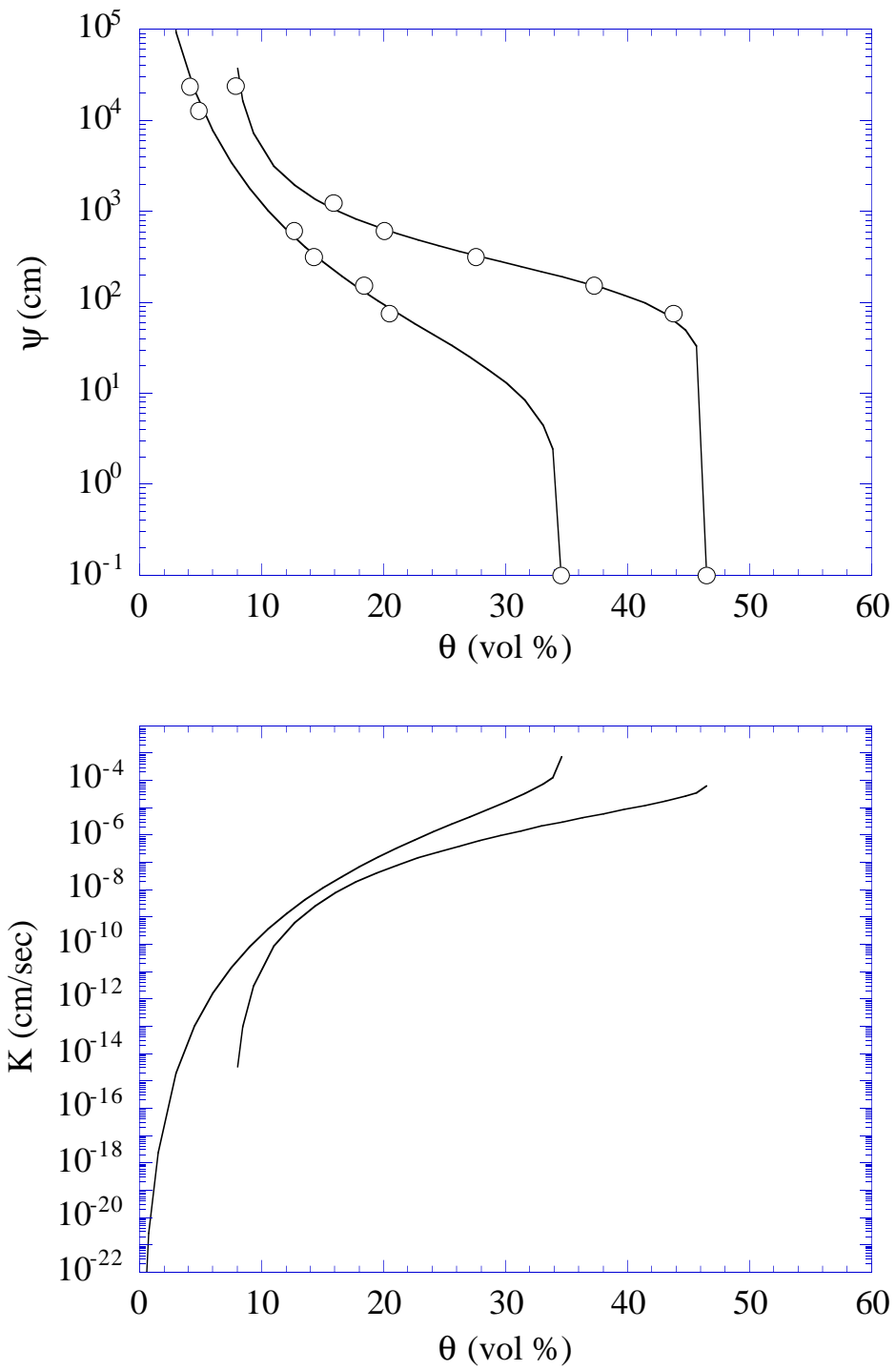
Figure 14. Composite of moisture characteristic (top) and unsaturated hydraulic conductivity (bottom) curves for the Alluvium.
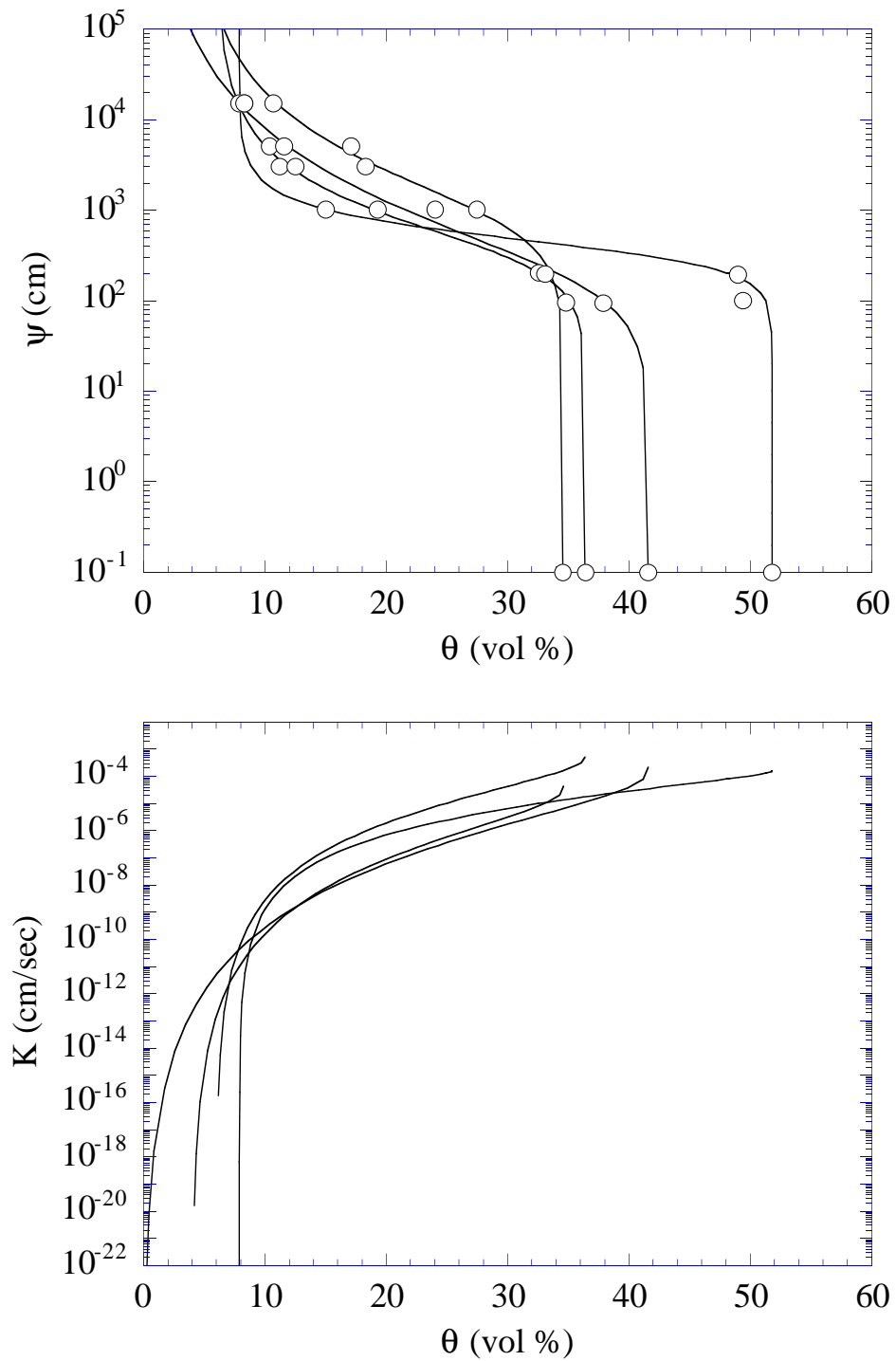
Figure 15. Composite of moisture characteristic (top) and unsaturated hydraulic conductivity (bottom) curves for Unit 3 of the Tshirege Member of the Bandelier Tuff.
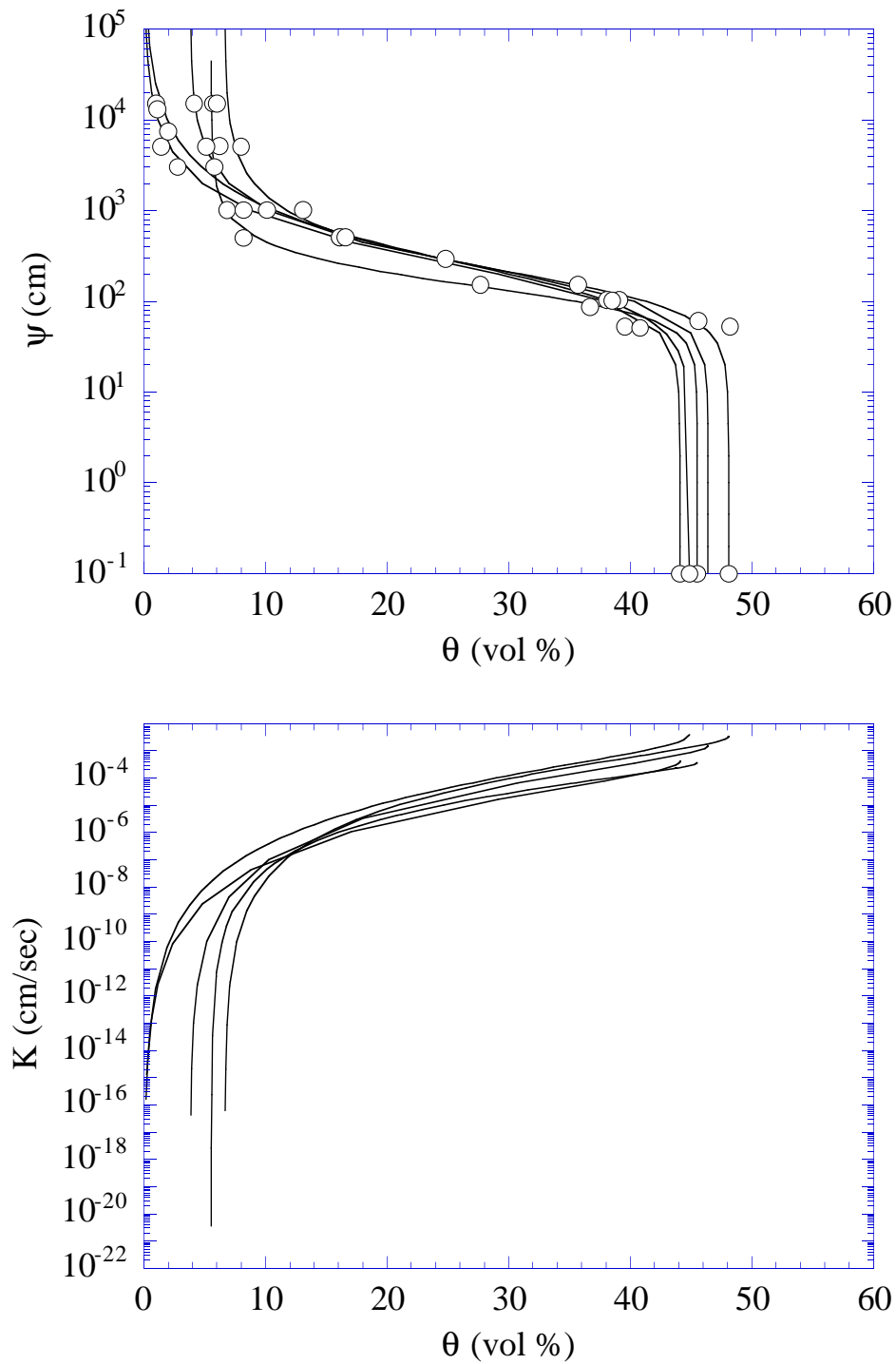
Figure 16. Composite of moisture characteristic (top) and unsaturated hydraulic conductivity (bottom) curves for Unit 2b of the Tshirege Member of the Bandelier Tuff.
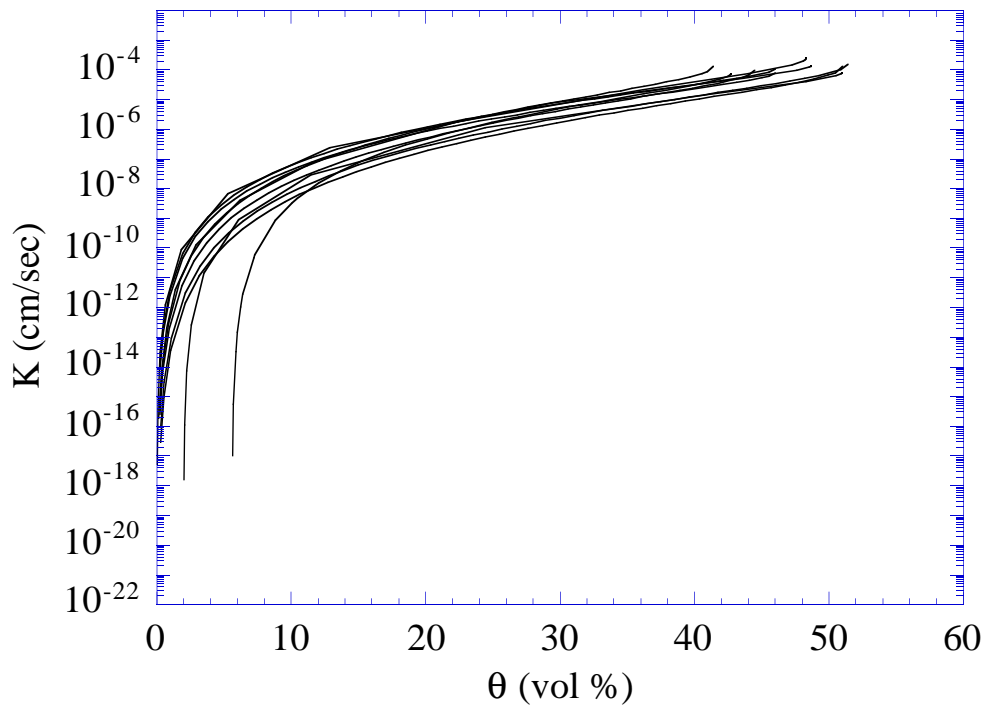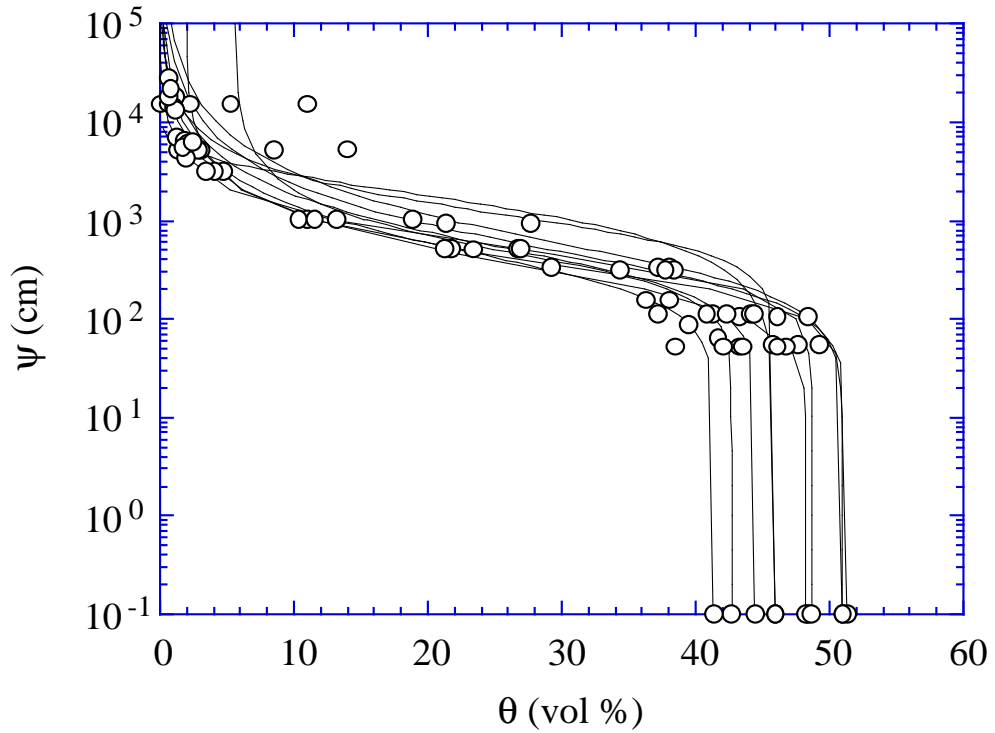
Figure 17. Composite of moisture characteristic (top) and unsaturated hydraulic conductivity (bottom) curves for Unit 2a of the Tshirege Member of the Bandelier Tuff.
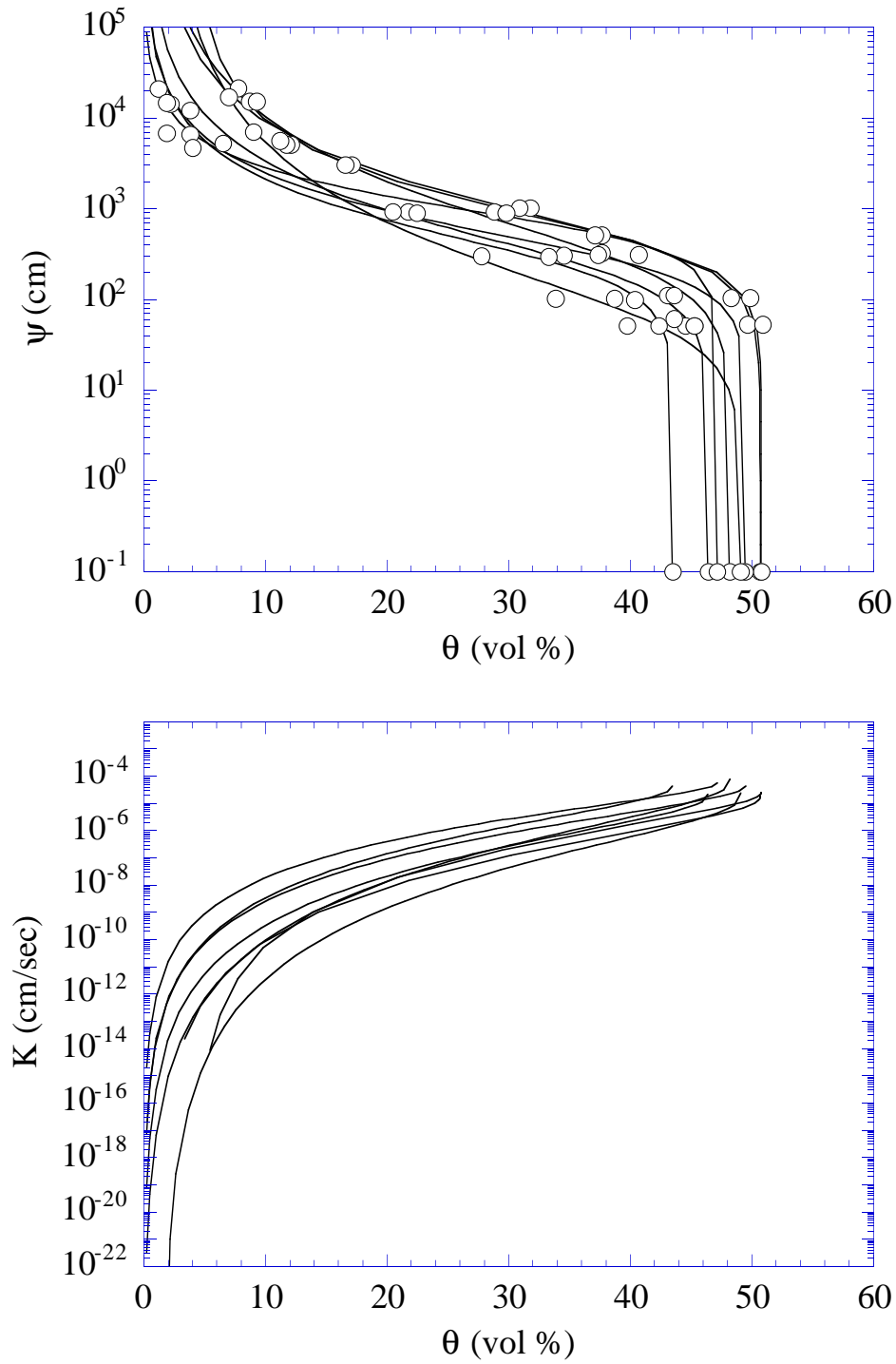
Figure 18. Composite of moisture characteristic (top) and unsaturated hydraulic conductivity (bottom) curves for Unit 1b of the Tshirege Member of the Bandelier Tuff.
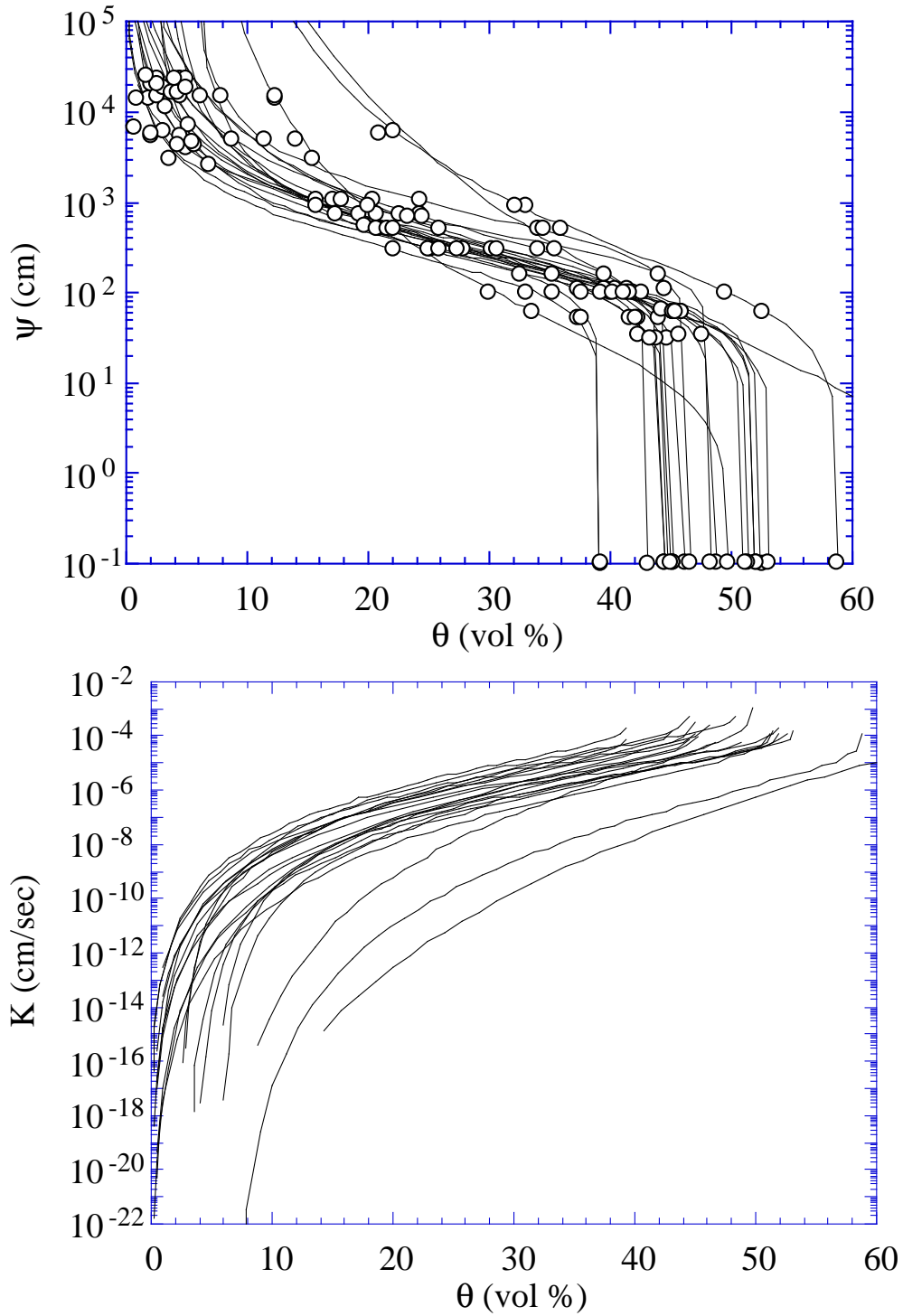
Figure 19. Composite of moisture characteristic (top) and unsaturated
hydraulic conductivity (bottom) curves for Unit 1a of the Tshirege
Member of the Bandelier Tuff.
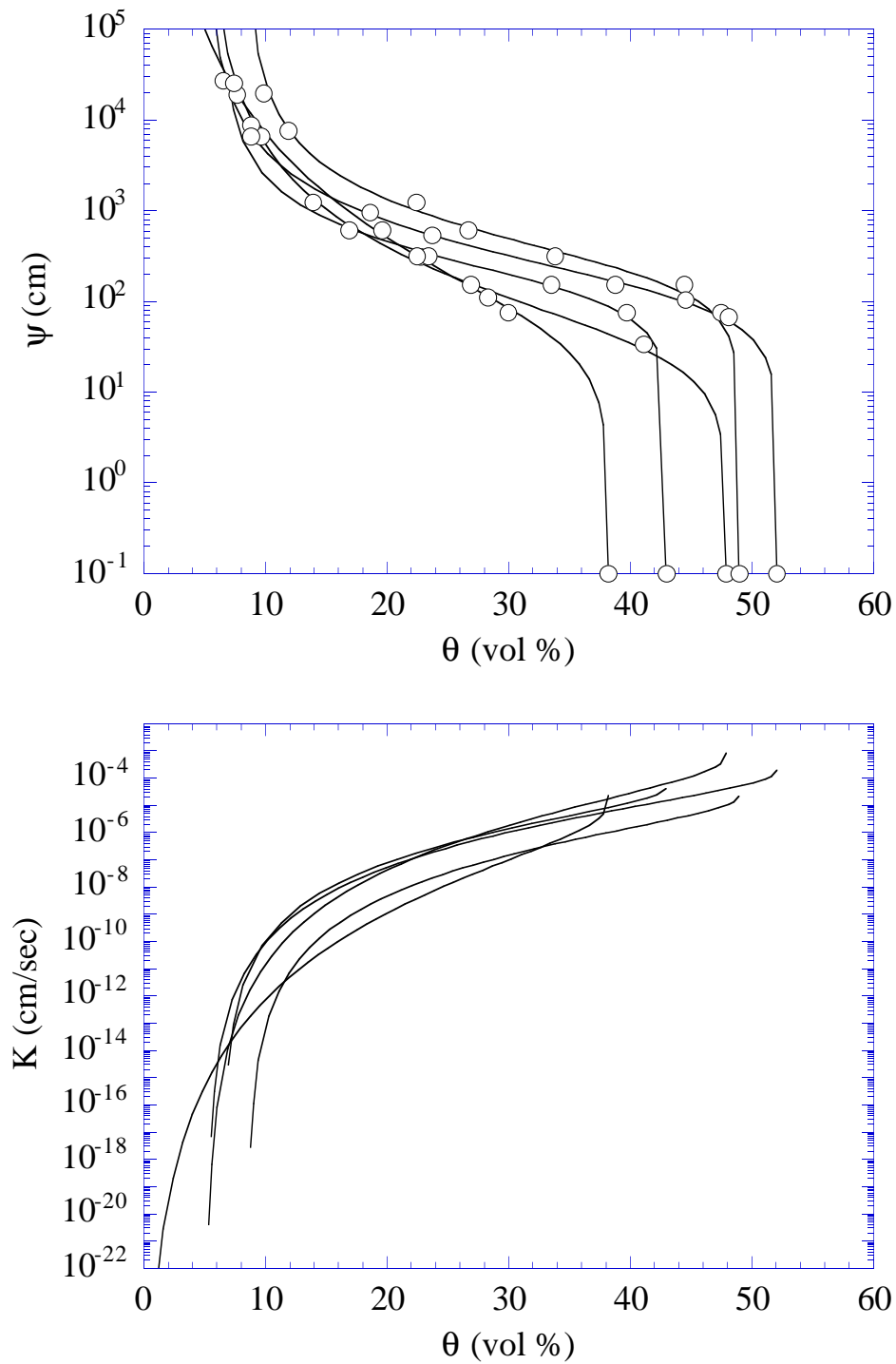
Figure 20. Composite of moisture characteristic (top) and unsaturated hydraulic conductivity (bottom) curves for Weathered Unit 1a of the Tshirege Member of the Bandelier Tuff.
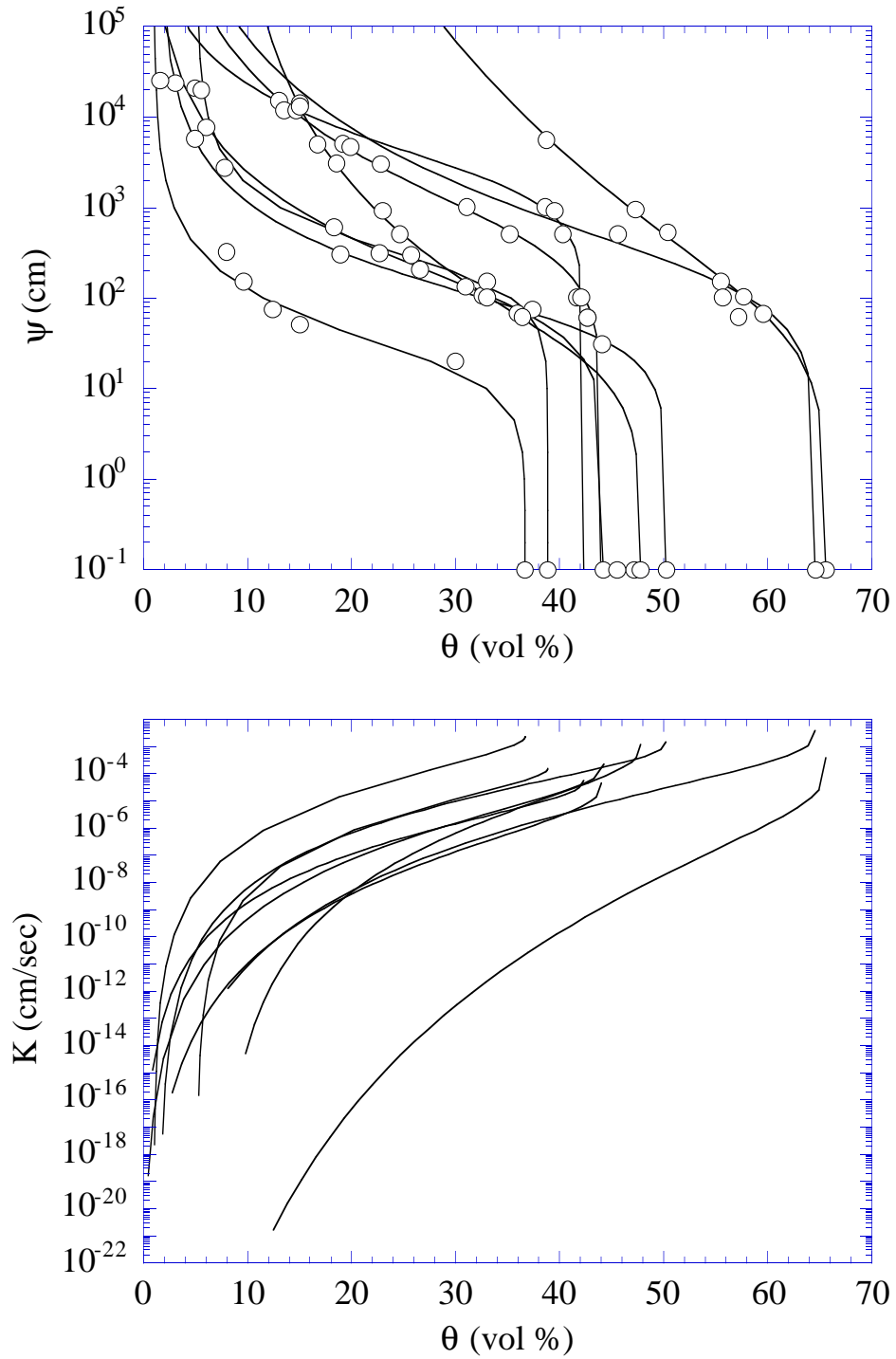
Figure 21. Composite of moisture characteristic (top) and unsaturated hydraulic conductivity (bottom) curves for the Tsankawi/Cerro Toledo Member of the Bandelier Tuff.
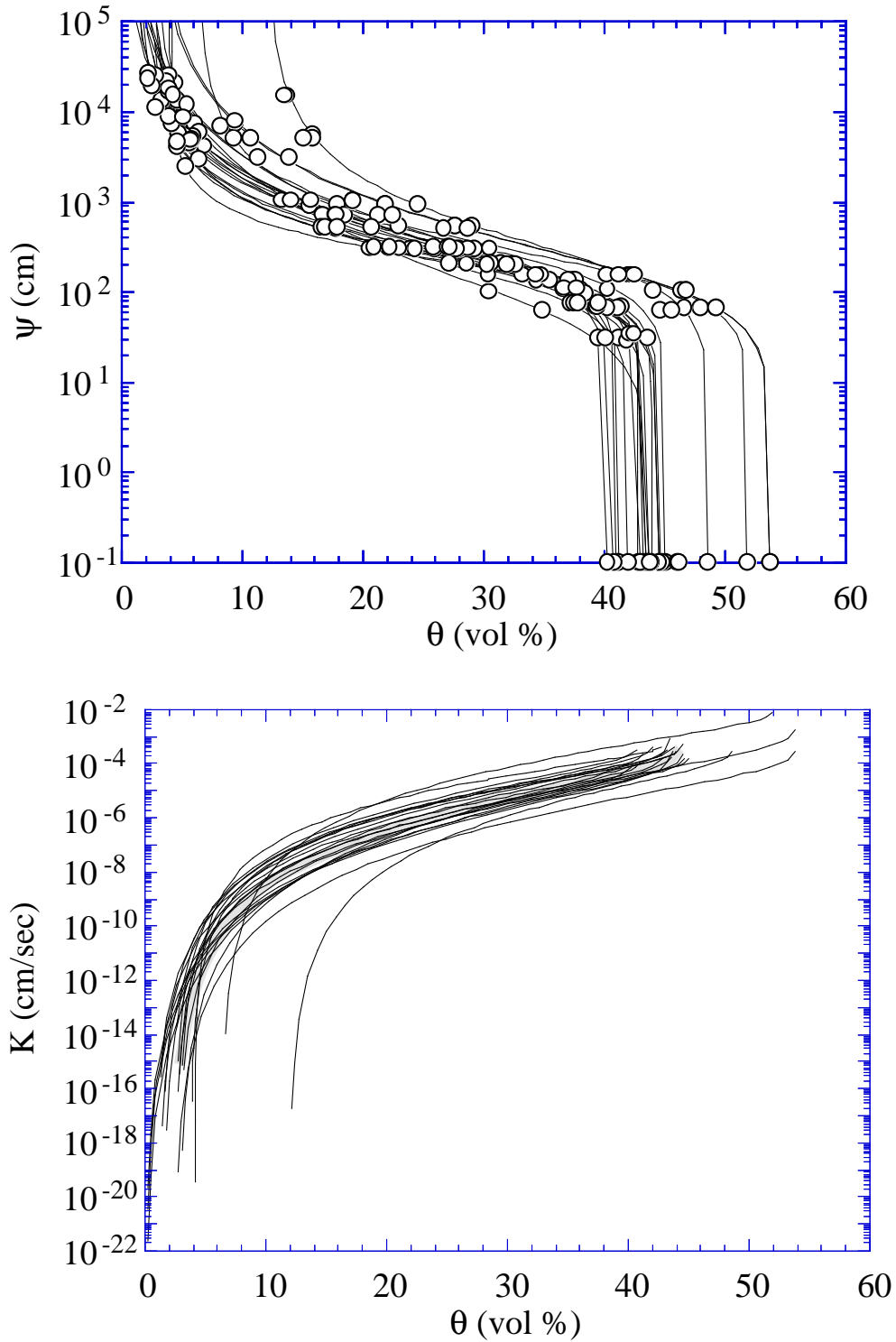
Figure 22. Composite of moisture characteristic (top) and unsaturated hydraulic conductivity (bottom) curves for the Otowi Member of the Bandelier Tuff.
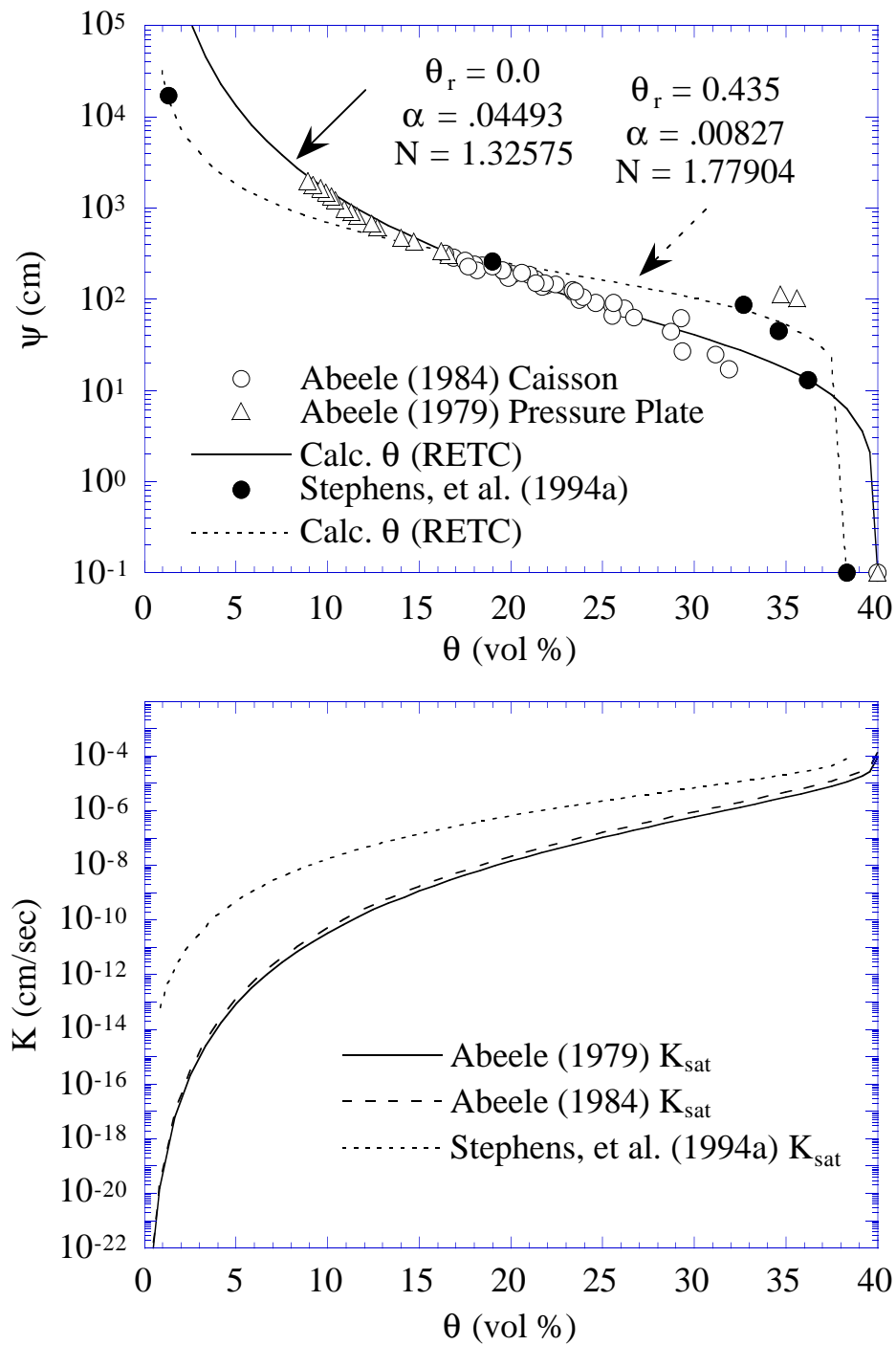
Figure 23. Composite of moisture characteristic (top) and unsaturated hydraulic conductivity (bottom) curves for samples of crushed Bandelier Tuff.
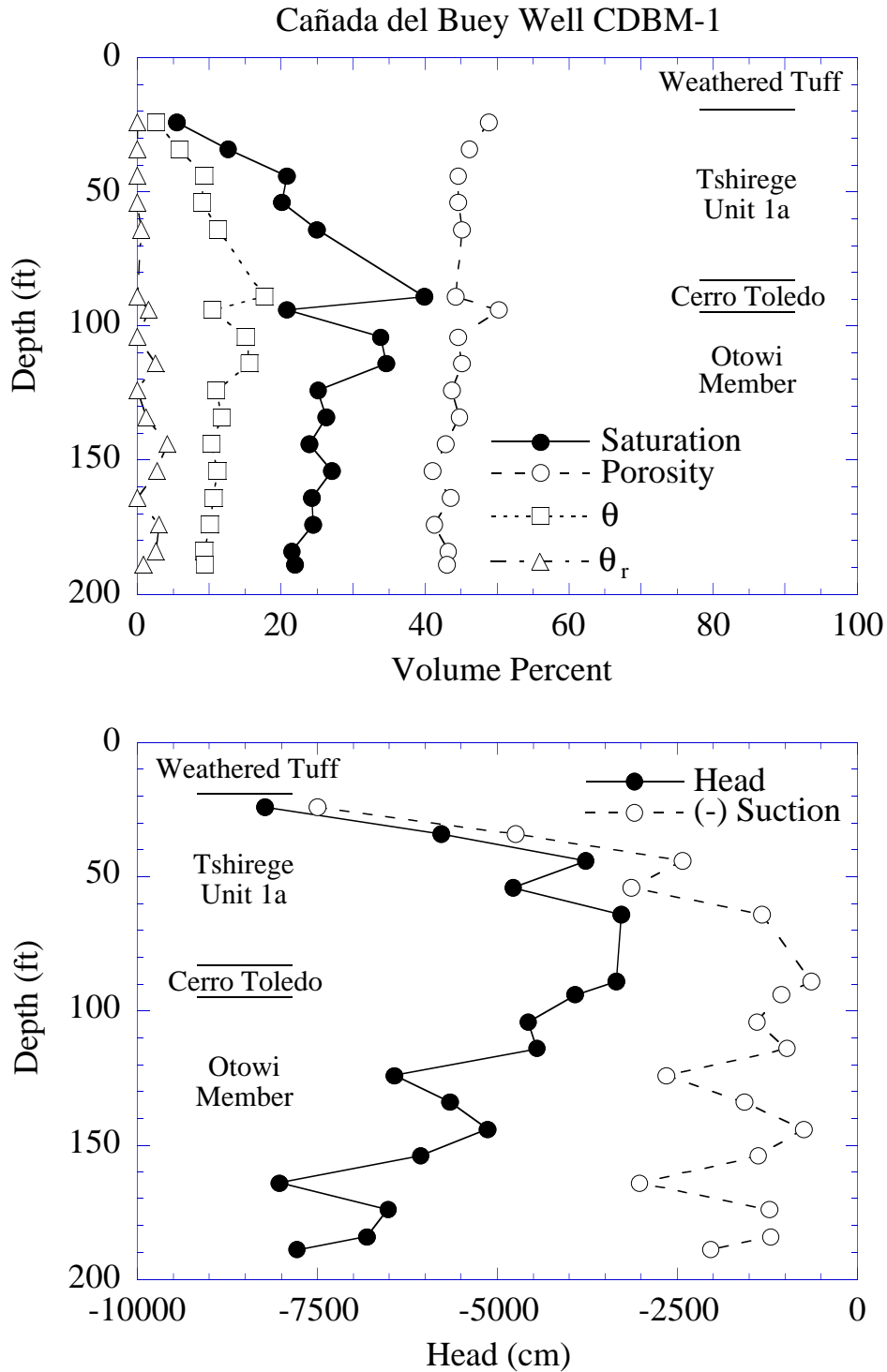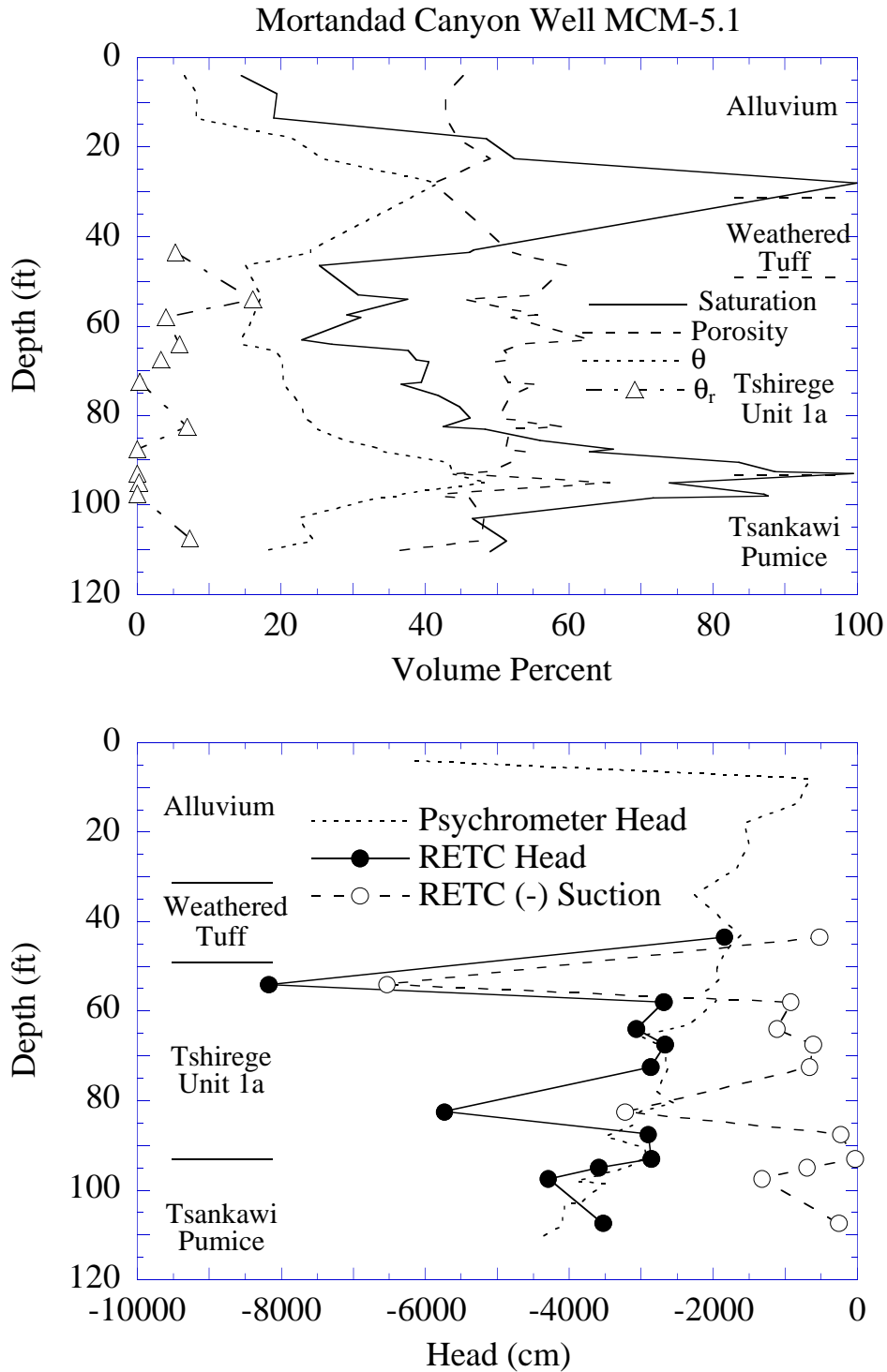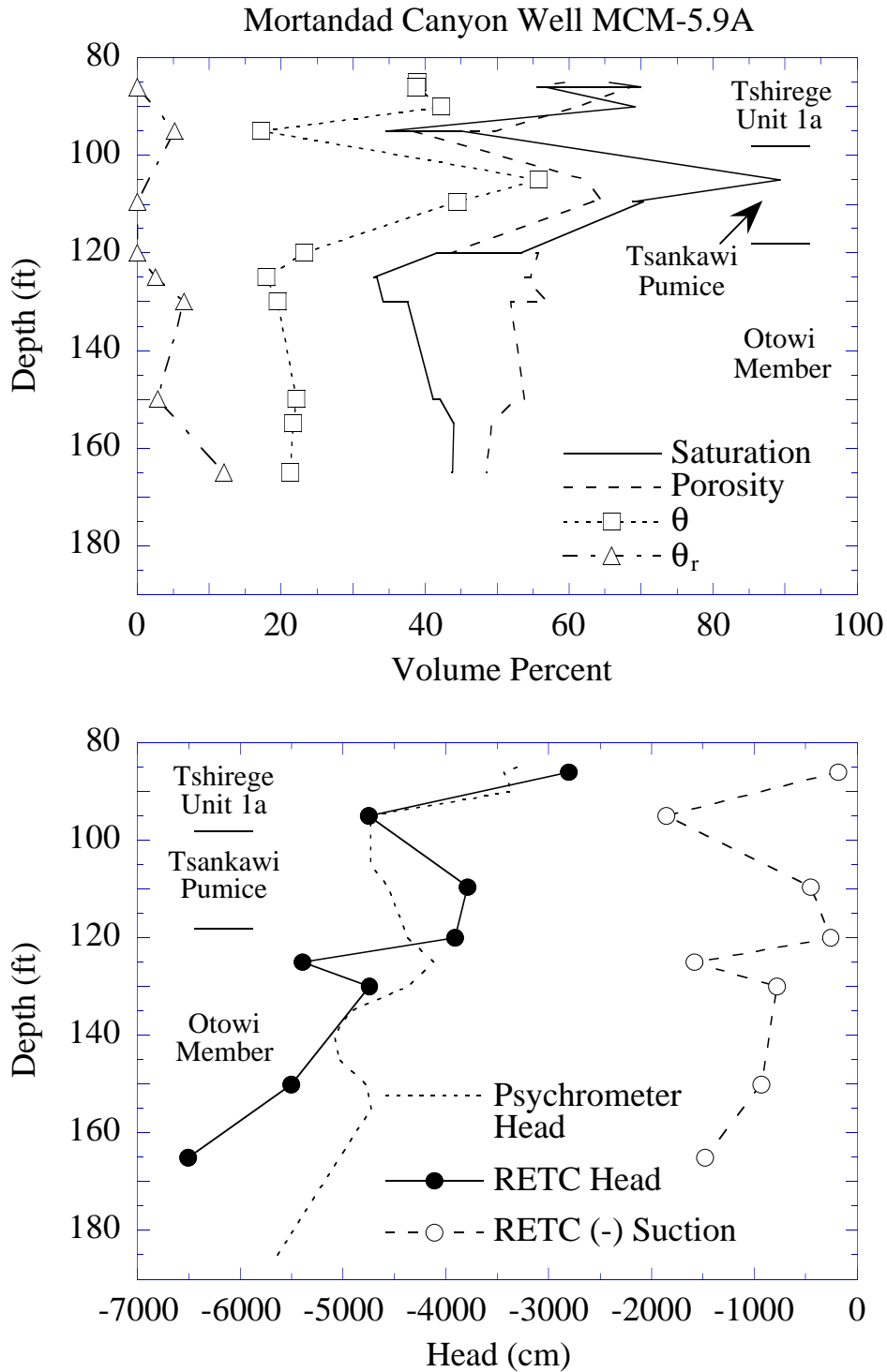
Figure 24. Cañada del Buey borehole CDBM-1 core sample depth profiles of (top) saturation, porosity, volumetric moisture content, and residual moisture content; and (bottom) head and (-) suction at in situ moisture content.
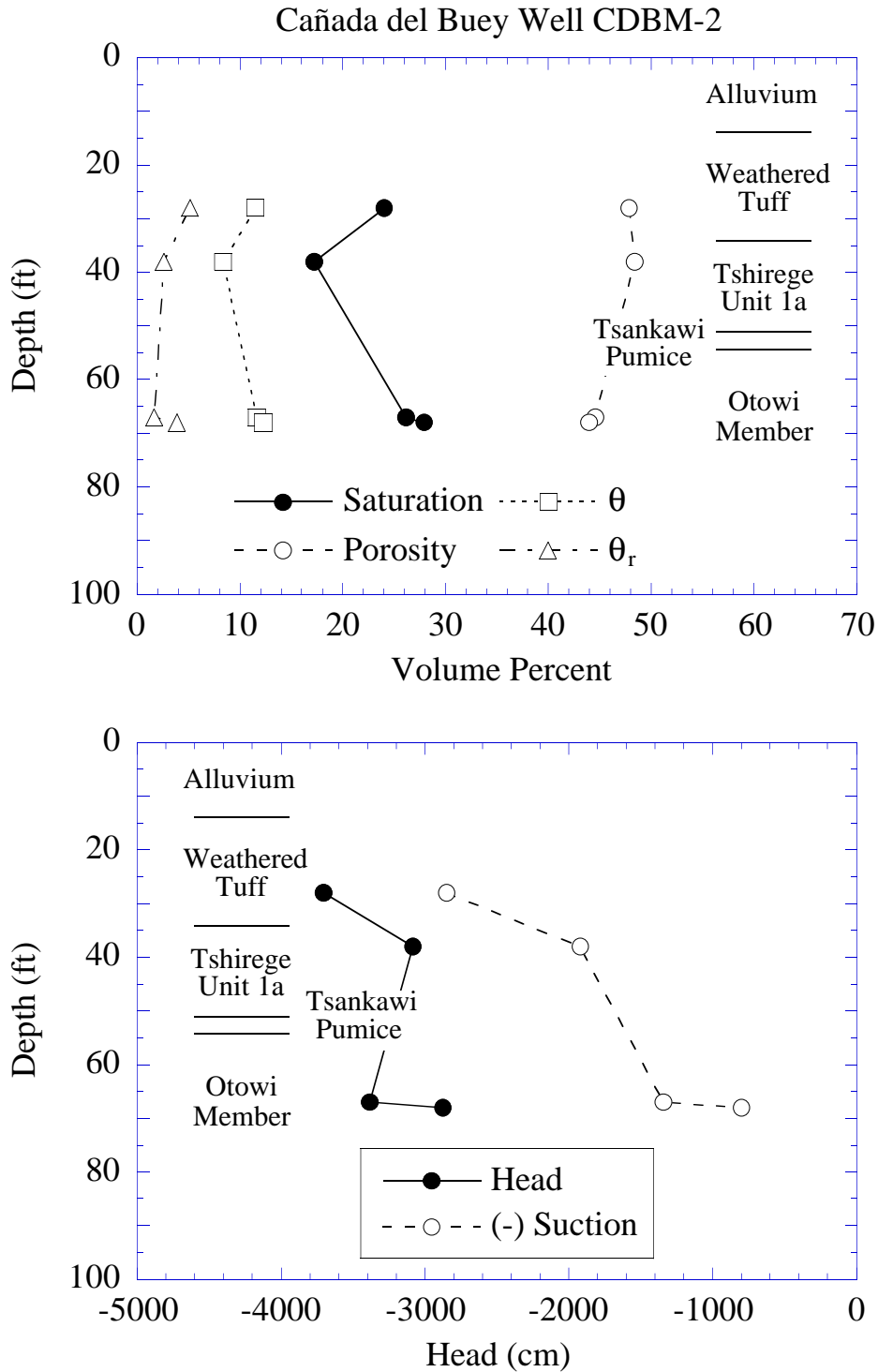
Figure 25. Cañada del Buey borehole CDBM-2 core sample depth profiles of (top) saturation, porosity, volumetric moisture content, and residual moisture content; and (bottom) head and (-) suction at in situ moisture content.
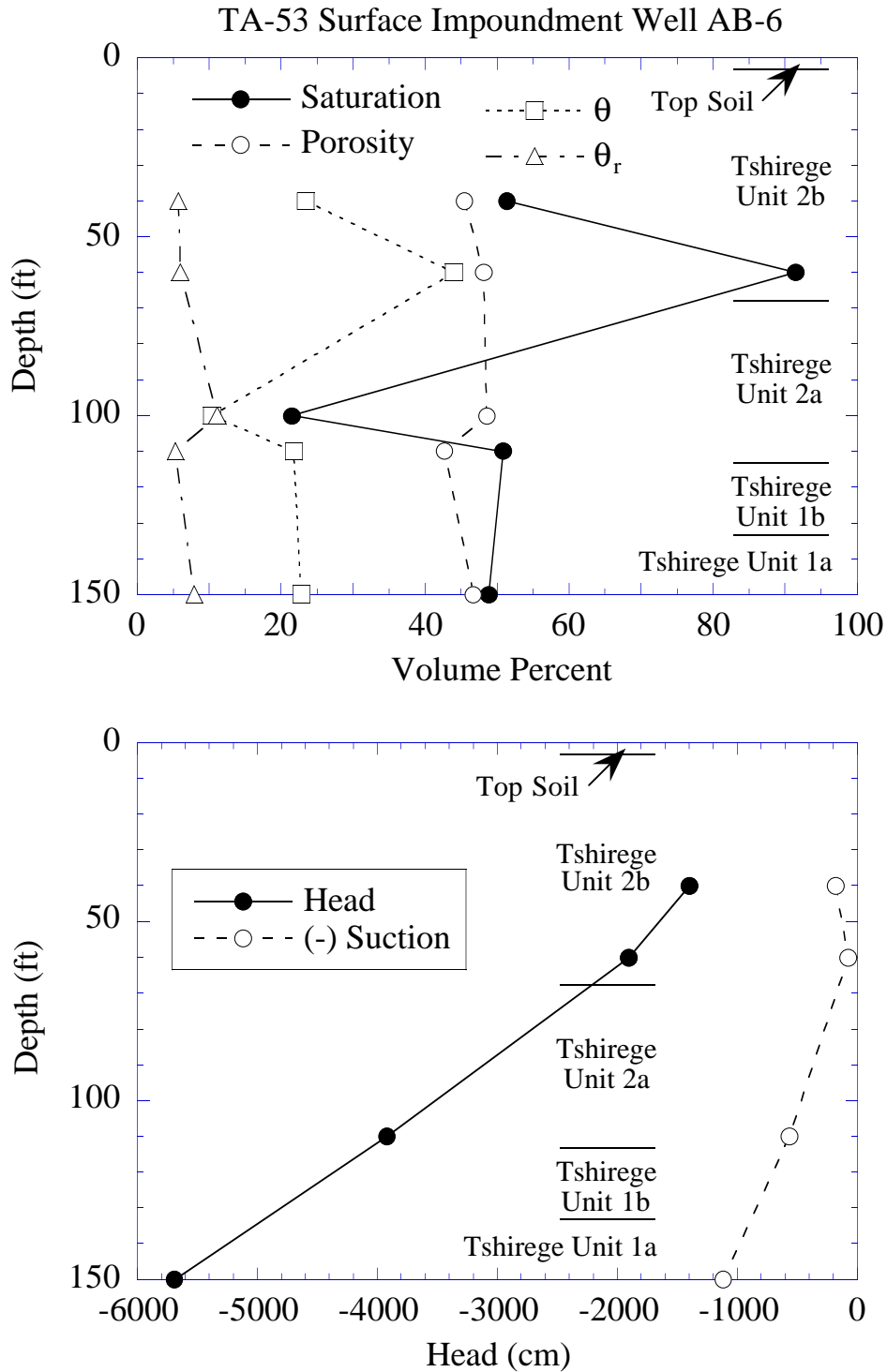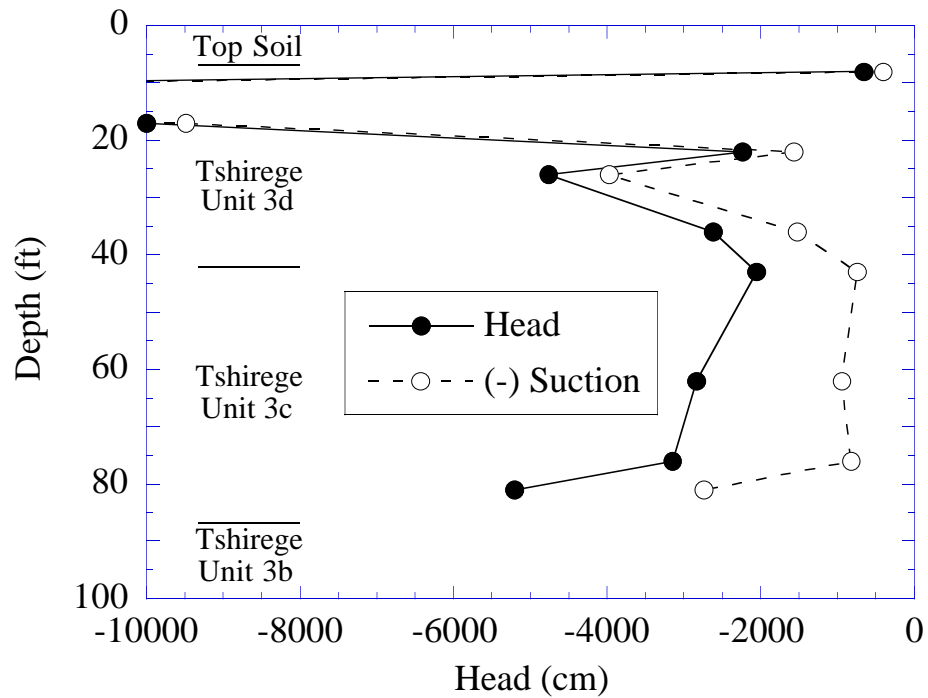
Figure 26. TA-53 borehole AB-6 core sample depth profiles of (top) saturation, porosity, volumetric moisture content, and residual moisture content; and (bottom) head and (-) suction at in situ moisture content.
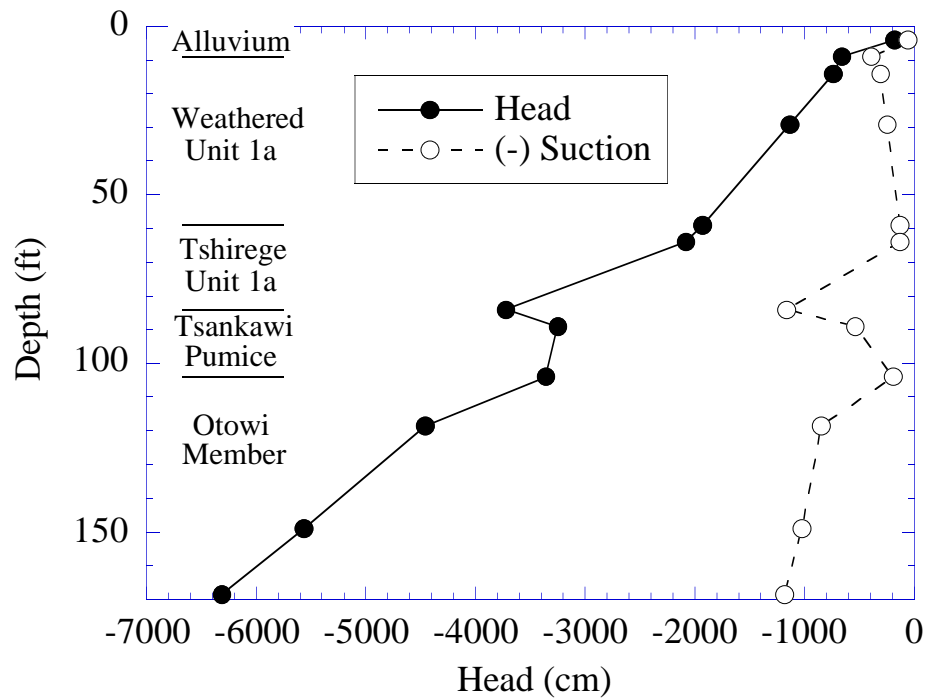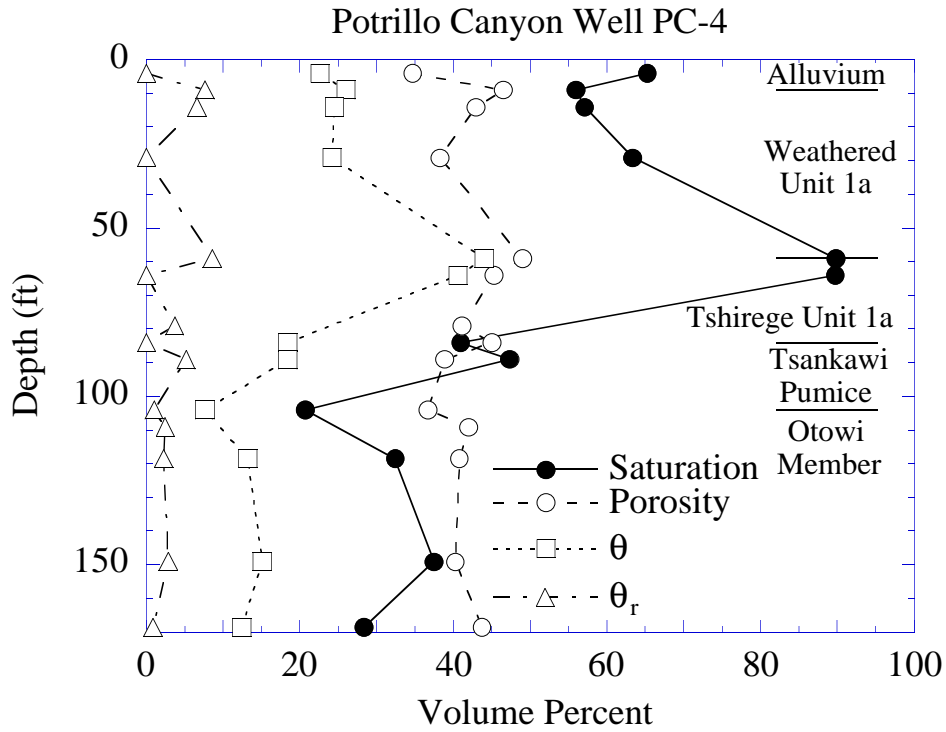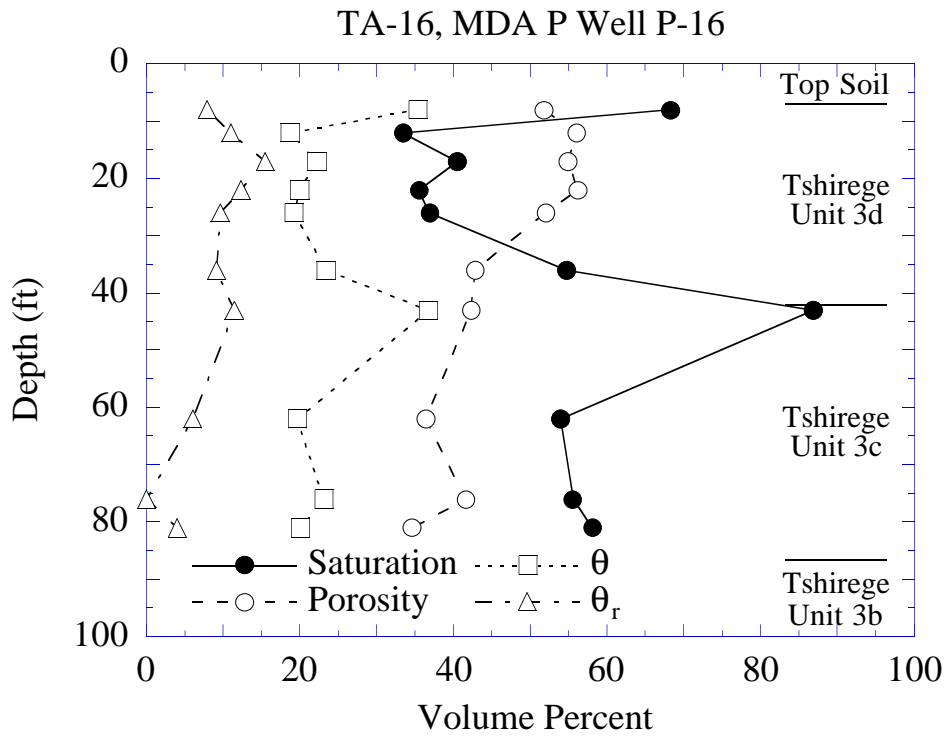
Figure 27. Potrillo Canyon borehole PC-4 core sample depth profiles of (top) saturation, porosity, volumetric moisture content, and residual moisture content; and (bottom) head and (-) suction at in situ moisture content.
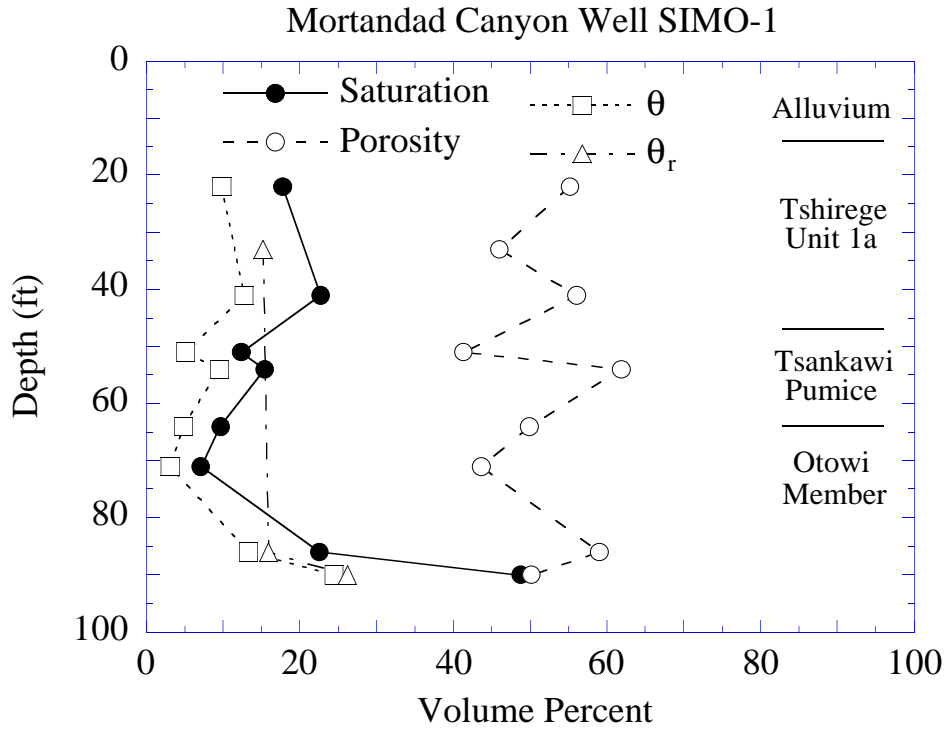
Figure 28. Mortandad Canyon borehole SIMO-1 core sample depth profiles of saturation, porosity, volumetric moisture content, and residual moisture content.

Mortandad Canyon Well MCM-5.1

Figure 29. Mortandad Canyon borehole MCM-5.1 core sample depth profiles of (top) saturation, porosity, volumetric moisture content, and residual moisture content; and (bottom) head and (-) suction (from retention curve) at in situ moisture content and sample psychrometer head.

Mortandad Canyon Well MCM-5.9A

Figure 30. Mortandad Canyon borehole MCM-5.9A core sample depth profiles of (top) saturation, porosity, volumetric moisture content, and residual moisture content; and (bottom) head and (-) suction (from retention curve) at in situ moisture content and sample psychometer head.
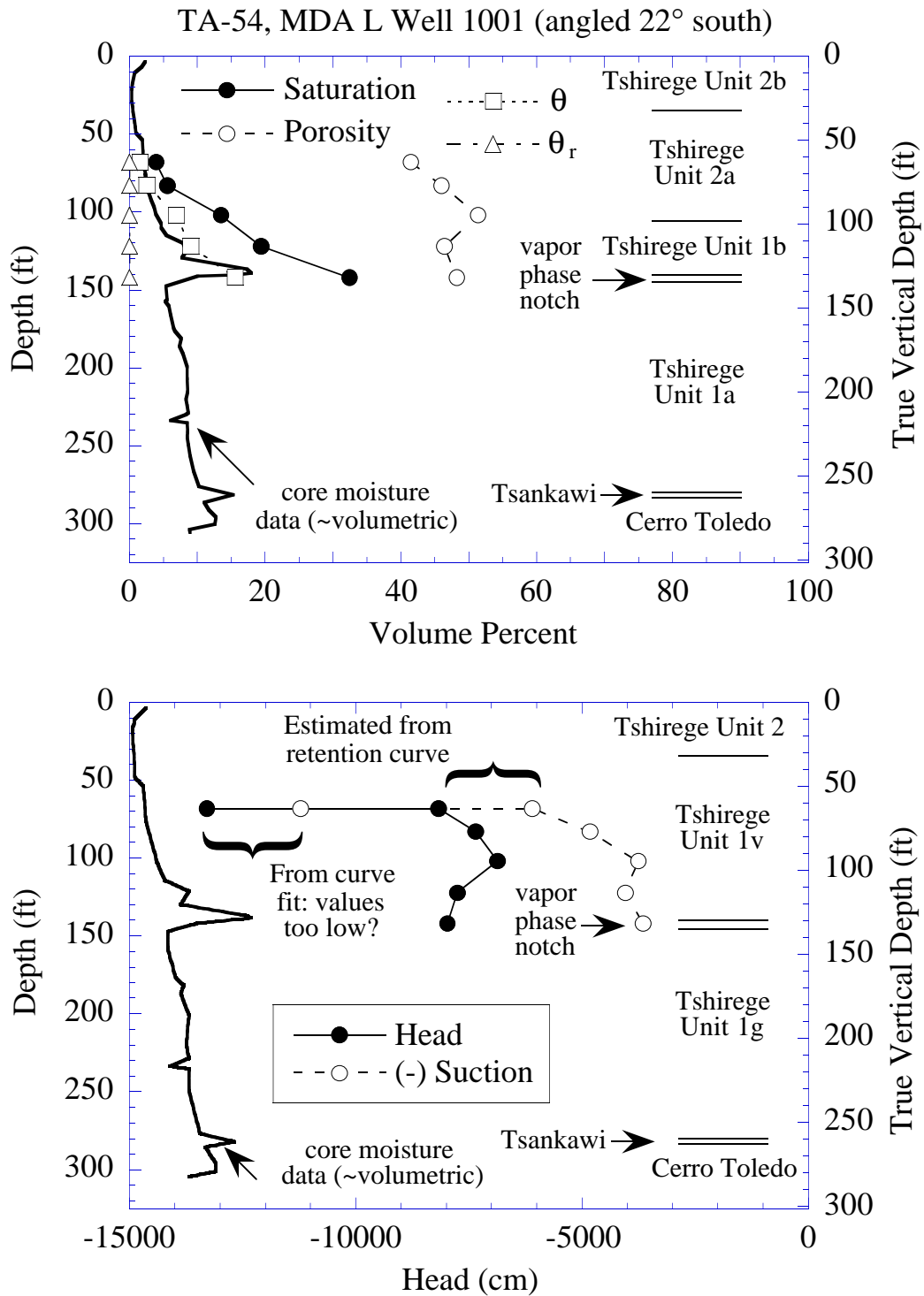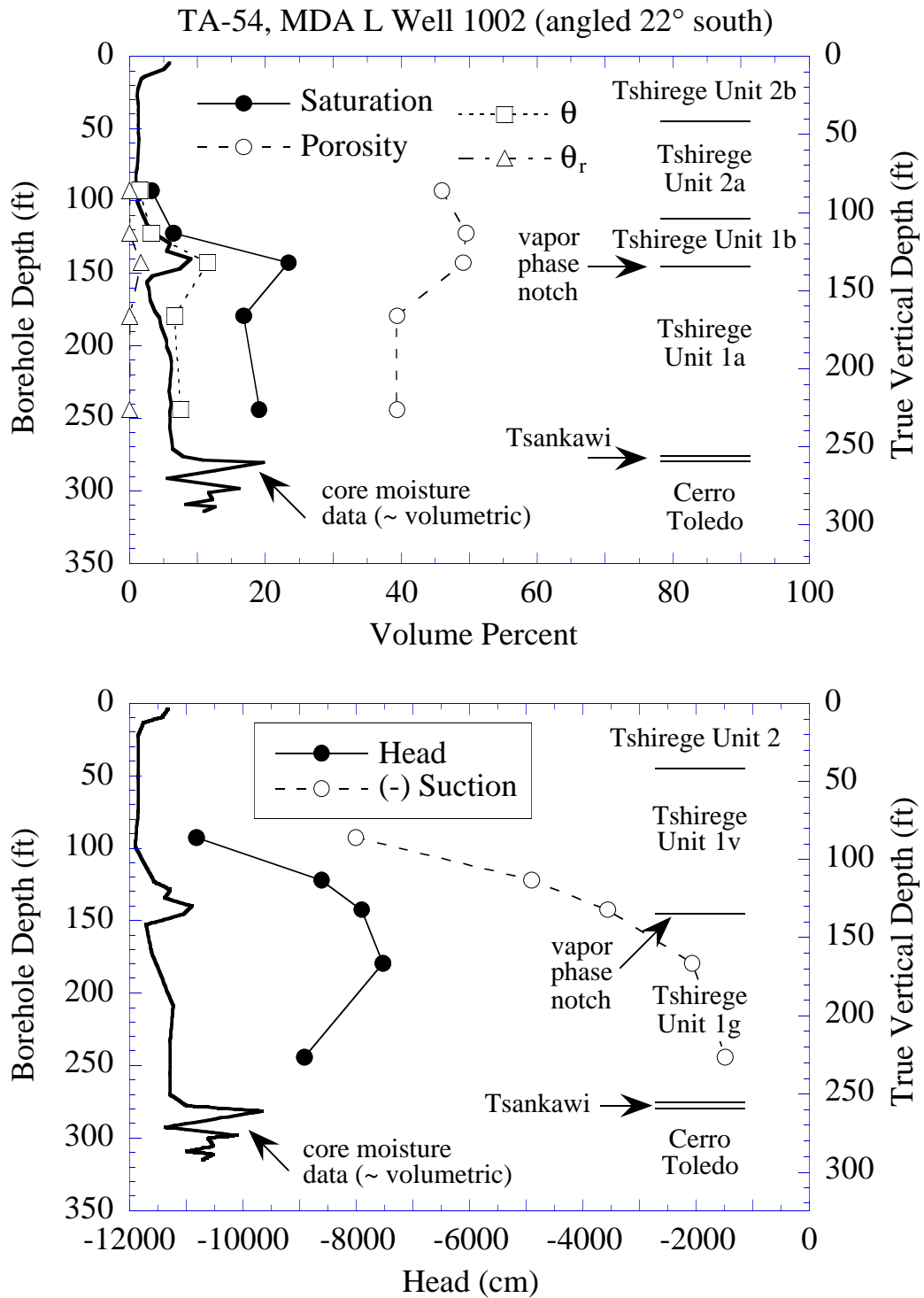
Figure 31. TA-16, MDA P borehole P-16 core sample depth profiles of (top) saturation, porosity, volumetric moisture content, and residual moisture content; and (bottom) head and (-) suction at in situ moisture content. Due to lack of psychrometer measurements to define the dry part of the retention curves, the suction and head values at low moisture contents are unreliable.

Figure 32. TA-54, MDA L borehole 54-1001 core sample depth profiles of (top) saturation, porosity, volumetric moisture content, and residual moisture content (with the addition of the core moisture data for the borehole); and (bottom) head and (-) suction at in situ moisture content.
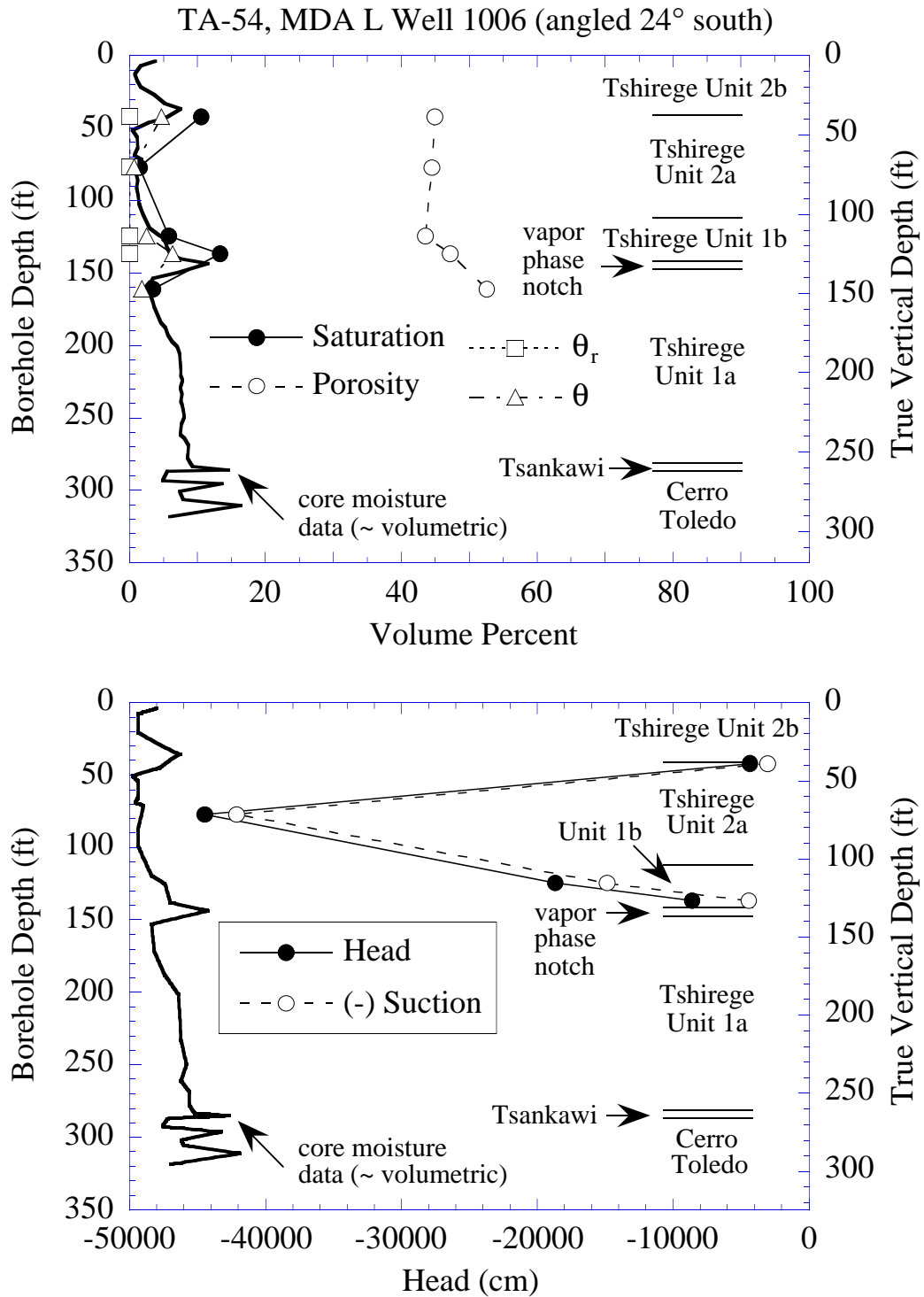
Figure 33. Borehole TA-54, MDA L borehole 54-1002 core sample depth profiles of (top) saturation, porosity, volumetric moisture content, and residual moisture content (with the addition of the core moisture data for the borehole); and (bottom) head and (-) suction at in situ moisture content.
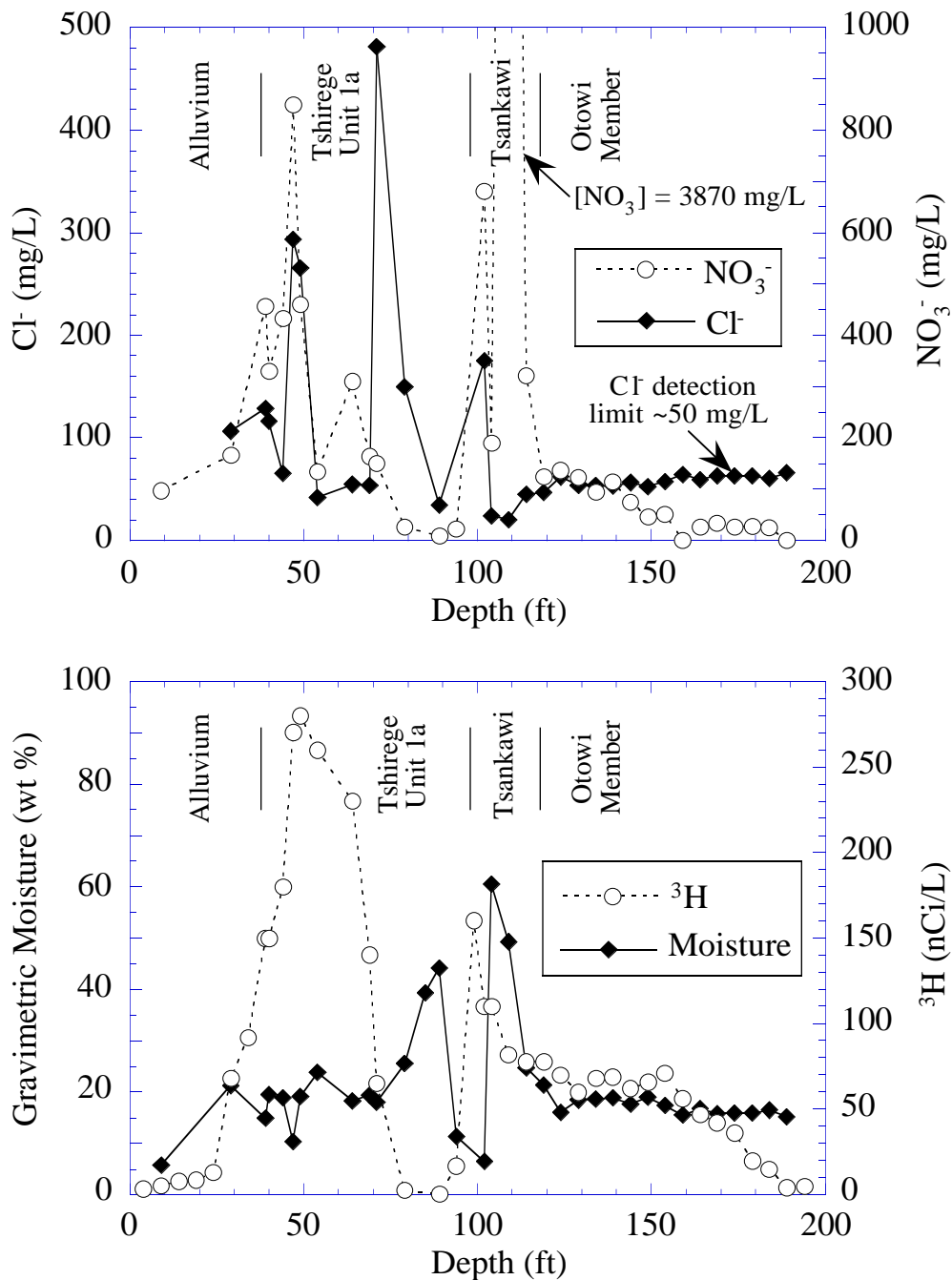
Figure 34. Borehole TA-54, MDA L borehole 54-1006 core sample depth profiles of (top) saturation, porosity, volumetric moisture content, and residual moisture content (with the addition of the core moisture data for the borehole); and (bottom) head and (-) suction at in situ moisture content.

Figure 35. Borehole MCM-5.9A profiles of Cl⁻ and NO₃⁻ (top) and gravimetric moisture and tritium (^{3}H) (bottom). The data are from Stoker et al. (1991). The Cl⁻ and NO₃⁻ concentrations were determined as μg/g by leaching core samples with water. The results were converted from μg/g to mg/L using the core gravimetric moisture content. The minimum detection limit for Cl⁻ was 10 μg/g, which converts to about 47–66 mg/L for a gravimetric moisture contents of 15%–21%.